Role of peroxisomes in inclusion body (IB) formation and cellular metabolism in the yeast model of human N88S seipinopathy

Vitor Daniel Ferreira Moreira
Master in Biochemistry
Faculty of Sciences of University of Porto and School of Medicine and Biomedical Sciences
2024-2025

Role of peroxisomes in inclusion body (IB) formation and cellular metabolism in the yeast model of human N88S seipinopathy

Vitor Daniel Ferreira Moreira

Dissertation carried out as part of the Master in Biochemistry
Yeast Signalling Networks
2024-2025

Supervisor
Vitor Teixeira, Assistant Researcher, i3S - Instituto de Investigação e Inovação em Saúde and ICBAS - Instituto de Ciências Biomédicas Abel Salazar, Universidade do Porto

Co-supervisor
Vítor Costa, Associate Professor, i3S - Instituto de Investigação e Inovação em Saúde and ICBAS - Instituto de Ciências Biomédicas Abel Salazar, Universidade do Porto

Dedicated to my parents

Acknowledgements

Já não era sem tempo, finalmente toda uma vida de estudos (que é a única realidade que conheço até agora) finalizada (por enquanto, pois não sei o que o futuro me reserva). Finalizada mais uma etapa importante da minha vida gostaria de deixar aqui uma mensagem de agradecimento a todos os que me acompanharam nesta jornada.

Começando por alguém que começou por ser meu professor, um enorme agradecimento ao meu orientador Dr. Vitor Teixeira. Se não fosse pelo destino de me ter calhado um dos seus temas para apresentação na cadeira de Estrutura e Função de Proteínas provavelmente o convite por sua parte para trabalhar consigo também não teria acontecido. O que me leva a mais um ponto, obrigado pela confiança que colocou na minha pessoa na altura e também pelo que aguentou ao ter que me aturar durante todo este ano letivo. Foi um prazer aprender, trabalhar e evoluir consigo ao meu lado. Tivemos os nossos altos e baixos, mas acho que é disso que se constroem boas relações e como tal só tenho a agradecer por tudo e espero que não percamos o contacto no futuro.

Também deixar umas palavras de agradecimento pela confiança e ajuda que o professor e líder de grupo Vítor Costa me proporcionou ao longo desta jornada. Bem como também a todos os meus colegas de grupo que me aturaram, atenderam aos meus pedidos e tornaram este ano de trabalho menos pesado e dificultoso. Os meus sinceros agradecimentos.

Gostaria também de expressar a minha gratidão às instituições que me acolheram e formaram ao longo da minha Licenciatura e Mestrado em Bioquímica: a Faculdade de Ciências da Universidade do Porto (FCUP), o Instituto de Ciências Biomédicas Abel Salazar (ICBAS) e a própria Universidade do Porto. Um agradecimento muito especial direciono à Professora Doutora Paula Gameiro, à Professora Doutora Eulália Pereira, ao Professor Doutor Jorge Azevedo e ao Professor Doutor Paulo Correia de Sá, pelo facto de nos terem orientado e esclarecido dúvidas que surgiram durante o percurso para que deste trabalho pudesse sair o maior aproveitamento possível.

Aos meus fantásticos pais, Vitor Moreira e Rosalina Nunes, uma gratidão eterna por sempre terem sido uns pais perfeitos que nunca me deram razão para me queixar, obrigado por sempre me terem apoiado nas minhas escolhas e me terem acompanhado ao longo desta jornada. Espero lhes ter deixado orgulhosos também o tanto que eu estou de vocês. Um beijo enorme a ambos e que isto seja apenas o início do orgulho que vos irei dar!

Também deixar um espacinho reservado aqui para agradecer a quatro pestes que tive de aturar e que foram o maior prémio que ganhei na universidade. À Clara, Joana, Helena e Ana um muitíssimo obrigado por todos os momentos que passamos e pelo apoio inegável que me deram nesta etapa da minha vida. Não consigo imaginar um universo paralelo onde a versão da minha pessoa passasse por este pesadelo todo sem a vossa presença para me ajudar a evoluir como pessoa e também me permitir divertir e esquecer de todo o estresse.

Agradecer também a todos os que conheci durante esta jornada que se apercebendo ou não tiveram influência no percurso que tive até à data de hoje.

Resumo

O Retículo Endoplasmático (RE) desempenha um papel crucial no metabolismo de lípidos e na formação de gotículas lipídicas. Proteínas-chave, como a seipina, codificada pelo gene *BSCL2* em mamíferos e *SEI1* em leveduras, são essenciais para a biogénese de gotículas lipídicas. A seipina, uma proteína de membrana do RE, ajuda a estabilizar os locais de contato entre o RE e as gotículas lipídicas, promovendo a transferência unidirecional de triglicerídeos (TG) e o armazenamento de lípidos na célula. Mutações na seipina, nomeadamente a mutação N88S, leva a uma neuropatia conhecida como seipinopatia, a qual é caracterizada pela degeneração de neurónios motores e desregulação do metabolismo lipídico. A mutação N88S na seipina é uma mutação classificada como ganho de função, a qual bloqueia a *N*-glicosilação da proteína, resultando numa alteração conformacional que está relacionada com ativação da resposta ao estresse do RE (UPR) e acumulação de corpos de inclusão contendo a proteína mutante, e também com elevados níveis de estresse oxidativo. Estudos com leveduras e modelos de mamíferos têm sido cruciais para entender em detalhe os mecanismos celulares da seipinopatia, procurando investigar de que forma o estresse no ER associado à mutação N88S resulta em alterações no proteoma e lipidoma das células, disfunção neuronal e morte celular. Este estudo constitui mais uma contribuição para estes estudos, e tem por objetivo avaliar a contribuição dos peroxissomas para os mecanismos moleculares subjacentes à seipinopatia. Nesta investigação, foi possível demonstrar que a função peroxissomal é crítica para combater o estresse oxidativo, e que as alterações do fluxo metabólico do acetil-coA, resultante da beta-oxidação, no ciclo do glioxilato e da mitocôndria conduzem a um ciclo lipídico fútil que contribui para a produção de espécies reativas de oxigénio.

Palavras-chave: Seipinopatia; Seipina; Peroxissomas; Ciclo do Glioxilato; Mitocôndria

Abstract

The Endoplasmic Reticulum (ER) plays a crucial role in lipid metabolism and the formation of lipid droplets. Key proteins, such as seipin, encoded by the *BSCL2* gene in mammals and *SEI1* in yeast, are essential for the biogenesis of lipid droplets (LDs). Seipin, an ER membrane protein, helps stabilize contact sites between the ER and nascent LDs, promoting the unidirectional transfer of triglycerides (TG) and the storage of lipids in the cell. Mutations in seipin, notably the N88S mutation, leads to a neuropathy known as seipinopathy, which is characterized by motor neuron degeneration and dysregulation of lipid metabolism. The N88S mutation in seipin is classified as a gain-of-function mutation, which blocks the *N*-glycosylation of the protein, resulting in a conformational change that is linked to the activation of the ER stress response (UPR) and the accumulation of inclusion bodies containing the mutant protein, as well as high levels of oxidative stress. Studies with yeast and mammalian models have been crucial for understanding in detail the cellular mechanisms of seipinopathy, aiming to investigate how ER stress associated with the N88S mutation results in changes to the cellular proteome and lipidome, neuronal dysfunction, and cell death. This study adds another contribution to this research and aims to assess the contribution of peroxisomes to the molecular mechanisms underlying seipinopathy. In this research, it was shown that peroxisomal function is critical to counter oxidative stress, and that changes in the metabolic flux of acetyl-CoA, resulting from β-oxidation, through the glyoxylate cycle and mitochondria lead to a futile lipid cycle that contributes to the production of reactive oxygen species (ROS).

Keywords: Seipinopathy; Seipin; Peroxisomes; Glyoxylate cycle; Mitochondria.

Table of Contents

List of Tables vii

List of Figures viii

List of Abbreviations x

1. Introduction 1

1.1. Lipid Droplets 3

1.1.1. Molecular mechanisms of LD biogenesis 4

1.1.1.1. Nucleation phase 4

1.1.1.2. Oil lens formation 5

1.1.1.3. LD maturation and cellular localization 7

1.1.2. LD dynamics and NL mobilization 10

1.2. Seipin 12

1.2.1. Molecular architecture and function of Seipin 13

1.2.2. N88S seipinopathy: a motor neuron degenerative disease 14

1.3. Peroxisomes 16

1.3.1. Peroxisome biogenesis: membrane assembly and protein targeting mechanisms 17

1.3.2. Matrix protein import: signals, receptors, and translocation machinery 18

1.4. Glyoxylate Cycle 19

1.4.1. The glyoxylate cycle: key reactions 20

1.4.2. Enzyme localization and metabolic flexibility 21

1.4.3. Regulation of the glyoxylate cycle 21

1.5. Acetyl-CoA synthesis and metabolism 23

1.6. *S. cerevisiae* as a disease model system 25

1.7. Aims of the project 25

2. Materials and Methods 28

2.1. Yeast strains and plasmids 28

2.2. Culture media and growth conditions 31

2.3. Construction of yeast mutants 32
2.4. Yeast transformation 33
2.5. *E. coli* transformation 34
2.6. β-Galactosidase activity assay 34
2.7. Western blotting analysis 35
2.8. Fluorescence microscopy 35
2.9. ROS staining and IB formation 36
2.10. Yeast spotting assay 36
2.11. β-Oxidation Measurement 36
2.12. Enzymatic activity assays 36
2.13. Lipid peroxidation assay 38
2.14. Measurement of glutathione levels 38
2.15. Statistical analysis 38
3. Results 39
3.1. Absence of peroxisomes lead to an increase in IBs formation 40
3.2. Peroxisome deficiency increases ROS production and disrupts redox balance without inducing ER stress 41
3.3. N88S seipin-expressing cells exhibit increased peroxisomal biogenesis and function 44
3.4. Downregulation of glyoxylate cycle enzymes activities is not related to changes in their enzymatic activity 46
3.5. *MPC1* overexpression exacerbates ER stress but does not contribute to ROS generation upon N88S seipin mutation 49
3.6. Cytosolic misrouting of acetyl-CoA potentiates ER stress and contributes to oxidative damage in N88S mutant cells 51
3.7. Cytosolic acetyl-CoA fuels lipid biosynthesis and promotes oxidative stress in N88S seipin expressing cells 55
4. Conclusion 57
References 60

List of Table

Table 1. Yeast strains used in this study 28
Table 2. Plasmids used in this study 31
Table 3. Primers used in this study. 32
Table 4. Conditions for the measurement of glyoxylate and TCA cycle enzyme activities. 37

List of Figures

Figure 1 – Lipid droplet (LD) architecture. 3
Figure 2 - Stages of LD biogenesis. 4
Figure 3 - Nucleation phase of LD biogenesis. 5
Figure 4 - Oil lens formation. 7
Figure 5 - Nascent LD and their maturation in LD biogenesis. 8
Figure 6 - LD-organelle membrane contact sites (MCS). 9
Figure 7 - Schematic representation of LD lipolysis. 10
Figure 8 - The metabolism of the FFA into Acetyl-CoA or membrane synthesis. 12
Figure 9 - Seipin structure. 13
Figure 10 - N88S human seipinopathy model. 15
Figure 11 - Peroxisome biogenesis. 17
Figure 12 - Glyoxylate cycle. 20
Figure 13 - Regulation of the glyoxylate cycle. 23
Figure 14 - Overview of the metabolic and organelle interactions linking ER, lipid droplets, peroxisomes, and the glyoxylate-TCA Network. 27
Figure 15 - GO-based functional categorization of DEPs with respect to biological processes. 39
Figure 16 - PEX3 and PEX19 deficiency increased IBs formation in cells expressing the N88S seipin mutation. 41
Figure 17 - PEX3 deficiency has no effect in the activation of the UPR in N88S seipin-expressing cells. 42
Figure 18 - Lack of peroxisomes (pex3-deficient cells) increases ROS levels in N88S mutant cells but does not impact ROS levels in WT cells. 43
Figure 19 - The loss of peroxisomes leads to an increase in total glutathione levels in N88S seipin-expressing cells. 43
Figure 20 - N88S strains presented higher levels of peroxisome biogenesis and activity. 44
Figure 21 - β-oxidation activity was not altered by the N88S seipin mutation. 45
Figure 22 - Lower incorporation of acetyl-CoA into ASP in N88S-seipin expressing cells. 45
Figure 23 - N88S-seipin expressing cells exhibited a prominent growth defect in the absence of peroxisomes. 46
Figure 24 - Activities of glyoxylate and TCA cycle enzymes were not affected in N88S mutant strains. 47

Figure 25 - *CIT2* expression is reduced in N88S mutant cells under both basal and non-fermentable growth conditions. 48
Figure 26 - N88S seipin mutant cells display growth comparable to WT in the presence of sodium arsenite (NaAs) independently of the carbon source. 49
Figure 27 - *MPC1* overexpression did not alter the levels of ROS production in WT and N88S seipin mutant cells. 50
Figure 28 - Changes in acetyl-CoA subcellular distribution triggers the UPR in WT and N88S seipin mutant cells. 52
Figure 29 - N88S cytosolic *CAT2* cells induced more ROS production. 53
Figure 30 - Mutant N88S cells expressing the cytosolic *CAT2* showed growth defects at STAT phase. 53
Figure 31 - Carnitine supplementation had no effect in ROS production in N88S seipin expressing cells. 54
Figure 32 - Cerulenin attenuates oxidative stress in WT and N88S seipin mutant cells expressing cytosolic *CAT2*. 55
Figure 33 - The activity of acetyl-coenzyme A synthetase (Acs) was increased in N88S mutant cells overexpressing cytosolic *CAT2*. 56

List of Abbreviations

aa	Amino acids
ACAT	Acyl-coa cholesterol o-acyltransferase
Aco	Aconitase
ACS	Acyl-CoA synthetases
AFT1	Activating transcription factor 1
AGPAT	Acylglycerol-3-phosphate acyltransferase
ATP	Adenosine triphosphate
BiP	Immunoglobulin heavy chain binding protein
BiFC	Bimolecular fluorescence complementation
BSA	Bovine serum albumin
BSCL2	Berardinelli-seip congenital lipodystrophy 2
bZIP	Basic leucine zipper
CAT2	Carnitine acetyltransferase 2
$CAT2_{cyt}$	Carnitine O-acetyltransferase 2 cytosolic
$CAT2_{mit}$	Carnitine O-acetyltransferase 2 mitochondrial
CCT1	Choline-phosphate cytidylyltransferase 1
CDP-DAG	Cytidine diphosphate-diacylglycerol
CDS1P	CDP-DAG synthase
CHO1	PS synthase
CHO2	Phosphatidylethanolamine methyltransferase
CIT	Citrate synthase
CoA	Coenzyme A
CR	Caloric restriction
CTH2	Putative cystathionine gamma-lyase 2
DAG	Diacylglycerols
DG	Diacylglycerol
DEG	Differentially expressed genes
DGAT	Acil-CoA:diacilglicerol aciltransferase
DHE	Dihydroethidium
DNA	Deoxyribonucleic acid
DTNB	5,5′-Dithiobis(2-nitrobenzoic acid)
EDTA	Ethylenediaminetetraacetic acid
ER	Endoplasmic reticulum
ERAD	Endoplasmic reticulum-associated degradation

EXP	Exponential
FA	Fatty acid
FAS	Fatty acid synthase
Fe	Iron chemical symbol
FET3	Iron transport multicopper oxidase
FFA	Free fatty acids
FIT	Facilitator of iron transport
FITMs	Fat storage inducing transmembrane proteins
G3P	Glycerol-3-phosphate
GAT	G3p acyltransferase
GO	Gene ontology
GPAT	Glycerol-3-phosphate acyltransferase
HOG	High-osmolarity glycerol
HSL	Hormone-sensitive lipase
IB	Inclusion body
Icl	Isocitrate lyase
INO1	Inositol-3-phosphate synthase
KEAP1	Kelch-like ech-associated protein 1
KO	Knock out
LA	Lithium acetate
LB	Lysogeny Broth
LD	Lipid droplet
LDAF1	Lipid droplet assembly factor 1
LRO1	Fosfolipídeo:diacilglicerol aciltransferase
LPA	Lysophosphatidic acid
MCS	Membrane contact sites
Mdh	Malate dehydrogenase
MG	Monoacylglycerol
MGL	Monoacylglycerol lipase
Mls	Malate synthase
MM	Minimum Medium
MND	Motor neuron diseases
MPC1	Mitochondrial pyruvate carrier 1
mRNA	Messenger ribonucleic acid
Msn2/Msn4	Multicopy suppressor of snf1 mutation proteins 2 and 4
NAD(P)	Nicotinamide adenine dinucleotide phosphate

NAFLD	Non-alcoholic fatty liver diseases
NB	Nuclear body
NL	Neutral lipid
NR	Nucleoplasmic reticulum
NRF2	Nuclear factor erythroid 2-related factor 2
ONPG	O-nitrophenyl-β-D-galactopyranoside
OPI3	Phospholipid methyltransferase
p38	Mitogen-activated protein kinase
PA	Phosphatidic acid
PAH1	Pa phosphatase
PC	Phosphatidylcholine
PCR	Polymerase chain reaction
PDH	Mitochondrial pyruvate dehydrogenase
PDS	Post-diauxic shift
PE	Phosphatidylethanolamine
PEG	Polyethylene glycol
PEX	Peroxins
PI	Phosphatidylinositol
PIS1	PI synthase
PML	Promyelocytic leukemia
PMP	Peroxisomal membrane protein
PS	Phosphatidylserine
PTS	Peroxisomal targeting signals
REEP1	Receptor expression-enhancing protein 1
RING	Really interesting new
ROS	Reactive oxygen species
RPM	Rotation per minute
SC	Synthetic Complete
SCFUCC1	Ubiquitination of citrate synthase in the glyoxylate cycle protein 1
SD	Standard deviation
SDS-PAGE	Sodium Dodecyl Sulfate Polyacrylamide Gel Electrophoresis
SE	Sterol esters
SLC1	1-acyl-g3p acyltransferase
STAT	Stationary phase
ssDNA	Single-stranded carrier DNA

TAE	Tris-acetate-EDTA
TBS	Tris buffered saline
TCA	Tricarboxylic acid
TE	Tris EDTA
TG	Triacylglycerols
Tris-HCL	Tris-Hydrochloride
TTBS	Tris-Tween buffered saline
UPR	Unfolded protein response
UPRE	Unfolded protein response element
VC	C-terminal fragment of Venus
VN	N-terminal fragment of Venus
WB	Western Blot
WT	Wild type
XBP1	X-box binding protein 1
YAP1	Yes-associated protein 1
YPD	Yeast peptone dextrose
β-gal	β-galactosidase

1. Introduction

The Endoplasmic Reticulum (ER) is a complex organelle composed of a tubular network of membranes found within the cytoplasm of eukaryotic cells. It contributes to various cellular functions, including protein synthesis, folding, and quality control; calcium ion storage and release; metabolite and lipid interorganellar flux and lipid synthesis [1]. Additionally, the ER serves as a site for lipid droplet (LD) biogenesis, which is essential for neutral lipid storage [1-3].

LD biogenesis begins with the synthesis of triacylglycerols (TG) and sterol esters (SE) within the ER membrane bilayer [4, 5]. As these neutral lipids accumulate, they cause the ER membrane to progressively curve inward, forming an initial structure called an oil lens, the precursor to mature LDs [5]. Crucially, this site harbors seipin, the central protein of this study. In humans, seipin is encoded by the Berardinelli-Seip congenital lipodystrophy 2 (*BSCL2)* gene (*SEI1* in yeast), and its primary role is to regulate the unidirectional flow of TG and SE into nascent LDs [6, 7]. Seipin forms an ER-bound homo-oligomeric complex located at ER-LD contact sites, where it ensures proper LD assembly and growth [8]. Notably, mutations in seipin, particularly the N88S and S90L variants, disrupt this function and are linked to seipinopathies, a group of motor neuron diseases (MNDs) [9, 10]. These disorders highlight the critical role of seipin in maintaining lipid homeostasis and neuronal integrity.

The N88S mutation, classified as a gain-of-function variant, disrupts the protein's *N*-glycosylation, a critical post-translational modification required for proper folding [4, 9, 11]. This loss of glycosylation leads to misfolding, causing seipin to aggregate into inclusion bodies (IBs) [9]. These aggregates further exacerbate ER stress, creating a vicious cycle that contributes to cellular dysfunction. Building on these findings, our laboratory previously engineered a humanized yeast model of N88S seipinopathy in *Saccharomyces* (*S.*) *cerevisiae*. This model successfully recapitulated the key cellular hallmarks of the human disease, including ER stress, the activation of the unfolded protein response (UPR) pathway and formation of IBs. Our model further extended our understanding of the disease, providing evidence of oxidative stress markers characterized by generation of reactive oxygen species (ROS), lipid peroxidation, and reduced antioxidant activity [4, 9]. By mirroring the disease's molecular pathology, this yeast model provides a powerful platform to dissect the mechanisms underlying seipinopathy and screen for potential therapeutic interventions.

Using this model, it was employed a multi-omics approach, integrating proteomic and genomic analyses. Through gene ontology (GO) enrichment, it was identified distinct groups of upregulated and downregulated proteins, with notable changes in key metabolic pathways, including glyoxylate cycle, carboxylic acid metabolism, fatty acid (FA) metabolic processes and tricarboxylic acid (TCA) cycle [10]. These pathways were prioritized due to their functional interdependence, a relationship that will be explored in detail in subsequent sections. Complementing this, genomic profiling aimed at defining gene networks involved in IB formation revealed a cluster of genes linked to peroxisome biogenesis and function, which were found to directly influence IBs formation [10]. This dual-omics strategy was the step stone for all the work developed after, where we pretend to demonstrate that seipinopathy is not just a proteinopathy but also a lipidopathy. To unravel these critical mechanisms, our research focused on understanding how peroxisomes influence disease progression by examining their biogenesis and functional capacity. We specifically investigated how the presence or absence of peroxisomes alters metabolic flux through interconnected pathways, particularly the glyoxylate cycle and mitochondrial TCA cycle. By systematically analyzing these pathways, we aimed to identify key enzymes that show altered activity or expression patterns, as well as metabolite transporters that facilitate communication between these organelles. A central aspect of this work involved the characterization the protein networks that mediate peroxisome-mitochondria crosstalk, with special attention to metabolite shuttle systems and redox coordination mechanisms. The ultimate goal is to reveal novel therapeutic targets at the interface of this interorganellar network involved in lipid turnover and energy production. Through this integrated approach, we seek to establish a detailed mechanistic link between peroxisomal activity, metabolic regulation, and disease pathology.

1.1. Lipid Droplets

Lipid Droplets (LDs) are monolayered membrane organelles present in different taxonomic domain groups including eukaryotes [4, 12, 13], bacteria [14] and archaea [15], that primarily serve as storage sites for neutral lipids (NLs), such as triacylglycerols (TG) and sterol esters (SE). Beyond their well-established function as lipid reservoirs, LDs play pivotal roles in maintaining cellular homeostasis (**Figure 1**).

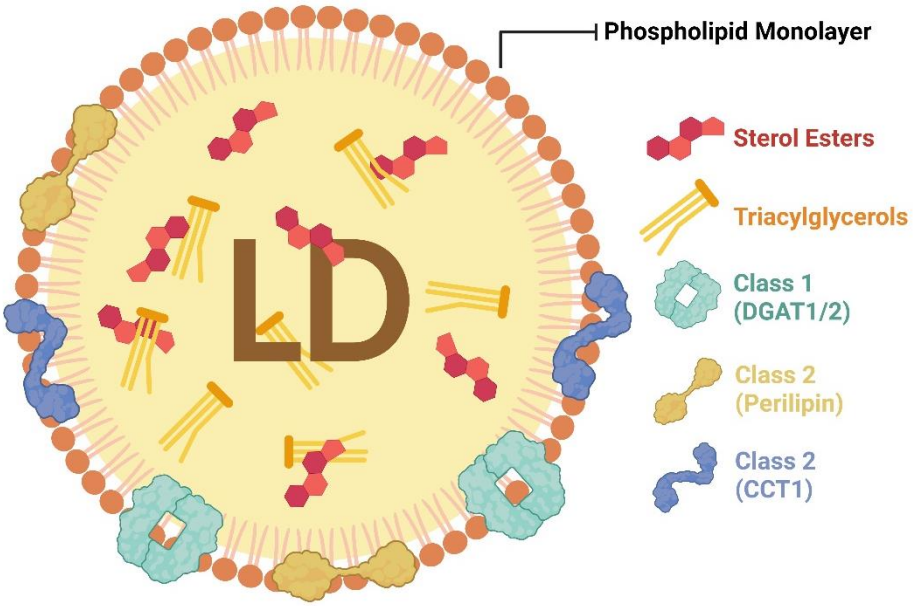

Figure 1. **Lipid droplet (LD) architecture.** An LD is enveloped by a single phospholipid layer that encases a central core of neutral lipids, primarily triacylglycerols and sterol esters. The LD surface is composed of various proteins that regulate biophysical aspects of the organelle, including size, morphology and number. Made in Biorender.com.

They act as buffers for unsaturated fatty acids (FAs), prevent the accumulation of oxidized and peroxidized lipids, and provide immediate protection against lipotoxicity and oxidative stress, thereby safeguarding cellular integrity and homeostasis [4]. The stored neutral lipids within LDs can later be mobilized for essential metabolic processes, such as β-oxidation to generate energy or for membrane lipid biosynthesis, highlighting their role as an energy and lipid source [3, 5]. Beyond energy storage, LDs regulate lipid and membrane homeostasis, sequester misfolded proteins, act as signaling platforms, and form contact sites with other organelles to coordinate metabolism, stress responses, and autophagy [3, 16, 17]. Their versatile roles in immunity, hormone synthesis, and cellular differentiation make LDs central to cellular health. However, dysregulation of LD biogenesis, size, or turnover has been increasingly linked to the pathogenesis of numerous human diseases. Excessive accumulation of LDs is often associated with

metabolic disorders, including obesity, type 2 diabetes mellitus, hepatic steatosis, cardiovascular diseases, non-alcoholic fatty liver disease (NAFLD), and atherosclerosis [18-20]. Conversely, a decrease or insufficient number of LDs can lead to conditions such as lipodystrophy, characterized by the abnormal distribution or absence of adipose tissue [5, 6, 20]. Therefore, understanding LD biogenesis, regulation and functions is therefore crucial for elucidating the mechanisms underlying metabolic health and disease.

1.1.1. Molecular mechanisms of LD biogenesis

The currently most accepted model of LD biogenesis proposes that the process begins with the accumulation of TG and SE within the phospholipid bilayer of the ER (**Figure 2**) [5]. LD formation proceeds through four successive stages: nucleation, oil lens formation, nascent LD, and maturation (**Figure 2**). These stages will be addressed in detail in the subsequent subsections [5].

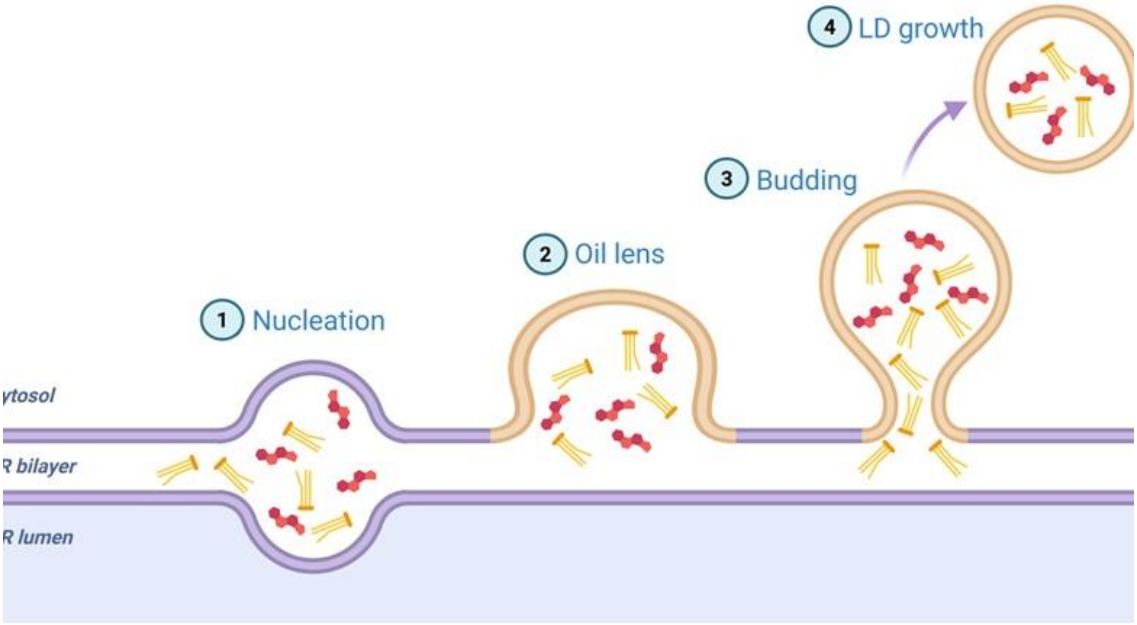

Figure 2. **Stages of LD biogenesis.** LD biogenesis consists of 4 phases: nucleation, oil lens formation, nascent LD and finally LD maturation. TGs are depicted in yellow and SEs in red. Made in Biorender.com.

1.1.1.1. Nucleation phase

The nucleation phase represents the initial stage of LD biogenesis, during which NL are synthesized within the ER bilayer (**Figure 3**). At this site, key enzymes such as Diacylglycerol acyltransferases (DGAT1/2) (Dga1 and Lro1 in yeast) [21] and Acyl-CoA cholesterol O-acyltransferase (ACAT1/2) (Are1 and Are2 in yeast) [22] catalyze the acetylation reactions leading to the production of TG and SE, respectively (**Figure 3**) [20]. The predominant pathway for triacylglycerol (TG) synthesis is the glycerol-3-phosphate pathway, in which three successive esterification reactions attach activated fatty acids to a glycerol-3-phosphate backbone. This process begins with glycerol-3-

phosphate acyltransferase (GPAT), which catalyzes the formation of lysophosphatidic acid (LPA). LPA is subsequently acylated by acylglycerol-3-phosphate acyltransferase (AGPAT) to produce phosphatidic acid (PA), which is then dephosphorylated to yield diacylglycerol (DG) (**Figure 3**). The final step is mediated by diacylglycerol acyltransferases (DGAT1/2), which cleave the thioester bond of fatty acyl-CoA (acyl donor) and transfer the acyl chain to the hydroxyl group of DG (acyl acceptor), generating TG at the ER (**Figure 3**) [21]. An alternative route, the monoacylglycerol (MG) pathway, involves the acylation of monoacylglycerol by monoacylglycerol acyltransferase (MGAT) to produce DG [21]. However, this pathway is more restricted and occurs predominantly in specialized cell types, such as enterocytes, hepatocytes, and adipocytes. In yeast, TGs can also be synthesized acyl-CoA- independent pathway catalyzed by Lro1 using phospholipids as acyl donors [23]. Although yeast cells remain viable without neutral lipids or lipid droplets, such mutants display increased sensitivity to fatty acid excess and lipotoxic stress [24].

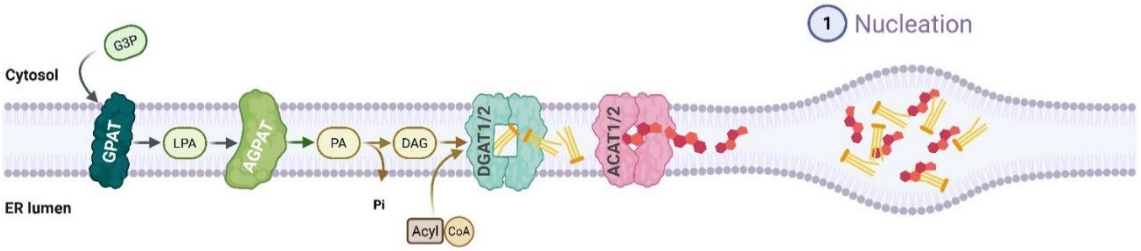

Figure 3. **Nucleation phase of LD biogenesis.** The initial step entails the enzymatic synthesis of TG (yellow) and SEs (red), leading to the accumulation of neutral lipids between the bilayers of the ER membrane. Abbreviations: GPAT: Glycerol-3-phosphate acyltransferase; AGPAT: 1-Acylglycerol-3-phosphate O-acyltransferase; PA: Phosphatidic acid; DAG: Diacylglycerol; DGAT: Diacylglycerol acyltransferase; ACAT: Acyl-CoA:cholesterol acyltransferase. Made in Biorender.com.

1.1.1.2. Oil lens formation

The budding of LDs is mediated by multiple ER-associated factors, many of which remain incompletely characterized. During oil lens formation, once the concentration of neutral lipids (NLs) within the ER bilayer surpasses a critical threshold, the outer leaflet of the ER membrane protrudes toward the cytosol [5]. This process is strongly influenced by membrane properties, particularly surface tension and phospholipid composition. For example, enrichment of phosphatidylcholine (PC) and phosphatidylinositol (PI) in the outer leaflet reduces surface tension [25], thereby favoring budding, whereas the presence of conical lipids such as diacylglycerol (DG) and phosphatidylethanolamine (PE) opposes it (**Figure 4**) [3, 25].

Among the protein regulators, fat storage inducing transmembrane proteins (FITMs), especially FITM2 (Scs3 and Yft2 in yeast), play a central role [26, 27]. FITM2 localizes to the luminal side of the ER and contributes to local remodeling of DG and PA, the precursor molecule for PL synthesis metabolism (**Figure 4**) [26]. By promoting the accumulation of DG and PE in the luminal leaflet, FITM2 prevents its budding. However, since these lipids can rapidly flip between leaflets and be reconverted into phospholipids, FITM2 indirectly replenishes the cytosolic monolayer with phospholipids, which constitutes the primary source of the LD surface (**Figure 4**) [3]. Loss of FITM activity disrupts LD formation and has been linked to lipodystrophy [27].

Additional regulatory factors act specifically at endoplasmic reticulum–lipid droplet (ER–LD) junctions to control droplet biogenesis and stability. In yeast, the perilipin homolog Pln1 is recruited early to nascent LDs (**Figure 4**), where it plays multiple protective roles: it stabilizes the emerging droplets, prevents their premature fusion, and shields mature LDs from untimely lipolysis [3]. Deletion of *PLN1* markedly delays droplet budding, highlighting its critical role in the early stages of LD formation. Pln1 also interacts functionally with FITM2 and with seipin, a highly conserved ER membrane protein that is indispensable for TG accumulation and stabilization of the ER-LD interface [28]. Seipin serves as a central organizing factor at LD nucleation sites, and its function is further linked to a network of associated proteins. For example, seipin interacts with Nem1 (**Figure 4**), the catalytic subunit of Nem1-Spo7 phosphatase holoenzyme that regulates nuclear/ER membrane association and activation of lipin Pah1, the phosphatidate phosphatase involved in the production of diacylglycerol DG for LD biogenesis [29]. It also interacts with Pex30 , a membrane-shaping protein that facilitates LD budding from the ER at specific ER subdomains [30, 31], and Erg6, which supports LD stabilization (**Figure 4**) [29]. Finally, ER-shaping proteins such as spastin, receptor expression-enhancing protein 1 (REEP1), spartin, and atlastin-1 further modulate LD assembly (**Figure 4**) [31-34]. These proteins are thought to locally deform the ER membrane, creating a permissive environment for the accumulation of neutral lipids. By acting in concert with seipin, they help define specialized ER subdomains that coordinate the efficient assembly, growth, and maturation of LDs. [31].

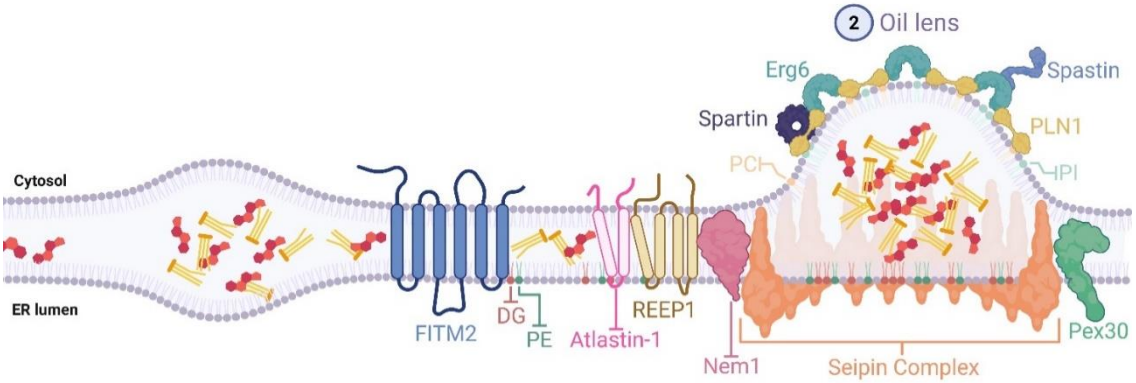

Figure 4. **Oil lens formation. FITM2 (dark blue)** (Scs3/Yft2 in yeast) remodels diacylglycerol (DG) and phosphatidic acid (PA) to regulate phospholipid balance and supply the cytosolic monolayer for LD surface formation. **Pln1 (yellow)** (perilipin homolog) stabilizes nascent LDs, prevents premature fusion, and protects mature LDs from lipolysis. **Seipin complex (orange)** organizes ER–LD junctions, promotes TG accumulation, and stabilizes the budding site. **Nem1 (red)** activates lipin Pah1 to generate DG for LD biogenesis. **Pex30 (green)** shapes ER membranes and facilitates site-specific LD budding. **Erg6 (cyan)** contributes to LD stabilization. **Spastin (lilac)**, **REEP1 (light brown)**, **spartin (purple)**, and **atlastin-1 (pink)** deform ER membranes to create permissive sites for neutral lipid accumulation and LD maturation**.** Made in Biorender.com.

1.1.1.3. LD maturation and cellular localization

Once they are fully formed, LDs can remain physically attached to the ER or detach and form distinct subpopulations in size and lipid composition. Cytosolic LDs can further grow employing different mechanisms [35]. Firstly, nascent LDs can increase in size by acquiring lipids from ER through ER-LD contact sites. Various protein machineries are involved in this process, through lipid transfer or mediating organelle contact. These include the FATP1-DGAT2 complex [36], the GBF1-Arf1-COPI complex [37], and the Rab18-NRZ-SNARE complex (**Figure 5**) [38]. Secondly, LD-associated enzymes, such as GPAT4 and DGAT2, can relocalize to the surface of the droplets and locally synthesize lipids to promote LD growth (**Figure 5**) [39].

The dynamic regulation of LD size and spatial distribution is also a highly orchestrated process that ensures cellular lipid homeostasis and proper metabolic adaptation [3, 40-42]. This regulation involves inter-organelle lipid exchange and structural remodeling events driven by distinct physical and biochemical mechanisms [5]. One major mechanism is homotypic fusion (**Figure 5**), where adjacent LDs merge through direct membrane contact, leading to rapid coalescence and formation of larger droplets. This process is typically completed within seconds and is facilitated by membrane-shaping proteins and phospholipid remodeling enzymes that reduce surface tension at the droplet interface [37, 43, 44]. A second key process is Ostwald ripening (**Figure 5**), a gradual mass transfer phenomenon where lipids move from smaller to larger droplets via molecular diffusion [35]. Unlike fusion, Ostwald ripening occurs over extended

timescales (minutes to hours) and contributes to LD heterogeneity by favoring the growth of larger droplets at the expense of smaller ones. Both mechanisms are tightly regulated by the cytoskeletal architecture, including microtubule and actin filament networks, which govern LD trafficking, positioning, and clustering within the cell. Motor proteins such as dynein and kinesin transport LDs along microtubules, enabling interactions with organelles like the endoplasmic reticulum (ER), mitochondria, and peroxisomes [45, 46]. Additionally, LD-associated proteins, such as seipin, perilipins, and members of the CIDE family, which act as molecular scaffolds to control droplet fusion, size restriction, and lipid transfer (**Figure 5**) [47, 48].

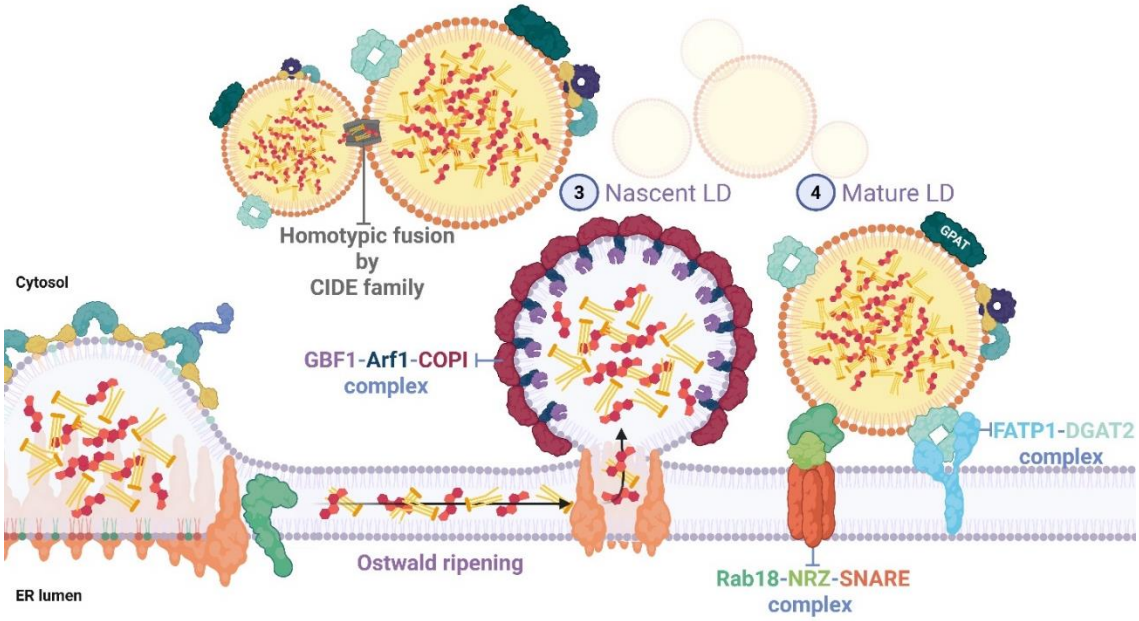

Figure 5. **Nascent LD and their maturation in LD biogenesis.** FATP1–DGAT2, GBF1–Arf1–COPI, and Rab18–NRZ–SNARE complexes mediate ER–LD contact and lipid transfer, enabling droplet enlargement. GPAT4 and DGAT2 relocate to LD surfaces to synthesize lipids locally. Homotypic fusion merges adjacent LDs through direct membrane contact, rapidly forming larger droplets. Ostwald ripening drives slower lipid diffusion from smaller to larger LDs, promoting size heterogeneity. Seipin, perilipins, and CIDE family proteins scaffold LD membranes, controlling fusion, lipid exchange, and size limitation. Made in Biorender.com.

Emerging evidence also highlights the role of lipid metabolism enzymes (e.g., ATGL, DGAT) and membrane contact site regulators in shaping LD morphology and dynamics [49, 50]. These factors ensure that LD expansion or shrinkage aligns with cellular energy demands, stress responses, and signaling pathways. Consequently, dysregulation of these processes contributes to metabolic disorders, lipodystrophies, and lipid storage diseases.

Detached LDs can localize to distinct cellular compartments (**Figure 6**) through specialized tethering mechanisms, enabling context-dependent metabolic functions [51]. At peroxisomal and mitochondrial interfaces, LD positioning is mediated by membrane

fusion and docking factors (perilipin-5 and MFN-2), respectively, creating efficient FAs conduits for β-oxidation [52-55]. Near the plasma membrane, particularly in macrophages and neurons, LDs facilitate localized lipid signaling and membrane repair [56]. At lysosomal/vacuolar surfaces, LDs engage with docking factors (perilipin-2) and the complex formed by heat shock cognate 71 kDa protein (HSC70) and lysosome-associated membrane protein 2A (LAMP2A), to couple LD turnover (e.g lipophagy or lipolysis) with lipid recycling during starvation [57-59]. Finally, nuclear-associated LDs interact with structural organizers like the promyelocytic leukemia (PML)-II nuclear body (NB) and type 1 nucleoplasmic reticulum (NR) in hepatocytes and adipocytes, where they may carry out potential roles in local lipid signaling and membrane biogenesis [60].

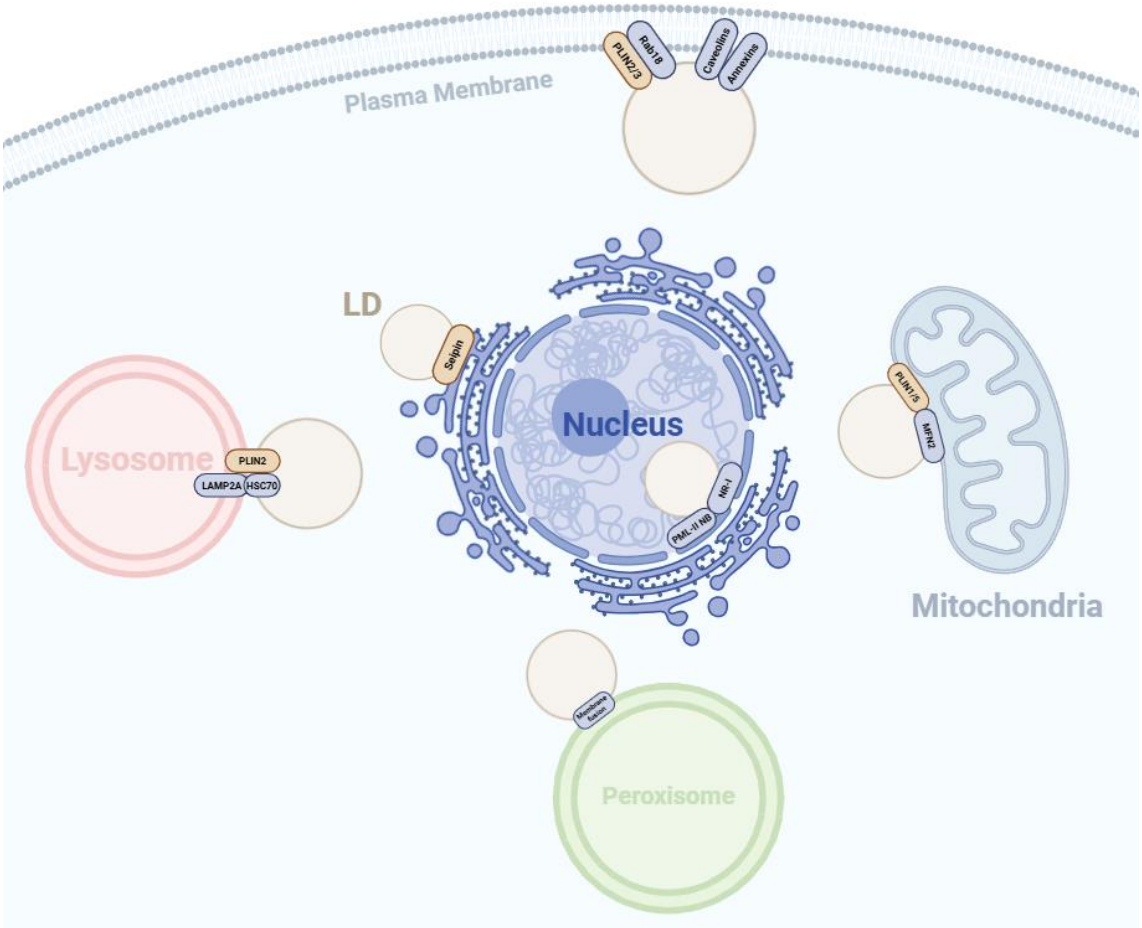

Figure 6. **LD-organelle membrane contact sites (MCS).** Identity of tethering factors at the interface of LDs with different organelles, being the ones in brown located at LDs and the grey ones are derived from the organelles at MCS. While the illustrated organelle contacts are presented as discrete and spatially segregated, individual LDs engage in simultaneous interactions with multiple organelles. **Abbreviations:** PLIN - perilipins; LAMP2A - lysosome-associated membrane protein 2A; HSC70 - heat shock cognate 71 kDa protein; MFN2 - mitofusin 2; Rab18 - Ras-related protein Rab-18. Made in Biorender.com.

1.1.2. LD dynamics and NL mobilization

LDs dynamically interact with various cellular compartments to facilitate the mobilization and utilization of stored neutral lipids, particularly TGs and SEs. The hydrolysis of these lipid reserves occurs through a tightly regulated enzymatic cascade. TGs are sequentially metabolized through the coordinated action of three key lipases: Adipose triglyceride lipase (ATGL) initiates the process by cleaving TGs into DGs and free fatty acids (FFAs), followed by Hormone-sensitive lipase (HSL) which further processes DGs to MGs and additional FFAs [61, 62]. The final hydrolysis step is mediated by Monoacylglycerol lipase (MGL), which yields glycerol and a third FFA molecule [61, 62]. Similarly, sterol esterases convert SEs into cholesterol and FFAs (**Figure 7**) [63].

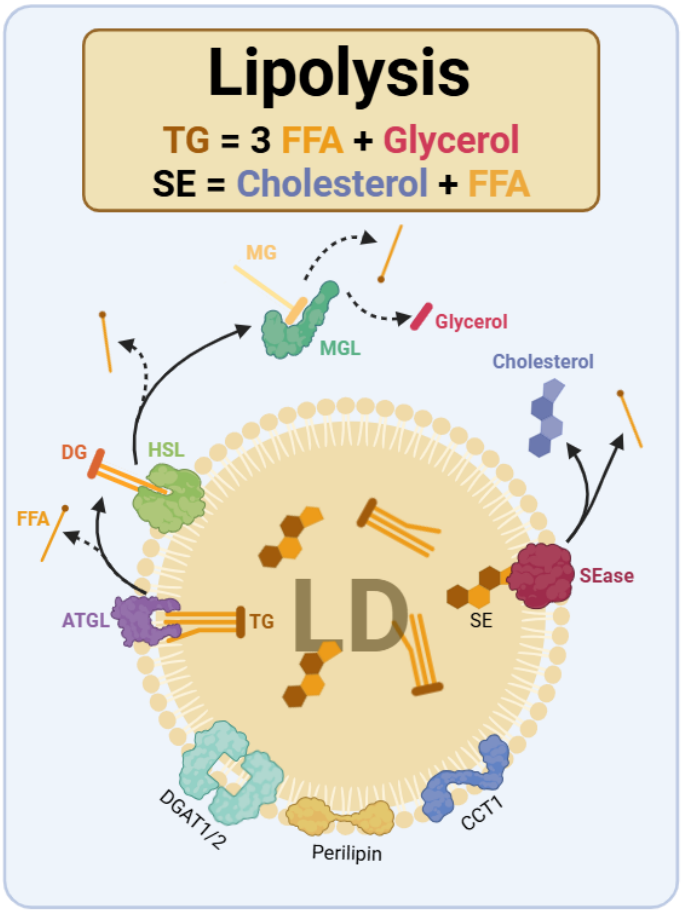

Figure 7. **Schematic representation of LD lipolysis.** In this image it's possible to see the mechanism through which the TG inside LDs are converted in three molecules of FFA and glycerol by the machinery that it is anchored to the LD membrane (respectively, lipases ATGL, HSL and MGL). The same goes for the SE, where sterol esterases (SEase) catalyze the hydrolysis of SEs to a molecule of free cholesterol and FFA. **Abbreviations:** MG: Monoacylglycerol; MGL: Monoacylglycerol lipase; DG: Diacylglycerol; HSL: Hormone-sensitive lipase; FFA: Free fatty acid; ATGL: Adipose triglyceride lipase; CCT1: CTP:phosphocholine cytidylyltransferase 1; DGAT: Diacylglycerol acyltransferase; SEase: Steryl ester hydrolase. Made in Biorender.com.

This lipolytic process is critically regulated by perilipin proteins [58], which serve dual roles in controlling lipase accessibility and maintaining the structural integrity of LD-organelle contact sites that are essential for efficient lipid transfer and metabolic coordination between cellular compartments (**Figure 6**). These newly released FFAs can subsequently be converted into acyl-CoA by acyl-CoA synthetases (ACSs), which catalyze the ATP-dependent formation of a thioester bond (**Figure 8**) [64]. The resulting acyl-CoA molecules can then enter β-oxidation pathways in either peroxisomes or mitochondria to origin acetyl-CoA. On the other hand the FFA can also be used for membrane synthesis (**Figure 8**), since the LD-derived acyl-CoAs serve as crucial precursors for PA synthesis, which begins with the sequential acylation of glycerol-3-phosphate (G3P) by G3P acyltransferase (Sct1/Gat2) and 1-acyl-G3P acyltransferase (Sct1/Slc1) to form PA [65]. This central lipid intermediate then functions as a metabolic hub, branching into both lipid storage and membrane biogenesis pathways. For storage metabolism, PA is converted to diacylglycerol (DG) by PA phosphatase (Pah1), which is subsequently acylated to TG by DG acyltransferase (Dga1/Lro1) [65]. For membrane biogenesis, PA is transformed to cytidine diphosphate-diacylglycerol (CDP-DAG) by CDP-DAG synthase (Cds1), initiating phospholipid production [65]. The CDP-DAG pathway diverges into three major biosynthetic routes: phosphatidylinositol (PI) synthesis through PI synthase (Pis1) using CDP-DAG and inositol (derived from glucose-6-phosphate via inositol-3-phosphate synthase, Ino1); phosphatidylserine (PS) production via PS synthase (Cho1)-mediated condensation of CDP-DAG and serine, which is subsequently decarboxylated to phosphatidylethanolamine (PE); and conversion of PE to phosphatidylcholine (PC) through three methylation reactions catalyzed by phosphatidylethanolamine methyltransferase (Cho2) and phospholipid methyltransferase (Opi3) [65]. This integrated metabolic network demonstrates how yeast coordinates lipid storage mobilization from LDs with membrane biogenesis through carefully regulated enzymatic conversions, with PA serving as the critical metabolic intersection point between these pathways.

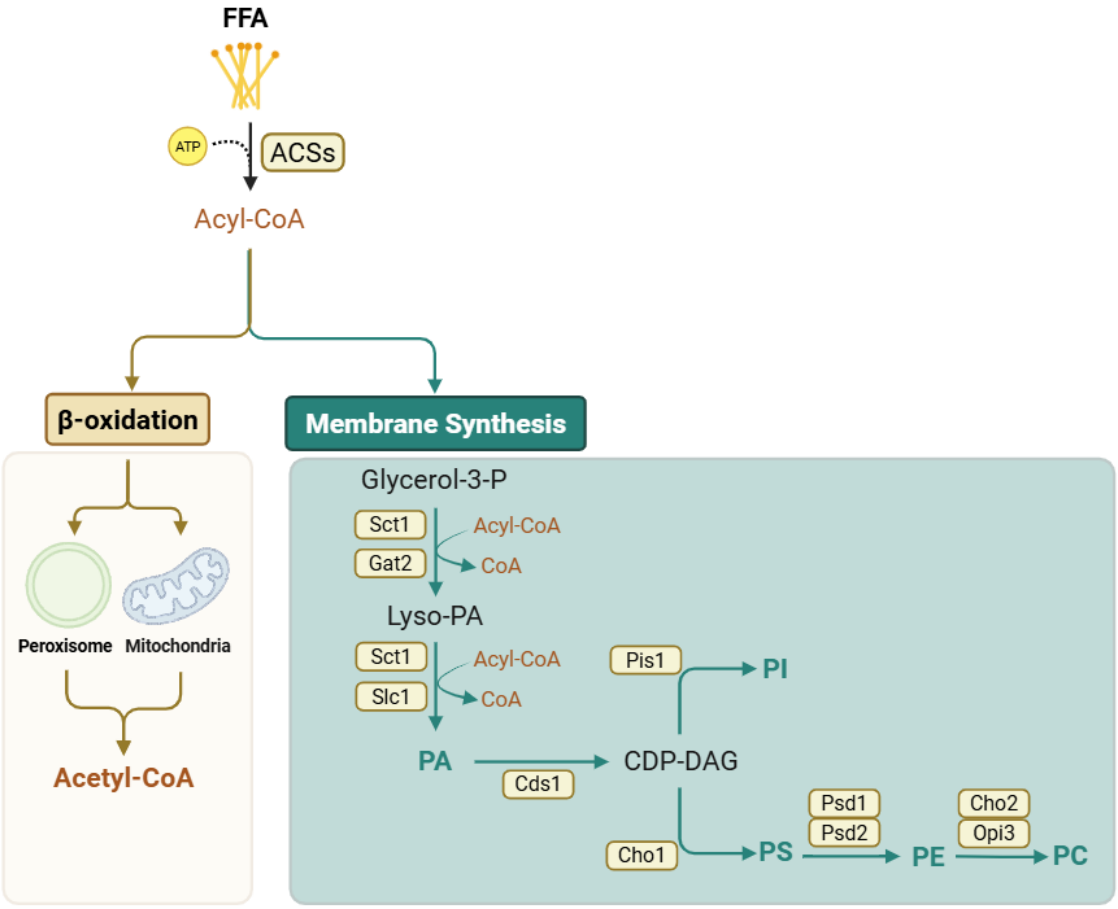

Figure 8. **The metabolism of the FFA into Acetyl-CoA or membrane synthesis.** Acyl-CoA synthetases convert FFA into acyl-CoA, which are eventually channeled for fatty acid synthesis, which in turn are targeted for β-oxidation either on peroxisome or mitochondria (*S. cerevisiae* exclusively peroxisomal) for energy generation. Acyl-coA can also be used as substrate for synthesis of PA and phospholipids (PS, PE and PC). And phosphatidylinositol (PI) and support membrane synthesis. **Abbreviations:** ATP: Adenosine triphosphate; PA: Phosphatidic acid; PI: Phosphatidylinositol; PS: Phosphatidylserine; PE: Phosphatidylethanolamine; PC: Phosphatidylcholine; CDP-DAG: CDP diacylglycerol. Made in Biorender.com.

1.2. Seipin

Seipin is an evolutionarily conserved membrane protein localized to the ER and is encoded by the human *BSCL2* gene and its yeast ortholog *SEI1* [66]. Mutations in *BSCL2*/seipin have been linked to a spectrum of human disorders, including Berardinelli-Seip congenital lipodystrophy (BSCL2), motor neuron diseases (MNDs), and congenital encephalopathy [67, 68]. While BSCL2 arises from loss of seipin function, MNDs are thought to result from the accumulation of toxic misfolded seipin oligomers. Mechanistically, seipin assembles into oligomeric complexes at ER-LD contact sites, where it is essential for LD biogenesis, making it a key regulator of adipogenesis and lipogenesis [69-71]. A central question in the field remains how dysfunction of seipin at these contact sites contributes to both metabolic and neuronal pathologies.

1.2.1. Molecular architecture and function of Seipin

Genomic analyses of the *BSCL2* gene have identified three transcript variants encoding distinct seipin isoforms. Isoform 1, considered the canonical form, consists of 398 amino acids (aa) and harbors more than 30 reported mutations. Isoforms 2 (287 aa) and 3 (462 aa) diverge from the canonical sequence through significant structural variations, specifically a truncated C-terminal region in isoform 2 and an extended N-terminal region in isoform 3 [72]. At a structural level, seipin oligomer forms a wheel-like undecamer in humans, featuring cytosolic *N*- and C-terminal domains that include two transmembrane domains, alongside a remarkably conserved loop that resides within the ER lumen (**Figure 9**) [6].

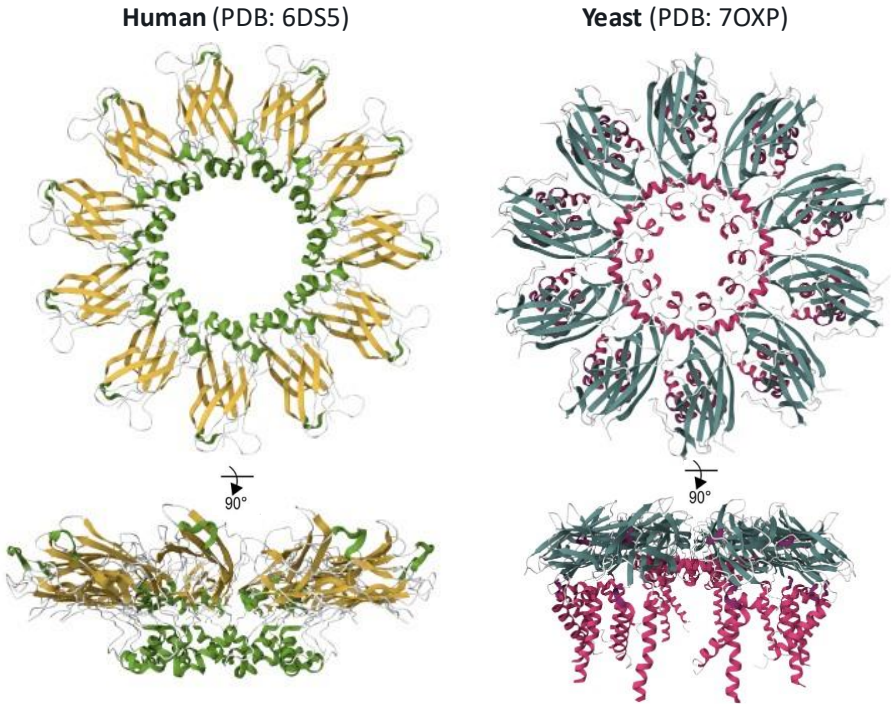

Figure 9. **Yeast Seipin structure**. Cryo-electron microscopy structures of seipin from human (PDB: 6DS5) and yeast (PDB: 7OXP) model organisms. The top panels show views from the cytosol toward the ER lumen, while the bottom panels display the structures rotated by 90°. Transmembrane domains at green and magenta; β-sandwich domain at yellow and cyan.

In *S. cerevisiae*, seipin exhibits a structurally similar architecture with a conserved central region of 250 aa, yet its composition differs genetically and stoichiometrically from its mammalian counterpart. Rather than being encoded by a single gene, the yeast complex requires two distinct genes (*SEI1* and *LDB16*) for proper assembly [6, 66]. The yeast proteins Sei1 and the ER-resident membrane protein Ldb16 form a stable complex that is critical for its stability and activity [6, 66]. Biochemical studies demonstrate that the seipin ring is assembled from 10 Sei1 protomers, contrasting with the undecameric or dodecameric ring of human and fly seipin complexes, respectively [6, 66, 73]. Sei1 is

essential for maintaining Ldb16 stability, as Ldb16 undergoes rapid endoplasmic reticulum-associated degradation (ERAD) in the absence of Sei1 [66, 74]. Conversely, while Sei1 remains stable in cells lacking *LDB16*, it loses its functional activity, indicating that Ldb16 is structurally required to carry out the biological function of the seipin complex [66, 74]. In agreement with this idea, the deletion of *SEI1* or *LDB16* renders cells harboring supersized LDs, which is a defining feature of seipin-deficient cells [66, 74]. This interdependence is further supported by a model in which Sei1 assembles into a homodecameric ring (**Figure 9**) that acts as a scaffold to position Ldb16. In this arrangement, Ldb16 functions as the principal TG binder and concentrator through specific hydroxy group-containing serine and threonine residues at the ER-LD contact sites, via a mechanism analogous to that observed in human and fly seipin proteins [66].

In yeast, the N-terminal domain of seipin is critical for the initiation and generation of LDs [75]. This specific role is mirrored in *Drosophila*, where the N-terminal domain exhibits similar functionality [73]. Despite variations in their structural traits, seipin universally contributes to the stabilization of the ER-LD contact sites, creating a diffusion barrier that helps to modulate the LD surface tension during their growth and budding, while promoting the unidirectional flux of TG from the ER to the nascent LD [66]. Additionally, seipin is involved in the regulation of acyl chain profiles in phospholipids [66]. As stated before the absence of functional seipin leads to significant abnormalities in LD morphology, namely the formation of supersized LDs and clusters of abnormally shaped droplets associated with significant changes in PC and PA composition [9, 71, 76]. Finally, seipin, beyond its role in LD biology and lipid metabolism, localizes to ER-mitochondria contact sites where it orchestrates mitochondrial calcium uptake through interactions with key calcium regulators, to support Krebs cycle metabolic flux and activity and ATP production in adipocytes. Disruption of seipin function underlies mitochondrial dysfunctions and metabolic defects observed in seipin deficiency-associated lipodystrophy [77].

1.2.2. N88S seipinopathy: a motor neuron degenerative disease

Seipin is highly expressed in neurons of the central nervous system, including motor neurons in the spinal cord and cortical neurons in the brain [68]. Whereas loss of function mutations in *BSCL2* gene lead to metabolic dysfunctions and lipodystrophy [69-71, 78], gain-of-function mutations in seipin are linked to MNDs such as hereditary spastic paraplegias and Celia's encephalopathy, which can lead to fatal outcomes in childhood [79]. Collectively known as seipinopathies, most mutations identified fall within the *N*-glycosylation motif (aa N88-S90, an N-X-V/S site) [9]. The two mutations that cause

neuronal seipinopathy, N88S and S90L, are located within the seipin´s loop, an 'aggregation-prone' segment in the protein. By disrupting *N*-glycosylation, these mutations promote protein aggregation and induce ER stress and cell death, a mechanism shared with other neurodegenerative disorders (**Figure 10**) [4].

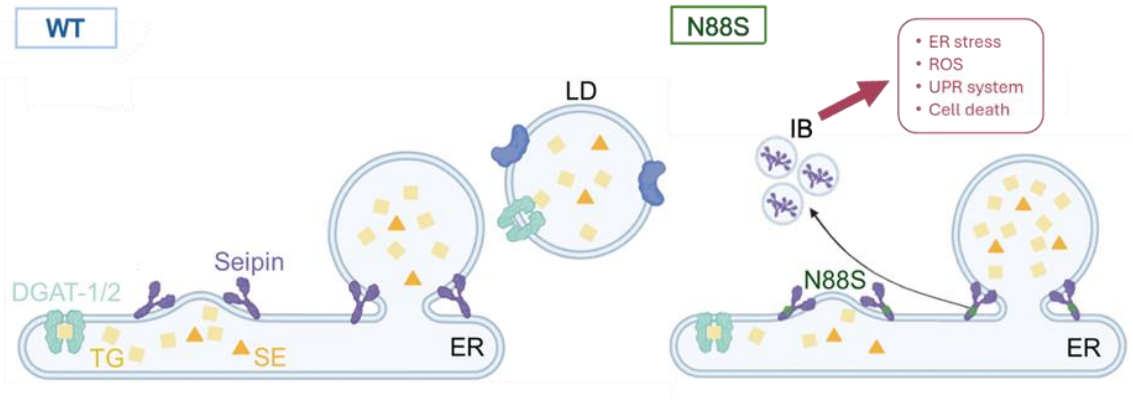

Figure 10. **N88S human seipinopathy model.** Misfolded N88S seipin accumulates in inclusion bodies (IBs) and triggers the Endoplasmic Reticulum (ER) stress response and oxidative damage, leading to neuronal cell death. **Abbreviations:** ROS: reactive oxygen species; UPR: unfolded protein response. Made in Biorender.com.

Also, seipin N88S is polyubiquitinated and degraded by the proteasome [4]. Importantly, protein aggregates segregate and accumulate into inclusion bodies (IBs), but their nature and composition remain to be established (**Figure 10**). Mouse models harboring the N88S seipin mutation have been developed to investigate the mechanisms of seipinopathy [80]. These models successfully mimic the neurological dysfunctions observed in human patients, including limb spasticity due to motor neuron degeneration and progressive muscle atrophy [80]. Here, neurons exhibit elevated ER stress, as evidenced by the increased expression of key stress markers such as immunoglobulin heavy chain binding protein (BiP), protein disulfide isomerase, and X-box binding protein 1 (XBP1), along with the formation of seipin aggregates [80]. Furthermore, the aggregation of mutant seipin is linked to the activation of autophagy, highlighting this process as a downstream response to ER stress [9, 80]. More recently, a humanized yeast model of N88S human seipinopathy revealed that N88S homo-oligomers expressing cells present reduced viability, decreased antioxidant activity, increased oxidative damage associated with higher reactive oxygen species (ROS) levels and elevated lipid peroxidation, and importantly this is correlated with the activation of the bZIP transcription factor Yap1, which is related to human Keap1-Nrf2 oxidative stress response pathway [4]. Notably, heterologous expression of human N88S seipin in a yeast seipin null background renders cells with normal LDs, albeit larger LDs with

different cell number distribution when compared to its human WT counterpart [9]. This indicates that the N88S mutation impacts both LD size and number. Later, proteomic and lipidomic studies with this model revealed changes in PA levels, which was linked to disrupted inositol metabolism and reduced flux towards phospholipid biosynthesis. Notably, inositol metabolism dysregulation exacerbated ER stress, independent of N88S seipin misfolding or IB formation [10]. The model also displayed disrupted iron (Fe) homeostasis throughout its lifespan, with N88S seipin-expressing cells showing diminished capacity to cope with iron deficiency [10]. This impairment was linked to changes in the expression of iron homeostasis genes regulated by the Fe-sensing transcription factor Aft1, including the mRNA-binding protein *CTH2* and the high-affinity iron transporter *FET3*, mediated through a p38/Hog1 kinase and stress responsive transcription factor Msn2/Msn4-dependent pathway [10].

1.3. Peroxisomes

Peroxisomes are dynamic organelles that play a critical role in cellular lipid metabolism. They are essential for bile acid synthesis, FA β-oxidation, generation of lipids required for myelin sheath formation, and maintenance of cellular redox homeostasis [81, 82]. Dysfunction of peroxisomes underlies severe human disorders such as Zellweger spectrum disorders, X-linked adrenoleukodystrophy, and deficiencies in peroxisomal β-oxidation enzymes, leading to neurological, hepatic, and metabolic defects [83]. Beyond their canonical functions in cellular lipid metabolism, peroxisomes have gained attention for their diverse non-metabolic roles. They are integral to cellular stress responses, redox balance, and the processes underlying healthy aging [83, 84]. Additionally, peroxisomes act as signaling platforms that contribute to pathogen defense and antiviral responses, reflecting a broader protective function [85]. Their number, size and protein composition are highly variable.

In yeast, the proliferation of peroxisomes is influenced by specific growth substrates. When glucose serves as the primary carbon source, it undergoes glycolysis to produce pyruvate and adenosine triphosphate (ATP) to support higher growth rates. In contrast, when C2 compounds serve as the primary carbon source, peroxisome biogenesis is markedly enhanced. In *S. cerevisiae*, peroxisomes are critical for the β-oxidation of C2 compounds, resulting in the production of acetyl-CoA, which is subsequently incorporated into the glyoxylate cycle to synthesize intermediates for the tricarboxylic acid cycle (TCA) [10, 82, 86]. This process is particularly vital during the diauxic shift, when yeast transitions from fermentative to oxidative metabolism, optimizing energy production under nutrient exhaustion [82, 86]. In higher eukaryotes, the abundance and

composition of peroxisomes are influenced by a variety of factors, including the specific organism, tissue type, and developmental stage [86]. Therefore, understanding the regulatory mechanisms governing peroxisome proliferation is essential for elucidating their diverse functions within different biological contexts.

1.3.1. Peroxisome biogenesis: membrane assembly and protein targeting mechanisms

Peroxins (PEX) are essential proteins that regulate peroxisome biogenesis and function, including the targeting of peroxisomal membrane proteins (PMPs) and matrix proteins (**Figure 11**) [87]. The assembly of the peroxisomal membrane is driven by specific peroxins such as Pex3, Pex16, and Pex19, which coordinate the incorporation of PMPs through direct or indirect pathways (**Figure 11**) [82, 88-90]. In the **direct pathway**, newly synthesized PMPs are recognized by Pex19, which acts as a receptor and chaperone, facilitating their insertion into the peroxisomal membrane with the assistance of Pex3 [82, 91]. In the **indirect pathway**, PMPs first accumulate at specialized ER subdomains via Pex16, giving rise to pre-peroxisomal vesicles that subsequently mature into functional peroxisomes [82, 91].

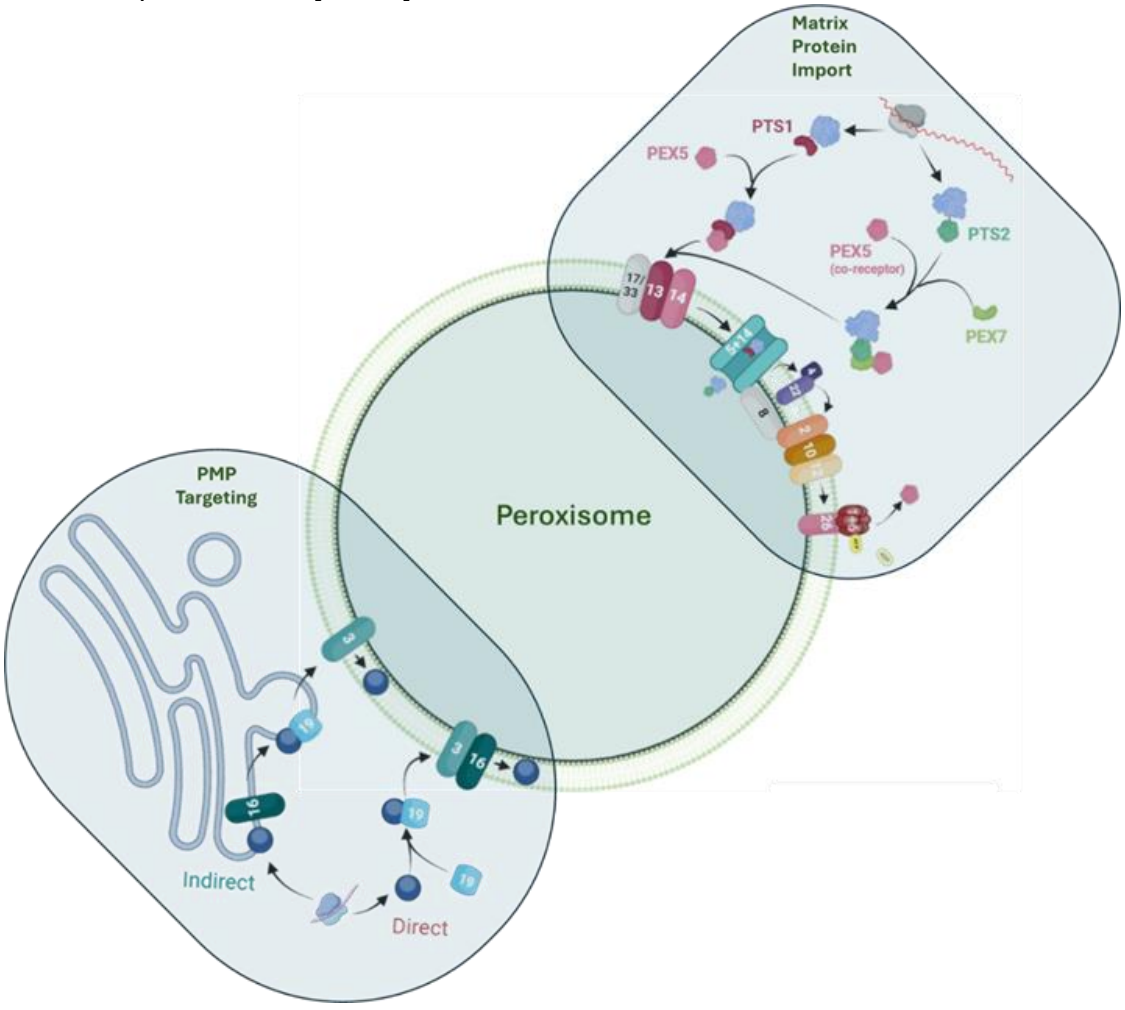

Figure 11. **Peroxisome biogenesis.** At bottom left: PMP targeting by direct and indirect pathways, using Pex3/16/19 protein complexes. At top right: Matrix Protein Import depending on it PTS1 and PTS2 sequence signals. Adapted from [82]. The image was created with Biorender.com.

1.3.2. Matrix protein import: signals, receptors, and translocation machinery

Peroxisomal matrix proteins typically possess one of two peroxisomal targeting signals (PTS), PTS1 or PTS2, which facilitate their import into peroxisomes (**Figure 11**) [92, 93]. Proteins bearing the PTS1 signal, which consists of the tripeptide S-K-L (or a conserved variant thereof) at the extreme carboxy termini of these proteins, are recognized by the cytosolic receptor Pex5. The PTS1 specifically interacts with the six tetratricopeptide repeat (TPR) motifs in the C-terminal half of Pex5. Here, Pex5 assists in the transport of these proteins to the peroxisomal membrane where they interact with docking proteins such as Pex13/14 for translocation [81]. The recycling of Pex5 from the peroxisomal membrane involves ubiquitination, mediated by a RING finger complex composed of Pex2/10/12 [81, 94]. Pex8 plays a supportive role within this complex by linking the docking and RING finger proteins, thereby assisting in the dissociation of the receptor-cargo complex [93]. A minor class of peroxisomal proteins contains the PTS2 signal, which consists of the sequence (R,K)-(L,V,I)-X_5-(H,Q)-(L,A,F) near the N terminus. PTS2-containing proteins utilize Pex7 as a receptor, which still requires Pex5 as a co-receptor during their transport process [95, 96]. The docking proteins for PTS2 are organized within a complex that includes Pex14, Pex17, and Pex18 [92]. Partial import defects observed in *PEX5* or *PEX7* null mutants reveal that, in yeast, the PTS1 and PTS2 import pathways operate independently [97]. In contrast, higher eukaryotes exhibit a greater interdependence as the absence of identified auxiliary factors is consistent with the observation that deletion of *PEX5* effectively abolishes both PTS1- and PTS2-mediated matrix protein import [98, 99].

In addition to the PTS1 and PTS2 pathways, at least one alternative import route exists for peroxisomal matrix proteins that lack recognizable PTS1 or PTS2 signals. These proteins may utilize a "piggyback" mechanism, hitching a ride with other proteins that possess recognized PTS motifs [100]. Alternatively, they may harbor an unidentified internal targeting signal. Evidence suggests that some proteins contain an internal, as-yet-uncharacterized PTS that interacts with the N-terminal domain of Pex5, facilitating their import [100].

1.4. Glyoxylate Cycle

The glyoxylate cycle is an anabolic variant of the tricarboxylic acid (TCA) cycle that functions as an anaplerotic pathway in most protists, plants, fungi, and many bacteria. Unlike these organisms, animals and human tissues generally lack this cycle, with the sole known exception being nematodes during early embryogenesis [101]. Its primary role is to enable growth when glucose is scarce and only C2 substrates such as acetate or ethanol are available as carbon sources [102]. Functionally, the glyoxylate cycle operates as a modified branch of the TCA cycle, sharing several enzymes, including malate dehydrogenase, citrate synthase, and aconitase, but bypassing the two oxidative decarboxylation steps catalyzed by isocitrate dehydrogenase and α-ketoglutarate dehydrogenase [103]. This bypass is achieved through the inclusion of two unique enzymes: isocitrate lyase and malate synthase (**Figure 12**). Isocitrate lyase cleaves isocitrate (C6) into glyoxylate (C2) and succinate (C4), after which malate synthase condenses glyoxylate with acetyl-CoA (C2) to form malate (C4) and free CoA [103]. The resulting malate replenishes the TCA cycle and serves as a precursor for oxaloacetate, which is essential for gluconeogenesis. Oxaloacetate is converted into phosphoenolpyruvate by phosphoenolpyruvate carboxykinase and subsequently into glucose through the gluconeogenic pathway, involving key enzymes such as fructose-1,6-bisphosphatase [104]. In essence, the glyoxylate cycle circumvents the carbon-loss steps of the TCA cycle, allowing organisms to synthesize carbohydrates from simple two-carbon compounds during glucose deprivation [105].

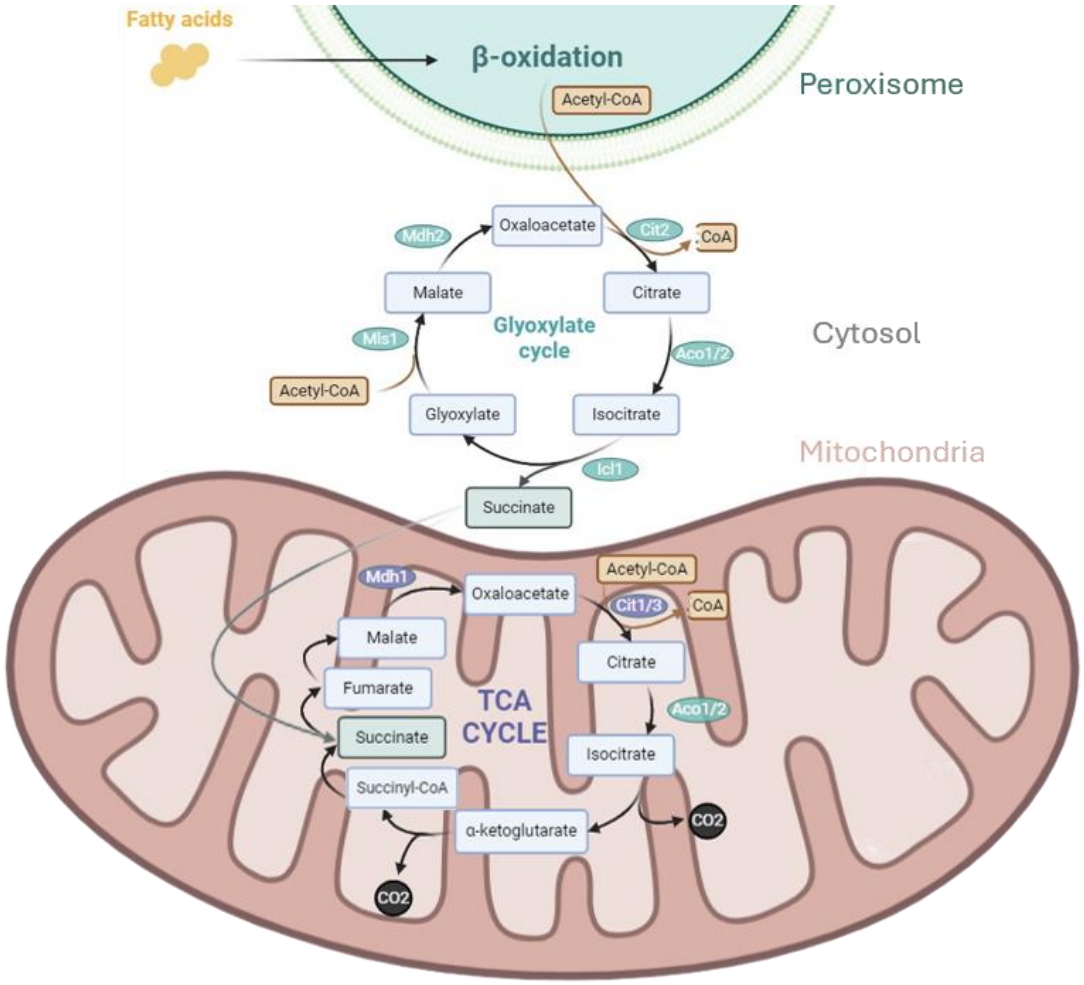

Figure 12. **Glyoxylate cycle.** Interplay between peroxisomes and mitochondria. In peroxisomes, β-oxidation of fatty acids generates acetyl-CoA, which fuels the glyoxylate cycle. This pathway produces intermediates such as succinate, which enter the mitochondrial tricarboxylic acid (TCA) cycle. **Abbreviations:** TCA, tricarboxylic acid cycle; CO_2, carbon dioxide. Figure created with BioRender.com.

1.4.1. The glyoxylate cycle: key reactions

Within the cycle, citrate synthase (Cit) isoenzyme Cit2, whose activity is controlled by ubiquitination, catalyzes the conversion of acetyl-CoA and oxaloacetate into citrate [105, 106]. The citrate then undergoes a series of enzymatic transformations, initially converting to isocitrate via aconitase (Aco1, Aco2), followed by cleavage by isocitrate lyase (Icl1) to yield glyoxylate and succinate. Despite sharing several intermediates with the TCA cycle, succinate is the primary product transported by its transporter Scf1 to the mitochondria, as it is preferentially carried by the dicarboxylate carrier located in the mitochondrial membrane (**Figure 12**) [102]. Concurrently, glyoxylate can react with another acetyl-CoA molecule, leading to its conversion into malate through the action of malate synthase (Mls1). Subsequently, malate dehydrogenase (Mdh2) regenerates oxaloacetate, thus closing the cycle [105].

1.4.2. Enzyme localization and metabolic flexibility

S. cerevisiae has three CIT genes encoding Cit1 and Cit3, which are located in the mitochondria and participate in the TCA cycle, and the peroxisomal PTS1-containing Cit2, which incorporates peroxisomal derived acetyl-CoA into the glyoxylate cycle (**Figure 12**) [107]. Aconitase isoenzymes Aco1 and Aco2 are distributed between cytosol and the mitochondria, supporting both cycles (**Figure 12**) [108]. The localization of glyoxylate cycle enzymes in yeast is dynamic and depends on the carbon source [107, 109, 110]. For example, Cit2 is primarily peroxisomal, while aconitase and other enzymes like isocitrate lyase Icl1 and malate synthase Mls1 localize differently depending on the presence of FAs or ethanol [111]. This flexibility ensures efficient metabolic adaptation to varying substrates. When growing on FAs, enzymes such as Mls1 are found in peroxisomes, optimizing local reactions and minimizing metabolite shuttling. In contrast, on ethanol, these enzymes localize to the cytosol to better interact with cytosolic acetyl-CoA pools. Additionally, *S. cerevisiae* possesses three isoforms of malate dehydrogenase: Mdh1 (mitochondrial), Mdh2 (cytosolic), and Mdh3 (peroxisomal), each tailored to specific metabolic compartments to enhance metabolic flexibility (**Figure 12**) [105, 112].

1.4.3. Regulation of the glyoxylate cycle

The choice between the TCA cycle and the glyoxylate cycle is regulated by the type and availability of carbon sources. In yeast, the key enzymes of the glyoxylate cycle, Icl1 and Mls1 and Mdh2, are regulated in response to the carbon source of the growth medium. Synthesis of these enzymes is repressed in cells grown on glucose and derepressed in media lacking glucose [111]. In *S. cerevisiae*, Snf1 kinase is the main activator of downstream glucose-repressed genes and is important for the activation of alternative carbon metabolism [113]. In general, Snf1 is induced in response to glucose-deficient conditions and deactivates the transcriptional repressor Mig1 by phosphorylation [114]. Dissociation of Mig1 from the co-repressor protein complex Ssn6-Tup1 leads to increased expression of Cat8, a transcriptional regulator that binds the carbon source-responsive element (CSRE) located at the promoter region of many glyoxylate cycle and gluconeogenic genes such as *ICL1*, *MLS1*, *FBP1* and *PCK1* [114-116].

The activation of the retrograde (RTG) pathway, which can be triggered by mitochondrial dysfunction, drives a transcriptional program via the Rtg1/3 bHLH–Zip factors that upregulates anaplerotic and glyoxylate-cycle-linked genes, including *CIT2*, which feeds acetyl-CoA-derived carbon into the glyoxylate shunt and TCA replenishment [117]. Mechanistically, RTG signaling increases precursors for biosynthesis (e.g., glutamate)

and supports TCA cycle during respiratory stress, thereby creating a metabolic context that requires and supports glyoxylate-cycle activation. The coordination with carbon-source regulation helps to couple the RTG response pathway to the glyoxylate cycle enzymes. Transcription factors Adr1 and Cat8, which drive derepression of non-fermentative metabolism, act as positive regulators of RTG-dependent transcription and intersect with induction of *ICL1* (isocitrate lyase) and *MLS1* (malate synthase) under conditions such as glucose limitation and caloric restriction [118, 119]. The expression of these genes is induced when cells rely on C2 substrates or undergo lifespan-extending caloric restriction (CR), placing glyoxylate-cycle control downstream of the RTG-carbon signaling axis. Genome-wide and physiological studies further support this linkage: during mitochondrial dysfunction or altered membrane biogenesis (e.g., cardiolipin deficiency), cells depend on RTG-driven anaplerosis and engage glyoxylate-cycle and related pathways to promote stress resistance [120, 121].

More recently, new mechanistic insights into the regulation of the glyoxylate cycle revealed that it occurs through an oxaloacetate-dependent positive feedback loop (**Figure 13**) [105]. In conditions where the TCA cycle is active, oxaloacetate is continuously consumed. However, in the presence of ethanol or acetate as the sole carbon source, oxaloacetate levels increase [105]. This accumulation enhances the interaction between Cit2 and oxaloacetate, stabilizing its closed conformation, which inhibits recognition of Cit2 by SCFUCC1, an E3 ligase responsible for its ubiquitination and degradation in the proteasome, thereby facilitating the activation of the glyoxylate cycle (**Figure 13**) [105]. Conversely, reduced oxaloacetate levels, driven by glucose presence, favor the inactivation of the glyoxylate cycle [105].

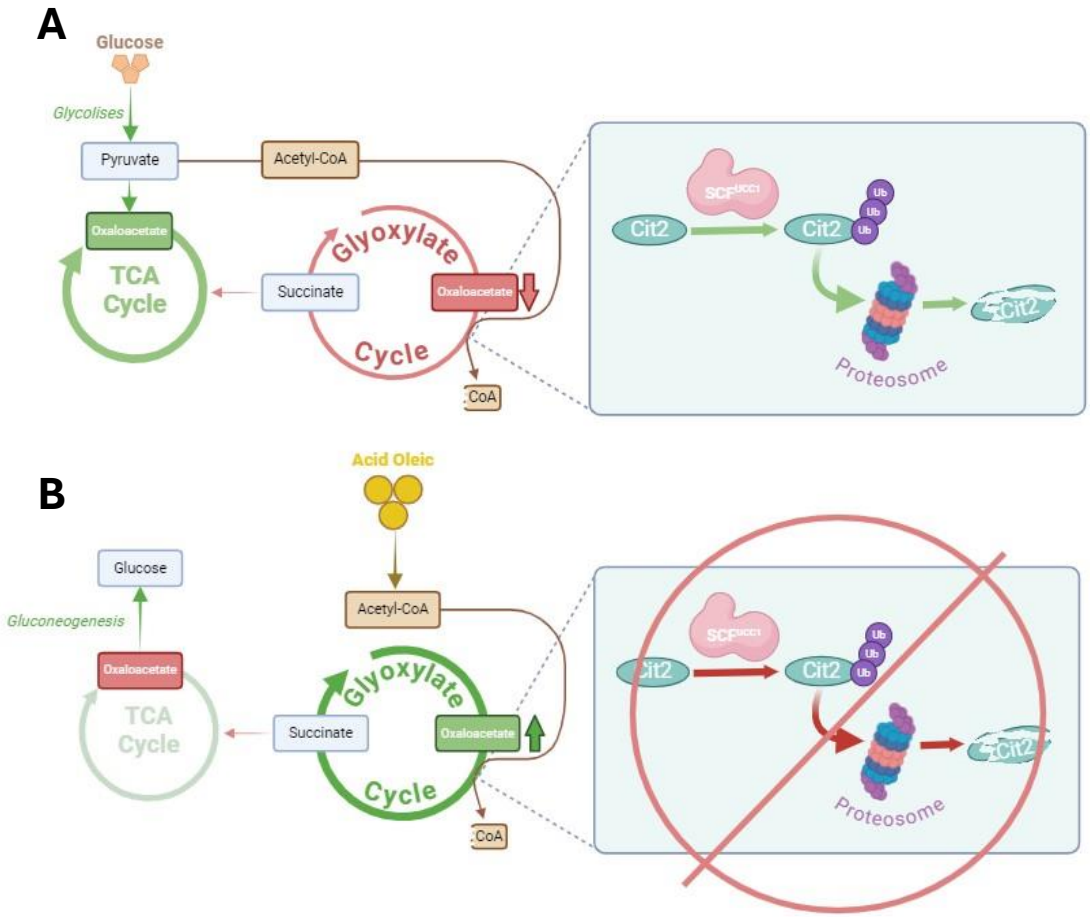

Figure 13. **Regulation of the glyoxylate cycle. (A)** When glucose is the carbon source used by yeast cells, oxaloacetate is consumed in the tricarboxylic acid (TCA) cycle, preventing inhibition of SCFUCC1-mediated Cit2 degradation. **(B)** With oleic acid as the carbon source, the glyoxylate cycle remains active; oxaloacetate is not consumed and thus inhibits Cit2 degradation. Adapted from [102]. Created with BioRender.com.

1.5. Acetyl-CoA synthesis and metabolism

Acetyl-CoA represents a central metabolite in *S. cerevisiae*, functioning as a key intermediate in energy production, biosynthetic pathways, and epigenetic regulation. It serves as the primary substrate for the TCA cycle, a precursor for lipid and sterol biosynthesis, and the donor of acetyl groups for protein acetylation, including histone modification, thereby linking cellular metabolic status to transcriptional regulation [122-124]. Despite its ubiquitous role, acetyl-CoA is compartmentalized within the mitochondria, cytosol, nucleus, and peroxisomes, with no direct membrane transport mechanism. Consequently, yeast cells have evolved multiple compartment-specific biosynthetic pathways and metabolite shuttles to sustain acetyl-CoA homeostasis under diverse nutrient conditions.

In *S. cerevisiae*, mitochondrial acetyl-CoA is predominantly synthesized by the pyruvate dehydrogenase (PDH) complex, which catalyzes the oxidative decarboxylation of pyruvate imported via the mitochondrial pyruvate carrier (*MPC1*) [125]. This acetyl-CoA pool primarily supports energy metabolism via the TCA cycle. In contrast, the cytosolic and nuclear pools of acetyl-CoA are generated through the action of acetyl-CoA synthetases (ACS), which activate acetate to acetyl-CoA in an ATP-dependent manner. Of the two ACS isoenzymes, Acs2 is essential for growth on glucose and plays a critical role in nuclear acetyl-CoA supply for histone acetylation, whereas Acs1 is induced under non-fermentative conditions, such as growth on ethanol or acetate [126]. In addition, peroxisomes represent a third site of acetyl-CoA synthesis, primarily via β-oxidation of FAs, which becomes essential when yeast utilizes lipids as a carbon source [127, 128].

The spatial separation of acetyl-CoA pools requires inter-compartmental transport systems, as acetyl-CoA itself cannot freely cross organellar membranes. This is achieved through several metabolite shuttles. First, the carnitine shuttle facilitates reversible acetyl group transfer between peroxisomes, mitochondria, and the cytosol. This system relies on carnitine acetyltransferase Cat2, which converts acetyl-CoA to acetyl-carnitine for transport across membranes, followed by reconversion to acetyl-CoA [129]. The carnitine shuttle is functionally active only in the presence of exogenous carnitine, as *S. cerevisiae* lacks carnitine biosynthesis capability [129]. In its absence, the glyoxylate cycle compensates for inter-organellar carbon transfer. This peroxisomal pathway, mediated by Icl1 and Mls1, incorporates acetyl-CoA into four-carbon intermediates (e.g., succinate), which can be exported to mitochondria or the cytosol, thereby replenishing the TCA cycle and supporting gluconeogenesis under non-fermentative conditions [130]. Functional redundancy between these two pathways is evident, as deletion of either *CIT2* or *CAT2* individually does not abolish growth on oleate, whereas simultaneous deletion is lethal under these conditions [131]. A third mechanism involves acetate-mediated exchange. The mitochondrial enzyme Ach1 catalyzes the conversion of acetyl-CoA to acetate, which freely diffuses to the cytosol, where ACS enzymes regenerate acetyl-CoA, thus maintaining communication between mitochondrial and cytosolic acetyl-CoA pools [132]. Collectively, these interconnected biosynthetic routes and transport mechanisms ensure robust acetyl-CoA distribution across cellular compartments, enabling *S. cerevisiae* to adapt to fluctuations in carbon availability and to coordinate energy metabolism with biosynthetic and regulatory processes.

1.6. *S. cerevisiae* as a disease model system

S. cerevisiae has emerged as a versatile model organism for studying neurodegenerative diseases, offering unique strengths while presenting certain limitations. One of the key advantages of *S. cerevisiae* is its genetic simplicity and conservation of cellular pathways. As a eukaryote, yeast shares many fundamental biological processes with human cells, including protein folding, secretion, trafficking, and degradation [133-136]. These processes are central to neurodegenerative diseases such as Alzheimer's, Parkinson's, seipinopathies, where misfolded proteins and impaired cellular homeostasis play critical roles. The yeast well-characterized genome [137] and ease of genetic manipulation make it an ideal platform for exploring these molecular mechanisms at a cellular level [138, 139]. Moreover, yeast's rapid growth and low-cost maintenance provide a practical edge for large-scale genetic and chemical screenings. For instance, high-throughput assays in yeast have been instrumental in understanding the processes contributing to cytotoxicity of misfolded proteins like α-synuclein, which is associated with Parkinson's disease, and in evaluating potential therapeutic strategies in human disease [140]. Despite its strengths, *S. cerevisiae* has notable limitations when considering key features of neurobiology. Its simplicity, while advantageous for studying fundamental processes, becomes a drawback when addressing aspects of multicellularity and organismal interactions [141]. Yeast unicellular nature limits its ability to capture and model complex intercellular interactions and tissue-specific features critical for understanding motor neuropathies, such as neuron-glia lipid and metabolic coupling, brain redox balance, and neurodegeneration [141]. Obviously, yeast lacks specialized neuronal structures, such as synapses, and does not replicate the multicellular environment of human tissues, which are critical to the pathology of neurodegenerative diseases. Nevertheless, humanized yeast models have been instrumental in identifying therapeutic targets, biomarkers, drug candidates, and functional disease networks, underscoring their utility in studying human disorders, as demonstrated in this work. However, validation in mammalian models remains essential to confirm their biological relevance to neurodegeneration.

1.7. Aims of the project

The N88S seipin mutation impairs seipin N-glycosylation, leading to protein misfolding and ER stress. Previously, we developed a humanized yeast model of N88S seipinopathy that recapitulates key features of the neuropathy, including pronounced ER stress and the formation of IBs composed of WT-N88S heteromers or N88S homomers

[4]. Our findings showed that cells expressing N88S homo-oligomers exhibit reduced viability and increased oxidative damage [4]. Using this model, we previously conducted a genome-wide screen to identify genetic modifiers of IB formation and unbiased proteomic profiling to define differentially expressed genes (DEGs) and map them onto functional interaction networks [10]. Through these analyses, we established gene interaction clusters using STRING and identified six major clusters [10]. Notably, one cluster was significantly enriched in proteins involved in peroxisomal targeting and peroxisomal membrane transport [10]. Furthermore, Gene Ontology (GO) analysis of proteomics data revealed enrichment in biological processes related to peroxisome biogenesis, as well as glyoxylate and dicarboxylate metabolism. Pathway enrichment analysis further confirmed that differentially expressed proteins (DEPs) associated with peroxisome dynamics strongly overlap with genes identified in our genomic screen [10]. Based on these observations, we hypothesize that peroxisomal dyshomeostasis contributes to the pathogenesis of seipinopathy. To test this, we investigated whether peroxisomal dysfunction influences IB formation, lipid metabolism, and redox signaling in our model. Specifically, this project focused on three interconnected metabolic pathways:

1. Peroxisomal β-oxidation, which generates acetyl-CoA from FAs
2. The glyoxylate cycle, which converts acetyl-CoA into TCA cycle intermediates
3. Mitochondrial TCA cycle activity

Our experimental approach involved metabolic flux analysis to trace acetyl-CoA compartmentalization and utilization, combined with integrated proteomics analyses to link metabolic alterations with protein network perturbations (**Figure 14**).

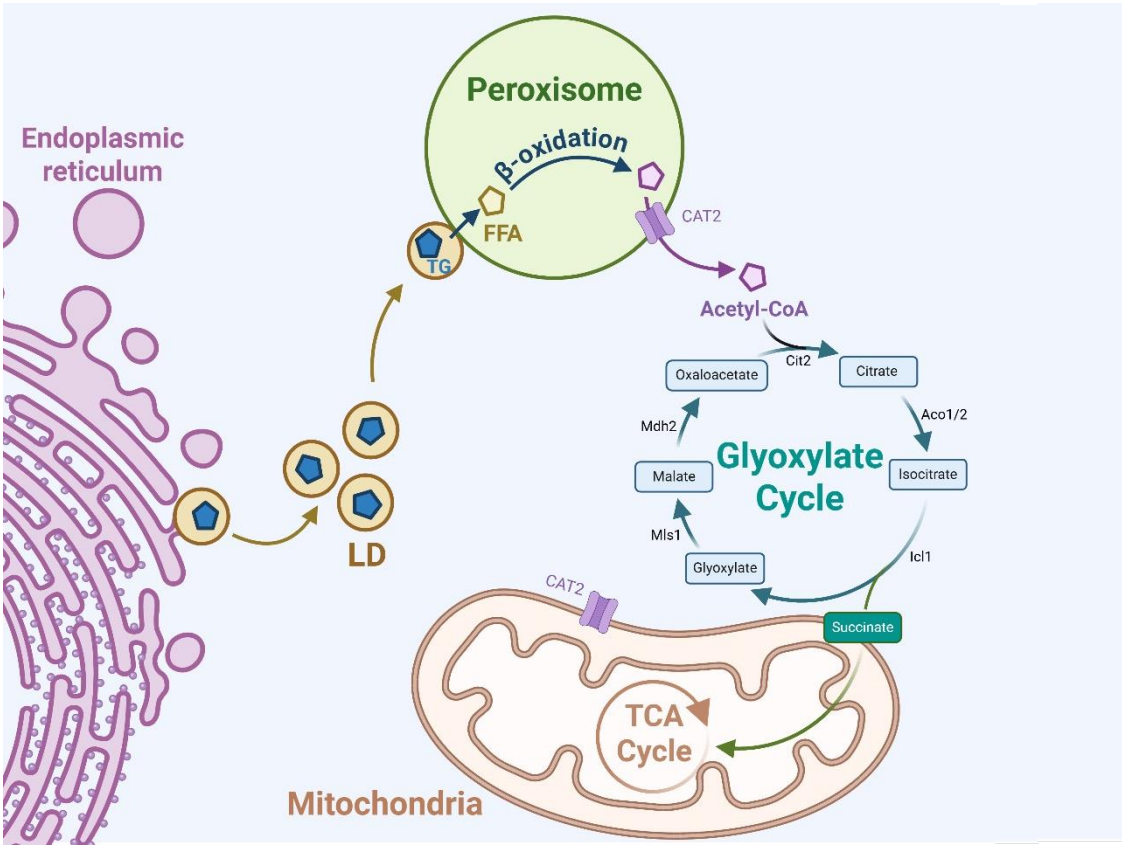

Figure 14. **Overview of the metabolic and organelle interactions linking ER, lipid droplets, peroxisomes, and the glyoxylate-TCA Network.** The figure illustrates a simplified schematic of the metabolic interplay between the ER, LDs, peroxisomes and the glyoxylate and TCA cycles. It highlights how TG synthesis and LD biogenesis are functionally linked to peroxisomal β-oxidation, wherein free fatty acids (FFAs) released by TG lipolysis are catabolized to produce acetyl-CoA. The resulting acetyl-CoA subsequently enters the glyoxylate and tricarboxylic acid (TCA) cycles, integrating lipid turnover with central carbon metabolism. Made in Biorender.com.

2. Materials and Methods

2.1. Yeast strains and plasmids

The *S. cerevisiae* strains utilized in this study were derived from the W303α parental strain and are detailed in **Table 1**. Using standard PCR-based homologous recombination techniques, processes like protein tagging and gene deletions were carried out [142, 143]. Primers for these procedures were designed using the Primers-4-Yeast tool [144] in conjunction with pFA6 plasmid set [142, 143].

Table 1. Yeast strains used in this study

Strain	Genotype	Source/Reference
WT-VN WT-VC	W303α *ldb16*Δ::natNT2 *fld1*Δ::hphmx4 pRS306-GPDpr-WTh*BSCL2*-VN-CYC1t pRS413-GPDpr-WTh*BSCL2*-VC-CYC1t	[9]
N88S-VN N88S-VC	W303α *ldb16*Δ::natNT2 *fld1*Δ::hphmx4 pRS306-GPDpr-N88Sh*BSCL2*-VN-CYC1t pRS413-GPDpr-N88Sh*BSCL2*-VC-CYC1t	[9]
WT-VN WT-VC *pex3*Δ	W303α *ldb16*Δ::natNT2 *fld1*Δ::hphmx4 pRS306-GPDpr-WTh*BSCL2*-VN-CYC1t pRS413-GPDpr-WTh*BSCL2*-VC-CYC1t *pex3*Δ::KANMX6	This study
N88S-VN N88S-VC *pex3*Δ	W303α *ldb16*Δ::natNT2 *fld1*Δ::hphmx4 pRS306-GPDpr-N88Sh*BSCL2*-VN-CYC1t pRS413-GPDpr-N88Sh*BSCL2*-VC-CYC1t *pex3*Δ::KANMX6	This study
WT-VN WT-VC PTS1	W303α *ldb16*Δ::natNT2 *fld1*Δ::hphmx4 pRS306-GPDpr-WTh*BSCL2*-VN-CYC1t pRS413-GPDpr-WTh*BSCL2*-VC-CYC1t pRS315-ADH1p-mCherry-PTS1	This study
N88S-VN N88S-VC PTS1	W303α *ldb16*Δ::natNT2 *fld1*Δ::hphmx4 pRS306-GPDpr-N88Sh*BSCL2*-VN-CYC1t pRS413-GPDpr-N88Sh*BSCL2*-VC-CYC1t pRS315-ADH1p-mCherry-PTS1	This study
N88S-VN N88S-VC *pex3*Δ PTS1	W303α *ldb16*Δ::natNT2 *fld1*Δ::hphmx4 pRS306-GPDpr-N88Sh*BSCL2*-VN-CYC1t pRS413-GPDpr-N88Sh*BSCL2*-VC-CYC1t *pex3*Δ::KANMX6 pRS315-ADH1p-mCherry-PTS1	This study
N88S-VN N88S-VC *pex19*Δ PTS1	W303α *ldb16*Δ::natNT2 *fld1*Δ::hphmx4 pRS306-GPDpr-N88Sh*BSCL2*-VN-CYC1t	This study

	pRS413-GPDpr-N88Sh*BSCL2*-VC-CYC1t *pex19*Δ::KANMX6 pRS315-ADH1p-mCherry-PTS1	
WT-VN WT-VC UPRE-LacZ	W303α *ldb16*Δ::natNT2 *fld1*Δ::hphmx4 pRS306-GPD-WTh*BSLC2*-VN-CYC1t pRS413-GPDpr-WTseipin-VC-CYC1t pRS315-UPRE-LacZ	[10]
N88S-VN N88S-VC UPRE-LacZ	W303α *ldb16*Δ::natNT2 *fld1*Δ::hphmx4 pRS306-GPD-N88Sh*BSLC2*-VN-CYC1t pRS413-GPDpr-N88Sseipin-VC-CYC1t pRS315-UPRE-LacZ	[10]
WT-VN WT-VC *pex3*Δ UPRE-LacZ	W303α *ldb16*Δ::natNT2 *fld1*Δ::hphmx4 pRS306-GPD-WTh*BSLC2*-VN-CYC1t pRS413-GPDpr-WTseipin-VC-CYC1t *pex3*Δ::KANMX6 pRS315-UPRE-LacZ	This study
N88S-VN N88S-VC *pex3*Δ UPRE-LacZ	W303α *ldb16*Δ::natNT2 *fld1*Δ::hphmx4 pRS306-GPD-N88Sh*BSLC2*-VN-CYC1t pRS413-GPDpr-N88Sseipin-VC-CYC1t *pex3*Δ::KANMX6 pRS315-UPRE-LacZ	This study
WT-VN WT-VC *CIT2*-LacZ	W303α *ldb16*Δ::natNT2 *fld1*Δ::hphmx4 pRS306-GPD-WTh*BSLC2*-VN-CYC1t pRS413-GPDpr-WTseipin-VC-CYC1t *CIT2*-LacZ-KANMX4	This study
N88S-VN N88S-VC *CIT2*-LacZ	W303α *ldb16*Δ::natNT2 *fld1*Δ::hphmx4 pRS306-GPD-N88Sh*BSLC2*-VN-CYC1t pRS413-GPDpr-N88Sseipin-VC-CYC1t *CIT2*-LacZ-KANMX4	This study
WT-VN WT-VC UPRE-LacZ *MPC1*	W303α *ldb16*Δ::natNT2 *fld1*Δ::hphmx4 pRS306-GPD-WTh*BSLC2*-VN-CYC1t pRS413-GPDpr-WTseipin-VC-CYC1t pRS315-UPRE-LacZ-ADH1pr-*MPC1*-ADH1t	This study
N88S-VN N88S-VC UPRE-LacZ *MPC1*	W303α *ldb16*Δ::natNT2 *fld1*Δ::hphmx4 pRS306-GPD-N88Sh*BSLC2*-VN-CYC1t pRS413-GPDpr-N88Sseipin-VC-CYC1t pRS315-UPRE-LacZ-ADH1pr-*MPC1*- ADH1t	This study
WT-VN WT-VC UPRE-LacZ *CAT2*$_{cyt}$	W303α *ldb16*Δ::natNT2 *fld1*Δ::hphmx4 pRS306-GPD-WTh*BSLC2*-VN-CYC1t pRS413-GPDpr-WTseipin-VC-CYC1t pRS315-UPRE-LacZ-ADH1pr-*CAT2*$_{cyt}$- ADH1t	This study

N88S-VN N88S-VC UPRE-LacZ *CAT2*$_{cyt}$	W303α *ldb16*Δ::natNT2 *fld1*Δ::hphmx4 pRS306-GPD-N88Sh*BSLC2*-VN-CYC1t pRS413-GPDpr-N88Sseipin-VC-CYC1t pRS315-UPRE-LacZ-ADH1pr-*CAT2*$_{cyt}$- ADH1t	This study
WT-VN WT-VC UPRE-LacZ *CAT2*$_{mit}$	W303α *ldb16*Δ::natNT2 *fld1*Δ::hphmx4 pRS306-GPD-WTh*BSLC2*-VN-CYC1t pRS413-GPDpr-WTseipin-VC-CYC1t pRS315-UPRE-LacZ-ADH1pr-*CAT2*$_{mit}$- ADH1t	This study
N88S-VN N88S-VC UPRE-LacZ *CAT2*$_{mit}$	W303α *ldb16*Δ::natNT2 *fld1*Δ::hphmx4 pRS306-GPD-N88Sh*BSLC2*-VN-CYC1t pRS413-GPDpr-N88Sseipin-VC-CYC1t pRS315-UPRE-LacZ-ADH1pr-*CAT2*$_{mit}$- ADH1t	This study

VN, Venus N-terminal fragment; **VC**, Venus C-terminal fragment

Plasmids used in this study are listed in **Table 2**. For cloning of ADH1pr-*MPC1*-ADH1t into the pRS315-UPRE-LacZ vector [10], the plasmid UG75-ADH-*CDS1*-3HA [145] was digested with ClaI and NheI and *MPC1* ORF was amplified by PCR, using BY4741 genomic DNA as template, and integrated into the same sites of the plasmid using specific primers as described in **Table 3**. Next, this newly generated plasmid was digested with SacII, and the resulting insert was cloned into the SacII restriction site of the pRS315-UPRE-LacZ vector. For cloning of ADH1pr-*CAT2*$_{cyt}$-ADH1t into the pRS315-UPRE-LacZ vector [10], the plasmid UG75-ADH-*CDS1*-3HA [145] was digested with BlpI and NheI and *CAT2* gene variants were amplified by PCR, using BY4741 genomic DNA as template, and integrated into the same sites of the plasmid using specific primers as described in **Table 3**. Next, this newly generated plasmid was digested with SacII, and the resulting insert was cloned into the SacII restriction site of the pRS315-UPRE-LacZ vector. *CAT2* encodes a protein with a mitochondrial targeting signal (MTS) at the N-terminus and a peroxisomal targeting signal (PTS) at the C-terminus (the tripeptide AKL). Here, the full-length *CAT2* ORF encodes a mitochondrial precursor protein of 670 amino acids, which is designated as *CAT2*$_{mit}$. We also constructed pRS315-UPRE-LacZ-ADH1pr-*CAT2*$_{cyt}$-ADHt, in which the PTS and the nucleotides encoding the first 22 amino acids of *CAT2* were deleted. The protein encoded by this construct is located both in the peroxisomes as well as the cytosol, and it was named cytosolic *CAT2* (*CAT2*$_{cyt}$) [146]. To monitor *CIT2*-LacZ expression, the indicated strains contained a EagI-cut *CIT2*-lacZ reporter gene integrated at the *CIT2* locus.

All constructs were verified either by sequencing (plasmids) or PCR (mutant strains). Strains were transformed using the standard lithium acetate procedure [148].

Table 2. Plasmids used in this study

Plasmids	Backbone	Description	Source/Reference
pFA6a-KANMX6	pFA6a	ORF deletion	[143]
PTS1-mCherry	pFL24	pFL24-ADH1p-mCherry-PTS1	[147]
UPRE-LacZ	pRS315	pRS315-UPRE-LacZ ADH1-CDS1-3HA	[10]
***MPC1O*Ex**	pRS315	pRS315- UPRE-LacZ-ADH1pr-*MPC1*-ADH1t	This study
***CIT2*-LacZ**	-	*CIT2*-LacZ-KANMX4	Dr Zhengchang Liu, University of New Orleans
***CAT2*$_{mit}$**	pRS315	pRS315-UPRE-LacZ-ADH1pr-*CAT2*$_{mit}$-ADH1t	This study
***CAT2*$_{cyt}$**	pRS315	pRS315-UPRE-LacZ-ADH1pr-*CAT2*$_{cyt}$-ADHt	This study

2.2. Culture media and growth conditions

Yeast cells were grown under aerobic conditions at 26 °C in Erlenmeyer flasks placed on a gyratory shaker set to 140 rpm. The growth medium volume was maintained at a 1:5 ratio relative to the flask volume. The liquid growth media used for yeast cultivation consisted of:

1. Yeast Peptone Dextrose (YPD): Containing 1% (wt/vol) yeast extract (Conda Pronadisa), 2% (wt/vol) bacto peptone (LabM), and 2% (wt/vol) glucose (Fisher Scientific).

2. Synthetic Complete (SC) Medium: Composed of 2% (wt/vol) of the indicated carbon source like glucose (Fisher Scientific)/ raffinose (Biosynth)/ sodium acetate (Thermo Scientific) and 0.67% (wt/vol) yeast nitrogen base (YNB) without amino acids (BD BioSciences), supplemented with the following amino acids and nucleotides: 0.008% (wt/vol) histidine (Sigma Aldrich), 0.008% (wt/vol) tryptophan (Sigma Aldrich), 0.04%

(wt/vol) leucine (Sigma Aldrich), 0.008% (wt/vol) uracil (Sigma Aldrich), and 0.008% (wt/vol) adenine (Sigma Aldrich).

3. Minimum Medium (MM): Containing 0.67% (wt/vol) yeast nitrogen base (YNB) without amino acids (BD BioSciences); 2% (wt/vol) of the preferred carbon source; supplemented with the following amino acids and nucleotides: 0.004% (wt/vol) histidine (Sigma Aldrich), 0.004% (wt/vol) tryptophan (Sigma Aldrich), 0.008% (wt/vol) leucine (Sigma Aldrich), 0.004% (wt/vol) uracil (Sigma Aldrich), 0.004% (wt/vol) adenine (Sigma Aldrich), and 0.004% (wt/vol) methionine (Sigma Aldrich).

For solid versions of previous media, 1.5% (wt/vol) agar (Conda Pronadisa) was incorporated.

Where indicated cerulunin was added to a final concentration of 1µg/mL for the inhibition of fatty acid synthase (FAS).

2.3. Construction of yeast mutants

Protein tagging and individual gene KO (**Table 3**) were based on the following PCR protocol. PCR reactions were performed in 20 µL reaction mixes containing NZYTech Proof polymerase mix and 200 ng of plasmid or 400 ng of DNA extract. PCR was performed in a T100 Thermo Cycler (Bio-Rad) with a heated lid using the following conditions: Initial denaturation step at 95ºC for 3 min, secondary denaturation step at 95 ºC for 45s (where PCR cycling starts), a primer annealing step with a temperature adjusted according to primer melting point for 45s, an elongation step at 72ºC for 1kb of PCR product/min (where PCR cycling ends) and a final elongation step of 10 min at 72ºC. Primers were designed using Primers-4 Yeast [149] for pFA6 [143] plasmid sets. Primers used in this work are described in **Table 3**.

Table 3. Primers used in this study.

ORF	Gene	Primer name	Sequence (5'→ 3')
YDR329C	*PEX3*	*PEX3* KO pFA6 F	GCAGAAGCACGAAACAAGGAGGCAAACCACTA AAAGGATGcggatccccgggttaattaa
YDR329C	*PEX3*	*PEX3* KO pFA6 R	ATATATTCTGGTGTGAGTGTCAGTACTTATTCAGA GATTAgaattcgagctcgtttaaac
YDL065C	*PEX19*	*PEX19* KO pFA6 F	ACGGAAAGAAGAAATGCCAAACATACAACACGA AGTAATGcggatccccgggttaattaa
YDL065C	*PEX19*	*PEX19* KO pFA6 R	TTTTTTTTTTTTTACTGTTATCATAAATATATATACC TTAgaattcgagctcgtttaaac

YGL080W	*MPC1*	*MPC1*_Fw_ClaI	TAAGCAATCGATATGTCTCAACCGGTTCAACGCG CTGCAG
YGL080W	*MPC1*	*MPC1*_Rv_NheI	TGCTTAGCTAGCTTACTGTTTACCAGTTTTTTCTT TCT
YML042W	*CAT2$_{cyt}$*	*CAT2* cyt_Fw_BlpI	TAAGCAgctaagcATGAGGATCTGTCATTCGAGAA CTCTCTC
YML042W	*CAT2$_{cyt}$*	*CAT2* cyt_Rv_NheI	TGCTTAGCTAGCTCATTTTCGTTTATTCTCATTTT CCAAGGCG
YML042W	*CAT2$_{mit}$*	*CAT2*_Fw_BlpI	TAAGCAgctaagcATGAGGATCTGTCATTCGAGAA CTCTCTC
YML042W	*CAT2$_{mit}$*	*CAT2*_Rv_NheI	TGCTTAGCTAGCTCATAACTTTGCTTTTCGTTTAT TCTCATTTTC

All PCR reaction products were analyzed by nucleic acid electrophoresis at 125V, using 1% (w/v) agarose gels with GreenSafe premium 0.04 µL/mL (NZYtech) and TAE buffer (40 mM Tris, 20 mM acetic acid, 1 mM EDTA). DNA bands were visualized through UV fluorescence and extracted from the gel using the NZYgelpure kit (Nzytech) according to the manufacturer's instructions. DNA quantification was done using Nanodrop 1000 (Thermofisher).

2.4. Yeast transformation

A modified lithium acetate (LiAc)/single-stranded carrier DNA (ssDNA)/polyethylene glycol (PEG) method [143] was employed for the transformation of *Saccharomyces cerevisiae*. Cells were initially cultured overnight in either YPD or synthetic complete (SC) selective medium until reaching an OD_{600} of 0.3–0.4. Following growth, cells were harvested via centrifugation, washed, and subsequently resuspended in 700 µL of a solution containing 1.0 M LiAc (Sigma-Aldrich), 10× Tris-EDTA (TE) buffer (pH 7.4), and sterile water. Aliquots of 120 µL from the resuspended cells were combined with a transformation mixture composed of 700 µL of 40% (w/v) PEG 3350 (Sigma-Aldrich), 20 µL of ssDNA (5 mg/mL), and the required amount of transforming DNA. This mixture was briefly vortexed to ensure homogenization, incubated at 26 °C for 30 minutes, and then subjected to heat shock at 42 °C for an additional 30 minutes. After transformation, YPD medium was added and cells were allowed to recover for 3 hours at 26 °C. The cultures were then centrifuged, resuspended in selective medium, and plated onto selective agar plates. For plasmid-based transformations, a simplified version of the protocol was utilized. A total of 3 µL of plasmid DNA and 3 µL of salmon sperm ssDNA were added to 100 µL of a transformation mix comprising 80 µL of 50% (w/v) PEG 3350, 10 µL of 1.0 M LiAc, and 10 µL of 10× TE buffer (pH 7.4). A small quantity of yeast cells, scraped directly

from a plate, was added to the reaction mixture, which was incubated at 26 °C for 4 hours. After incubation, cells were directly plated on selective media.

2.5. *E. coli* transformation

Chemically competent *Escherichia (E.) coli* cells were prepared using the calcium chloride soaking method and gently thawed on ice prior to transformation. An aliquot of 50 µL of competent cells was combined with 3 µL of plasmid DNA and maintained on ice for 30 minutes to allow DNA uptake. This was followed by a heat shock step at 42 °C for 90 seconds, after which the cells were immediately returned to ice for an additional 2 minutes to stabilize the membranes. Subsequently, 1 mL of LB medium was added to the cells to facilitate recovery, and the suspension was incubated at 37 °C for 1 hour with gentle shaking. After the recovery phase, the transformed cells were plated on LB agar containing ampicillin (100 mg/mL) and incubated overnight at 37 °C to allow colony formation.

2.6. β-Galactosidase activity assay

Cells containing LacZ-reporter fusion plasmids were cultured in SC medium. After growth, the cells were collected by centrifugation, resuspended in breaking buffer (100 mM Tris, 1 mM DTT, 10% (vol/vol) glycerol) supplemented with protease inhibitors (Complete Mini EDTA-free Protease Inhibitor Cocktail tablets), and mechanically disrupted using zirconium beads for 5 minutes. The cell debris was removed by centrifugation at 14,000 × g for 15 minutes at 4 °C, and the supernatant was collected for protein quantification. Total protein concentrations were determined using the Lowry method, with a standard curve generated from bovine serum albumin. Aliquots containing 15-100 µg of total protein were diluted to a final volume of 800 µL with β-galactosidase assay buffer (60 mM Na_2HPO_4, 40 mM NaH_2PO_4, 10 mM KCl, 1 mM $MgSO_4$, 50 mM β-mercaptoethanol). The samples were then incubated at 30 °C for 5 minutes in the presence of 200 µL of the substrate *o*-nitrophenyl-β-D-galactopyranoside (ONPG; Merck, Kenilworth, NJ, USA), as previously described [150]. The reaction was stopped by adding 400 µL of 1 M Na_2CO_3 once a yellow color developed. Absorbance was measured at 420 nm, and β-galactosidase activity was calculated using the following equation:

$$\beta - Galactosidase\ Activity = \frac{Abs420nm \times 1.40}{0.0045 \times protein\ (mg) \times t\ (\min)} nmol.min^{-1}mg^{-1}$$

2.7. Western blotting analysis

To evaluate the total protein levels of **Pex5**, **Pot1**, **acetyl-H3** and **histone-H3** in WT-VN WT-VC and N88S-VN N88S-VC strains, cells were cultured until they reached either the exponential (EXP) or post-diauxic shift (PDS) phase in SC-glucose medium at 26 °C. The cells were then washed and collected by centrifugation at 4000 rpm for 4 minutes at 4 °C. Protein extraction was performed using alkaline lysis, and the samples were prepared in Laemmli sample buffer. Proteins were separated by SDS-PAGE using 10% polyacrylamide gels for detecting Pex5, Por1, histone-H3 and acetyl-H3 total levels. The separated proteins were transferred to nitrocellulose membranes (Hybond-ECL, GE Healthcare) using a semi-dry transfer system for 1 hour. The membranes of Pex5, Pot1p and histone-H3 were blocked with 5% (wt/vol) nonfat dry milk in TTBS buffer (20 mM Tris, 140 mM NaCl, 0.05% (vol/vol) Tween-20, pH 7.6), and the membrane of acetyl-H3 blocked with 5% (wt/vol) BSA in the same TTBS buffer, all for 1 hour at room temperature. The membranes were then incubated with primary antibodies: polyclonal rabbit anti-Pex5, anti-Pot1 antibody (1:10000 dilution, Prof. Ralf Erdmann), anti-histone-H3 and anti-acetyl-H3 (1:3000 dilution, abcam-ab1791 and Cell Signalling mAB #7627, respectively), overnight at 4ºC. After washing with TTBS, the membranes were treated with an anti-rabbit secondary antibody (1:5000 dilution), 1 hour at room temperature. Immunodetection was carried out using chemiluminescence with WesternBright ECL reagent (Advansta), and the membranes were exposed to LucentBlue X-ray films (Advansta). Band intensities were quantified using a GS-900 Calibrated Densitometer (Bio-Rad). For membrane stripping, the membranes were washed with TTBS and incubated in stripping buffer (62.5 mM Tris-HCl, pH 6.8, 2% (wt/vol) SDS, 10 mM 2-mercaptoethanol) for 30 minutes at 50 °C. After several washes with water, the blots were visualized using enhanced chemiluminescence reagents (Perkin Elmer, Inc., Waltham, MA, USA), and band intensities were analyzed using ImageJ software.

2.8. Fluorescence microscopy

To examine the intracellular localization of IBs using the Venus signal upon reconstitution of the VN and VC fragments and peroxisomes (using *PTS1*-mCherry), cells were grown to the exponential phase in SC-glucose medium. The cells were centrifuged at 13400 rpm during 1 min, then washed with 1 mL of water, centrifuged again in same conditions and resuspended in 25 µL of SC-glucose and finally visualized using fluorescence microscopy (Zeiss Axio Imager Z1 Apotome or Leica TCS SP8). Z-stacks were captured for the DIC, mCherry, and Venus channels. Final images and quantification analyses were processed using ImageJ software (version 2.0.0-rc-69/1.52p). Where applicable,

all quantifications were based on at least two independent experiments, with over 100 cells evaluated per condition. Data were recorded in Excel (Microsoft) and analyzed using Prism 8.0 (GraphPad Software). Adjustments to brightness and contrast were made using Inkscape (The Inkscape Project).

2.9. ROS staining and IB formation

To assess ROS, cells grown in SC-glucose medium at specified phases were incubated with 5 µg/mL dihydroethidium (DHE, Molecular Probes) for 10 min at room temperature in the dark. The quantification of Venus fluorescence intensity, normalized to the number of cells, was used as a means to monitor IB formation [9]. Then, cells were centrifuged, washed twice and resuspended in PBS [9]. Flow cytometry analysis was performed using the FL1 (533/30) for IB monitoring, and FL3 (670 LP) channels (BD Accuri C6 Flow cytometer) for ROS quantification via DHE staining. Data were evaluated with FlowJow software (v. 10.6.1).

2.10. Yeast spotting assay

Growth assays were conducted by applying serial 1:10 dilutions of exponentially-grown cell cultures onto SC-glucose or SC-acetate plates containing sodium arsenite (NaAs) at the final concentration of 250 µM. Growth was monitored and documented following a period between 2-day and 5-day after incubation at 26 °C.

2.11. β-Oxidation Measurement

β-oxidation activity was measured using 11 µM of [1-^{14}C]-labelled octanoate (C8:0) as substrate (American Radiolabeled Chemical, St. Louis, MO, USA), as described previously [151]. The sum of the end products of β-oxidation, which includes [^{14}C]-labelled CO_2 and acid-soluble products (ASP), was taken as a measure of β-oxidation activity.

2.12. Enzymatic activity assays

Cells were grown to PDS phase in SC-glucose medium and harvested by centrifugation for 5 minutes at 4000 rpm (4 ºC). Cells were resuspended in their respectively buffer as indicated in **Table 4** containing protease inhibitors (Complete, EDTA-free Protease Inhibitor Cocktail, Roche). The protein extracts were obtained by mechanical disruption of the cells by vortexing in the presence of glass beads for 10 minutes. Cell debris was removed by centrifugation at 3000 rpm for 15 minutes at 4 ºC, and protein concentration was determined by the method of Lowry, using Bovine serum albumin (BSA) as a standard. Measurements of the activities of enzyme were done spectrophotometrically

at 25ºC adding the respective reagents as described in **Table 4** [152]. 1 unit of enzyme activity was defined as 1 nmol of protein substrate converted per minute and per mg of protein. Acetyl-coenzyme A synthetase activity was determined as previously described [153]. Cells were grown to PDS phase in SC-medium lacking histidine and leucine, and 0.2 mg protein extract or the equivalent volume of buffer was used (control).

Table 4. Conditions for the measurement of glyoxylate and TCA cycle enzyme activities.

Enzyme	Buffer (mM)	Other addition(s) [brand] (mM)	Wavelength (nm)	ε (M^{-1} cm^{-1} × 10^{-8})
Citrate synthase (EC 4.1.3.7)	100 Tris–HCl, pH 8.5	Oxaloacetate [Sigma-Aldrich] (0.25), acetyl-CoA [Sigma-Aldrich] (0.04), DTNB [Sigma-Aldrich] (0.1)	412	13.60
NAD-dependent isocitrate dehydrogenase (EC 1.1.1.41)	100 Tris–HCl, pH 7.4	D,L-Isocitrate [Sigma-Aldrich] (5), NAD [Sigma-Aldrich] (1.7),AMP [Thermo Scientific] (0.8), MgCl2 [Merck] (3)	340	6.22
NADP-dependent isocitrate dehydrogenase (EC 1.1.1.42)	100 Tris–HCl, pH 7.4	D,L-Isocitrate (5), NADP [Sigma-Aldrich] (0.6), MgCl2 (3)	340	6.22
Malate dehydrogenase (EC 1.1.1.37)	100 Tris–HCl, pH 7.4	Oxaloacetate (0.15), NADH (0.1)	340	6.22
Isocitrate lyase (EC 4.1.3.1)	100 KPi, pH 7.4	D,L-Isocitrate (8), cysteine [Sigma-Aldrich] (2), phenylhydrazine [Sigma-Aldrich] (3.3), MgCl2 (3)	324	17.00
Malate synthase (EC 4.1.3.2)	100 Tris–HCl, pH 8.5	Glyoxalate (5), acetyl-CoA (0.1), MgCl2 (10), DTNB (0.33)	412	13.6

2.13. Lipid peroxidation assay

For lipid peroxidation analysis, cells were grown in SC-glucose lacking histidine and leucine to stationary phase. Yeast extracts were prepared in 20 mM sodium phosphate buffer (pH 7.2), by vigorous shaking of the cell suspension, in the presence of glass beads, for 5 min. Trichloroacetic acid (10% w/v) was added and two more pulses of 1 min were performed. Total protein levels were quantified by the Lowry method using a bovine serum albumin standard curve. Lipid peroxidation was assayed in 600 µL of 1% (w/v) thiobarbituric acid, 0.05 M NaOH, 0.025% (w/v) butylated hydroxytoluene, 100 µL of 0.1 M EDTA, and 100 µL of total protein extract. Malondialdehyde (MDA) concentration was determined spectrophotometrically at 532 nm and expressed as nanomoles of MDA.(mg of protein)$^{-1}$ [154].

2.14. Measurement of glutathione levels

Cells were grown in SC-glucose lacking histidine and to PDS phase. The Glutathione GSH/GSSG Assay Kit (MAK 440, Sigma-Aldrich) was used to measure total, reduced and oxidized glutathione levels in samples using an enzymatic method that utilizes Ellman′s Reagent (DTNB) and glutathione reductase. 10 OD_{600} cells were used to perform the measurements according to the manufacturer's instructions. Yeast extracts were prepared in 20 mM sodium phosphate buffer (pH 7.2), by vigorous shaking of the cell suspension, in the presence of glass beads, for 5 min.

2.15. Statistical analysis

Unless otherwise stated, the results were obtained from at least three independent experiments. The images displayed are representative of these outcomes. Quantitative data are expressed as the mean ± standard deviation (SD). Statistical analyses were performed using unpaired, two-tailed Student's *t*-tests or one-way ANOVA, carried out with Prism 8.0 software (GraphPad Software). *P*-values < 0.05 were considered significant: * $p \leq 0.05$; ** $p \leq 0.01$; *** $p \leq 0.001$; **** $p \leq 0.0001$.

3. Results

Here, we used a well-established yeast model of human N88S-linked seipinopathy previously developed in our laboratory via a bimolecular fluorescence complementation (BiFC) strategy [4, 9]. This yeast model was constructed in a seipin-deficient background (*sei1*Δ *ldb16*Δ), in which human wild-type (WT) or N88S mutant forms of seipin were expressed as fusions to either the N-terminal (VN) or C-terminal (VC) fragments of the Venus fluorescent protein [4, 9, 10]. Quantitative untargeted mass spectrometric proteomic analysis was conducted to examine changes in protein abundance in wild-type (WT) versus N88S seipin-expressing mutant cells [9, 10]. Using YEASTRACT +, a Gene Ontology (GO) analysis and KEGG pathway analysis for differentially expressed proteins (DEPs) revealed an enrichment in proteins related to tricarboxylic acid cycle (TCA) (GO:0006099; p-value = 5,34 × 10^{-8}), fatty acid (FA) metabolic process (GO:0006631; p-value = 1,29 × 10^{-5}), carboxylic acid metabolic process (GO:0019752; p-value = 2,17 × 10^{-6}) and glyoxylate cycle (GO:0006097; p-value = 2,49 × 10^{-6}) (**Figure 15**). Peroxisomes support cellular metabolism by linking FA and carboxylic acid metabolism with the glyoxylate and TCA cycles to provide metabolic intermediates and support energy homeostasis. A previous genomic screening for IB formation modifiers also revealed a gene cluster enriched in protein targeting to peroxisome and peroxisomal membrane transport (data not shown). Altogether, we posit that peroxisome function is altered in N88S seipin-expressing cells, possibly contributing to alterations in lipid metabolism and flux observed in the mutant.

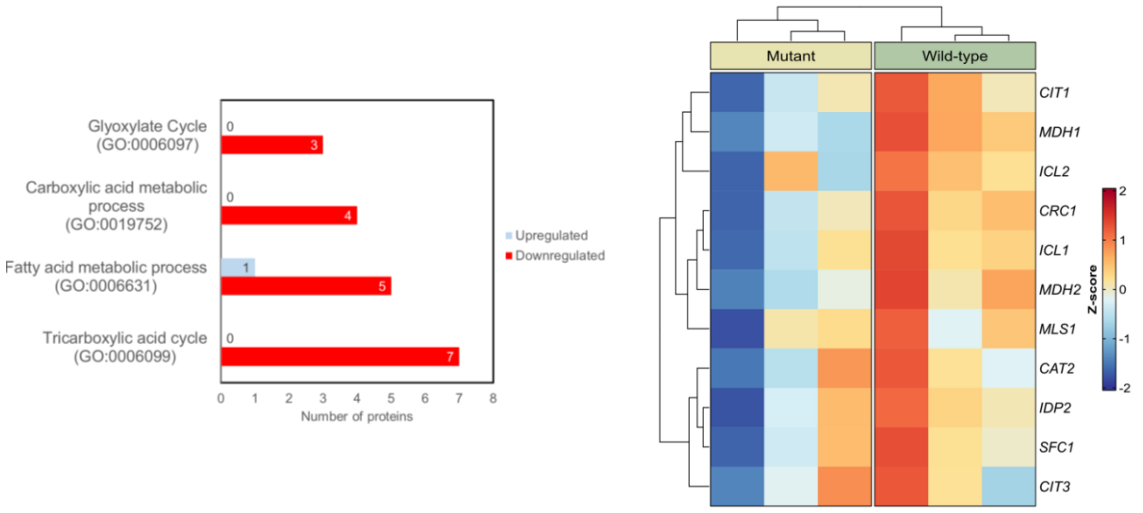

Figure 15. **GO-based functional categorization of DEPs with respect to biological processes.** Proteins that were significantly altered in N88S seipin-expressing cells were subjected to Gene Ontology (GO) enrichment analysis within the indicated biological process categories (left panel). Heat map analyses of total protein level changes of enzymes and metabolite transporters pathway in WT and N88S seipin-expressing cells (right panel, for 3 independent experiments per strain).

3.1. Absence of peroxisomes lead to an increase in IBs formation

The initial phase of this project focused on investigating the relationship between peroxisome morphology, number, and IB accumulation in WT and N88S seipin-expressing cells. To achieve this, we used fluorescence microscopy, tracking the Venus signal to monitor IB formation, and the *PTS1*-mCherry signal was used as a peroxisomal marker. The results revealed that N88S mutant cells exhibited a higher number of peroxisomes (**Figure 16 A and B**) than WT cells. although their overall morphology remained similar. To explore the correlation between peroxisomal genes and IB formation, we generated peroxisome ***pex3-*** or ***pex19*-deficient cells**. These cells are defective in peroxisomal membrane biogenesis and therefore lack functional peroxisomes, and all matrix enzymes reside in the cytosol [155]. In fact, *PTS1*-mCherry was observed in the cytosol in N88S mutant cells in both genetic backgrounds (**Figure 16 A**). Importantly, the lack of functional peroxisomes markedly increased IB formation in N88S seipin-expressing cells (**Figure 16 A and C**), indicating a metabolic link between peroxisomes and IB generation. Together, these findings indicate that expression of N88S seipin increases peroxisome abundance, and that peroxisomal function is required to restrain IB formation.

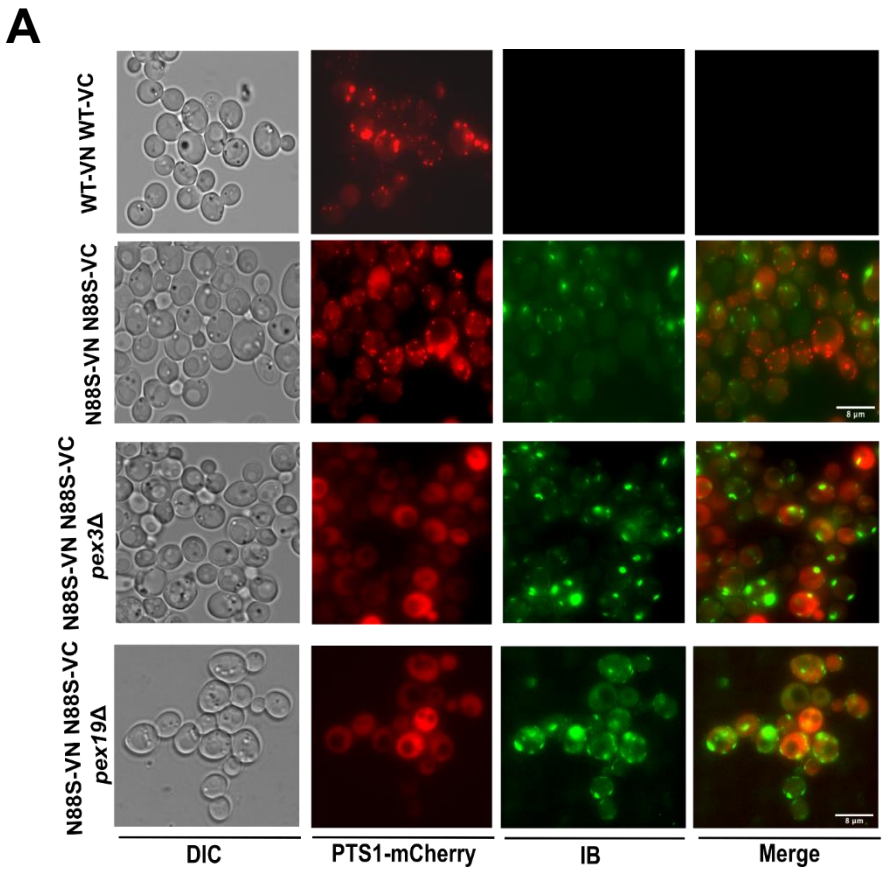

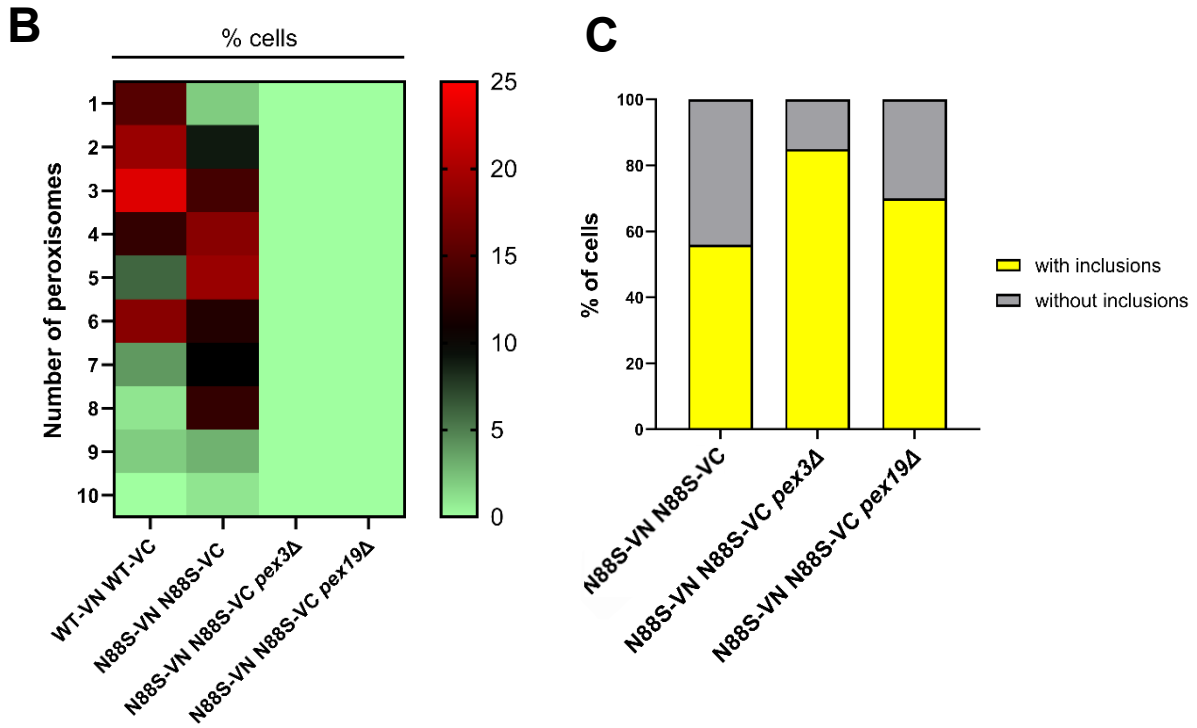

***Figure 16. PEX3* and *PEX19* deficiency increased IBs formation in cells expressing the N88S seipin mutation. (A)** Formation of IBs was monitored by fluorescence microscopy using the YFP/Venus channel (third column), and peroxisome number and morphology was assessed using a *PTS1*-mCherry fusion construct, in cells grown to the exponential phase in SC-glucose medium. DIC: Differential interference contrast. Bar scale, 8 µm. **(B)** Heat map illustrating the frequency distribution of peroxisome number per cell. The y-axis denotes the number of peroxisomes per cell, while the color scale represents the corresponding cell counts. Lower frequencies are depicted in green, and higher frequencies in red. Data were combined from 2 independent experiments. **(C)** Quantification is defined as percentage of cells displaying IB foci (n>100 cells). Data were combined from 2 independent experiments.

3.2. Peroxisome deficiency increases ROS production and disrupts redox balance without inducing ER stress

Peroxisomes are dynamic, multifunctional organelles that play a central role in maintaining cellular homeostasis by coordinating lipid metabolism with adaptive stress responses. To further understand the potential role of peroxisomes in the disease, we started by examining their impact on key phenotypes, including the ER stress response. We then analyzed how *PEX3* deficiency affects the activity of the UPRE-LacZ ER stress reporter. Consistent with earlier observations, cells expressing the N88S seipin variant exhibited increased β-galactosidase (β-gal) activity of the reporter fusion when compared to its WT counterpart at all growth stages (**Figure 17**), which correlates with higher ER stress levels [9, 10]. Importantly, *PEX3* deletion did not significantly alter UPR activation in WT- and N88S-seipin expressing cells (**Figure 17**), suggesting that changes in peroxisome number and metabolism are not associated with the induction of the ER stress response in the mutant strain.

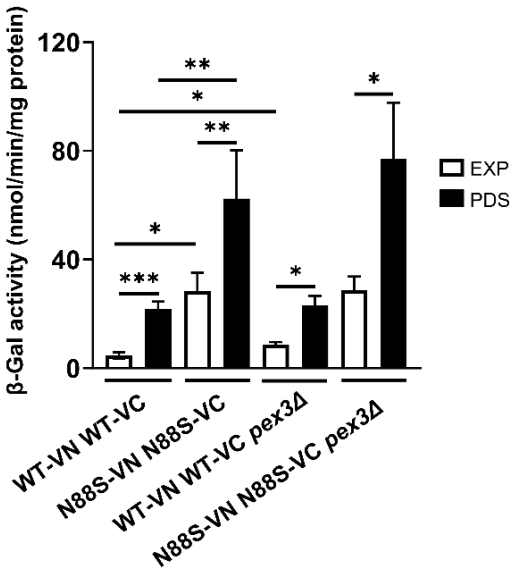

***Figure 17. PEX3* deficiency has no effect in the activation of the UPR in N88S seipin-expressing cells.** Cells with the specified genotypes expressing UPRE-LacZ were grown in SC-glucose medium lacking leucine and allowed to reach the exponential (EXP) and post-diauxic shift (PDS) phases. At least 3 independent experiments for each strain were performed. Protein extracts were prepared, and specific β-galactosidase (β-Gal) activity was measured using o-nitrophenyl-β-D-galactopyranoside (ONPG) as a substrate, with the amount of o-nitrophenol released indicating enzyme activity. * $p \leq 0.05$; ** $p \leq 0.01$; *** $p \leq 0.001$ (unpaired *t*-test with Welch´s correction).

Peroxisomes are key organelles that maintain cellular redox balance and homeostasis by linking lipid metabolism with ROS detoxification. We previously demonstrated that ROS levels were elevated in N88S seipin-expressing cells [9, 10]. Here, we examined whether alterations in peroxisome dynamics influence ROS production in these cells. For this purpose, cells were grown to the stationary phase, and ROS levels were measured using the dihydroethidium (DHE) probe. Our results showed that *PEX3* deficiency increased ROS levels by approximately 75% in N88S cells, while ROS levels in WT cells remained unaffected (**Figure 18**). These findings suggest that increased number of peroxisomes may help mitigate oxidative damage in cells expressing the N88S seipin mutation.

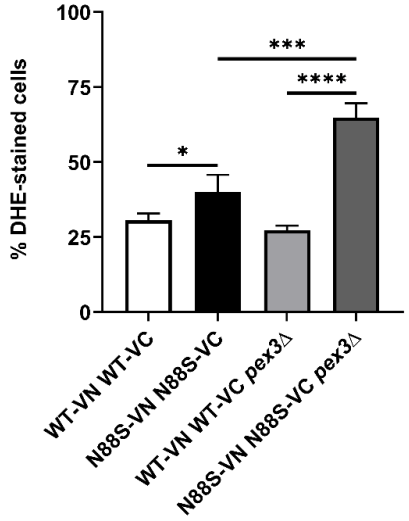

Figure 18. **Lack of peroxisomes (*pex3*-deficient cells) increases ROS levels in N88S mutant cells but does not impact ROS levels in WT cells.** Cells with the indicated genotypes were grown in SC-glucose medium until stationary (STAT) phase, and ROS levels were assessed in cells labeled with dihydroethidium (DHE) via flow cytometry using the FL3 channel. Data were generated from at least 3 independent experiments for each strain. * $p \leq 0.05$; *** $p \leq 0.001$; **** $p \leq 0.0001$ (unpaired *t*-test with Welch´s correction).

Peroxisomes contribute to cellular redox homeostasis in part by regulating glutathione levels, a key antioxidant that protects against oxidative stress [156]. Based on this, we evaluated the levels of glutathione. Glutathione exists in two states: oxidized (GSSG) and reduced (GSH). The results showed that total glutathione levels were increased in the N88S *pex3*Δ mutant when compared to N88S seipin-expressing cells (**Figure 19**), reinforcing the importance of peroxisomes in maintaining redox balance. Although no differences were observed in GSH levels and in the ratio GSSG/GSH between WT cells and the N88S seipin mutant, GSSG levels were lower in N88S seipin-expressing cells (**Figure 19**). The observation of increased ROS concurrent with normal GSH levels and a reduced GSSG pool implies that the glutathione system is actively maintaining redox homeostasis in the mutant, partially compensating for impaired antioxidant defenses, including the previously reported decrease in catalase activity in N88S seipin-expressing cells [9]. Possible explanations for this result include enhanced glutathione reductase activity or accelerated GSH synthesis and/or export of GSSG, which would prevent accumulation of intracellular GSSG. Altogether, these findings indicate that redox imbalance observed in the yeast model of human N88S seipinopathy might be linked to alterations in glutathione metabolism.

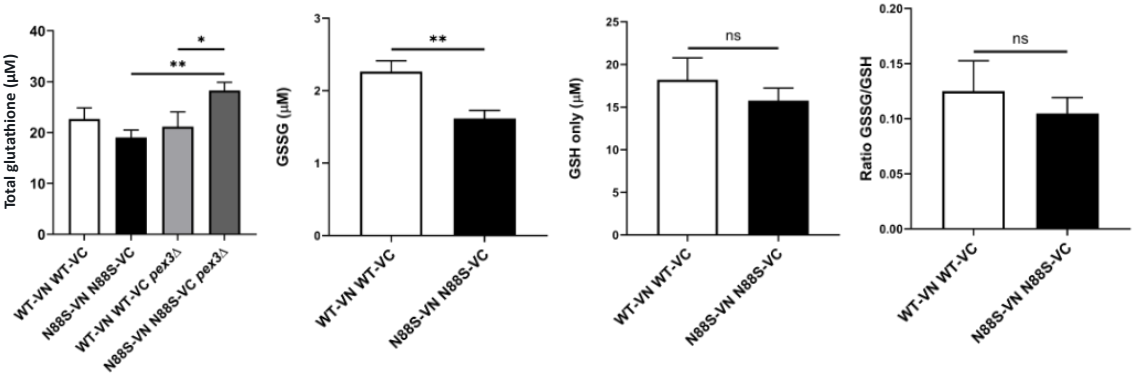

Figure 19. **The loss of peroxisomes leads to an increase in total glutathione levels in N88S seipin-expressing cells.** Total glutathione, oxidized (GSSG), reduced (GSH) glutathione levels and the ratio of GSSG to GSH were determined in cells grown in SC-glucose medium to PDS phase. At least 3 independent experiments were performed, as described in Materials and Methods (2.14). * $p \leq 0.05$; ** $p \leq 0.01$; ns - non-significant (unpaired *t*-test with Welch´s correction).

3.3. N88S seipin-expressing cells exhibit increased peroxisomal biogenesis and function

Fluorescence microscopy data revealed an increase in peroxisome number in cells expressing the N88S seipin mutation (**Figure 16**), prompting us to examine changes in the levels of Pex5 and Pot1, which are key proteins involved in peroxisomal biogenesis and function, respectively. Pex5 mediates the import of newly synthesized proteins containing a *PTS1* signal into peroxisomes, while Pot1 is a crucial enzyme for FA β-oxidation, reflecting peroxisomal metabolic activity [157]. Western blot analyses revealed higher levels Pex5 and Pot1 protein levels at post-diauxic phase (PDS) phase (**Figure 20**) for N88S-seipin expressing cells when compared to its WT counterpart, which corroborate with peroxisome proliferation and increased organellar activity. This indicates that peroxisomes are fully functional in cells carrying the N88S seipin mutation.

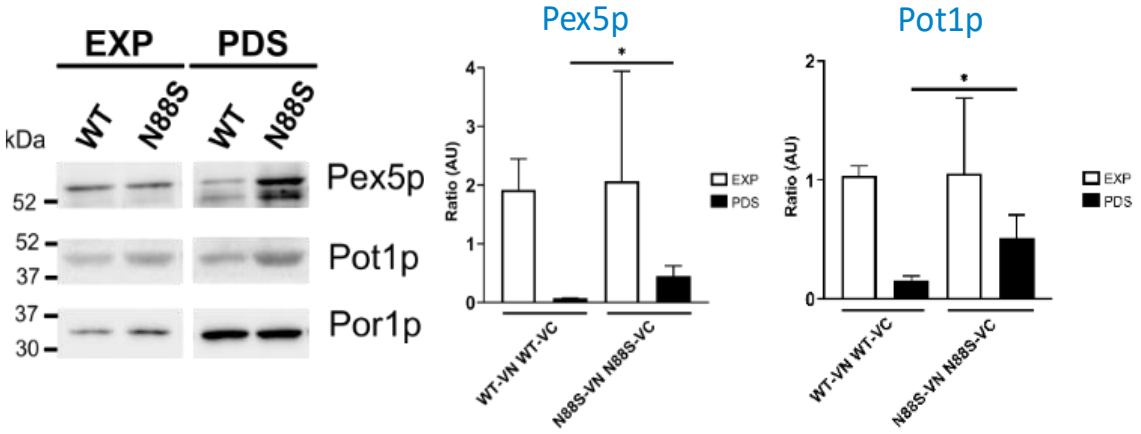

Figure 20. **N88S strains presented higher levels of peroxisome biogenesis and activity.** WT and N88S seipin expressing cells were grown in SC-glucose medium and allowed to reach the exponential (EXP) and post-diauxic shift (PDS) phases. Aliquots were collected at these stages, and Western blot analysis were performed for assessment of Pex5 and Pot1 protein levels. Por1 was used as loading control (left panel). Quantification is based on the ratio between the indicated protein and the loading control as measured by densitometry (right panel). * $p \leq 0.05$ (unpaired *t*-test).

In order to further analyze peroxisomal function, we determined the activity of the β-oxidation using radiolabeled [1-^{14}C]-labelled octanoate (C8:0) as substrate, which was oxidized to acid-soluble products (ASP) and CO_2. To achieve this, we used *pex3*-deficient strains as negative controls and conducted comparative analyses between the WT and N88S strains. The results revealed that although FA β-oxidation rates are similar between WT and N88S mutant cells (**Figure 21**), ASP levels are decreased by ~30% in N88S seipin-expressing cells (**Figure 22 A**), while no difference was observed for %CO_2 generated in TCA cycle (**Figure 22 B**). It was previously shown that [1-^{14}C]-labelled octanoate (C8:0) is primarily oxidized to oxaloacetate and malate ASPs, which are

glyoxylate and TCA cycle metabolites, and carbon dioxide (CO_2) [158]. This observation indicates that the metabolic flux and incorporation of acetyl-CoA generated from FA β-oxidation into the glyoxylate and TCA cycles are impaired (**Figure 12**).

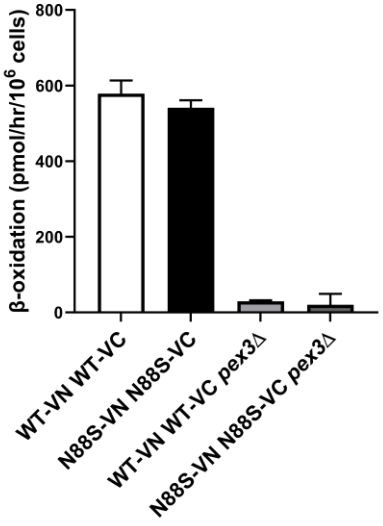

Figure 21. **β-oxidation activity was not altered by the N88S seipin mutation**. FA β-oxidation was assessed using radiolabeled [1-^{14}C] octanoate (C8:0) as a substrate and quantified as described in Materials and Methods (Section 2.11). Two independent experiments were performed for each strain.

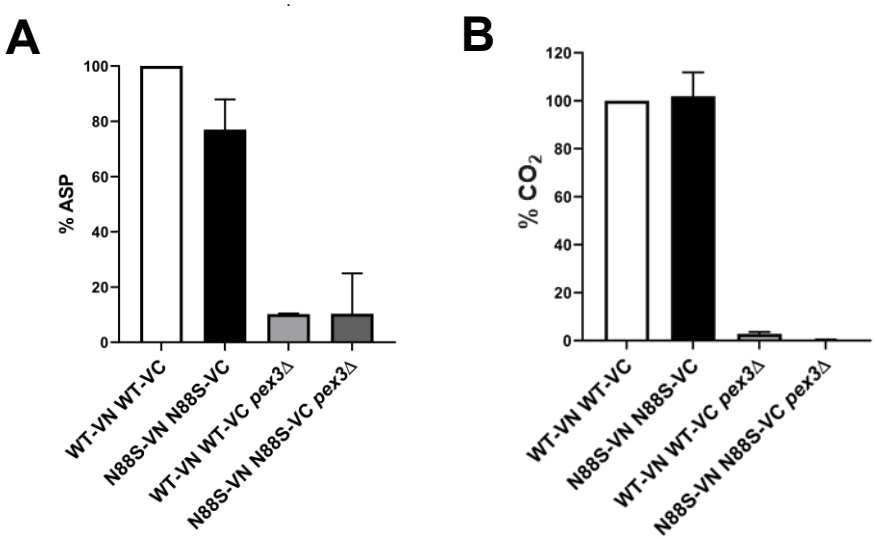

Figure 22. **Lower incorporation of acetyl-CoA into ASP in N88S-seipin expressing cells.** Cells with the indicated genotypes were cultured under the conditions described in Figure 21. Following extraction, the **A)** ASP-containing supernatant and **B)** CO_2-containing supernatant were transferred to liquid scintillation vials, and radioactivity was quantified using a liquid scintillation counter (LSC). ASP and CO_2 production in mutant strains were normalized relative to the WT strain, which was set at 100%.

Finally, growth measurement assays comparing WT and N88S cells with their respective *pex3*-deficient counterparts revealed that loss of peroxisomes impaired growth, with the effect being more pronounced in N88S cells (**Figure 23**). Together, these findings

indicate that peroxisome dynamics is critical for managing oxidative stress and IB formation, and for sustaining growth in the yeast model of N88S seipinopathy.

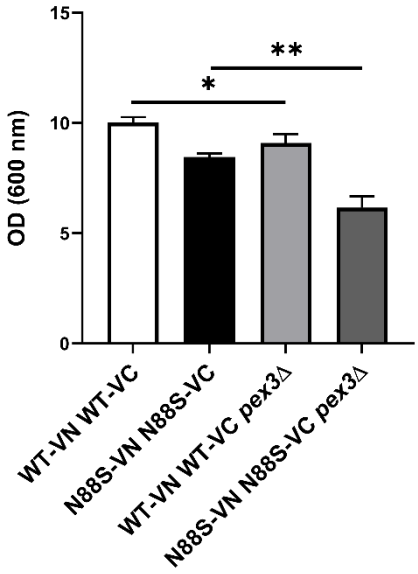

***Figure 23*. N88S-seipin expressing cells exhibited a prominent growth defect in the absence of peroxisomes.** Overnight precultures of cells grown in SC-glucose medium were diluted to OD_{600}=0.15 in fresh medium. The growth was monitored by OD_{600} and determined accordingly after a 48-hour incubation period. Both graphs were obtained from at least 3 independent experiments for each strain. * $p \leq 0.05$; ** $p \leq 0.01$ (unpaired *t*-test with Welch´s correction).

3.4. Downregulation of glyoxylate cycle enzymes activities is not related to changes in their enzymatic activity

Previous observations indicated altered ASP generation from FA β-oxidation in N88S cells. In addition, proteomic profiling and KEGG analysis revealed that the levels of proteins involved in glyoxylate cycle (Icl1, Mls1, Mdh2, Cit2) and TCA cycle (Cit1/3, Mdh1) are significantly reduced (**Figure 15**) [10]. This suggests that although peroxisomal β-oxidation remains active, reduced flux through downstream these metabolic pathways may limit the mobilization and conversion of acetyl-CoA into gluconeogenic or energy-yielding intermediates, potentially compromising energy homeostasis and metabolic adaptability under stress conditions. To explore whether decreased protein levels correlate with functional impairment, we measured basal activities of key enzymes from these pathways, including citrate synthase (TCA), malate dehydrogenase (glyoxylate/TCA), malate synthase (glyoxylate), NAD-dependent isocitrate dehydrogenase (mitochondrial), and NADP-dependent isocitrate dehydrogenase (cytosolic) in cells grown to PDS phase in SC-glucose medium, thus matching the conditions used for our previous proteomic analysis [10]. The results revealed no significant changes between WT and N88S seipin-expressing cells (**Figure**

24). These findings indicate that, despite reduced enzyme abundance, flux through these pathways may remain largely unchanged under basal conditions, likely due to compensatory mechanisms. However, a diminished enzyme pool (**Figure 15**) may constrain the metabolic flexibility of the cell, thereby limiting its capacity to adjust in response to alterations in carbon source and energy demand.

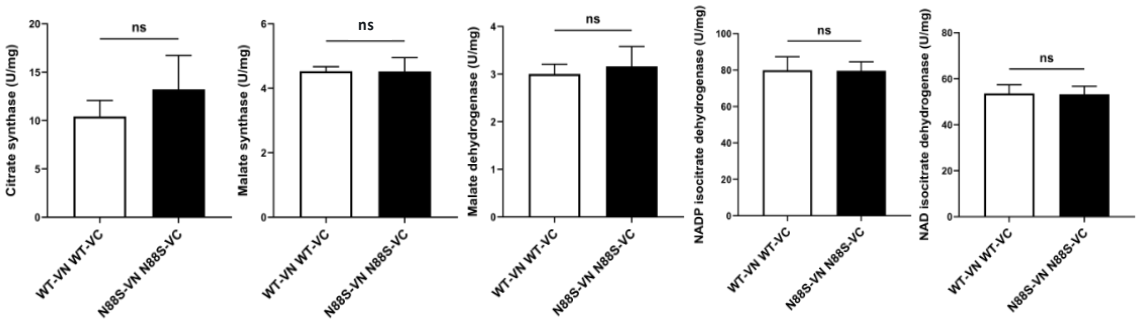

Figure 24. **Activities of glyoxylate and TCA cycle enzymes were not affected in N88S mutant strains.** Enzyme activities were measured in PDS-grown cells cultured in SC-glucose medium. Data represents the mean ± SD from at least three independent experiments per strain. ns - non-significant (unpaired *t*-test with Welch´s correction).

In yeast, enzymes required for the glyoxylate cycle are upregulated when cells grow on non-fermentable carbon sources (e.g. acetate or raffinose) or during the diauxic shift [159, 160]. Under these conditions, mitochondrial respiration becomes essential for generating energy from acetyl-CoA via the TCA cycle. This adaptive response underscores the physiological relevance of signaling pathways that adjust metabolism in response to mitochondrial function. Numerous nuclear genes are transcriptionally regulated by the mitochondrial state, namely *CIT2*, which encodes a glyoxylate cycle isoform of citrate synthase. Its transcription is strongly induced in response to loss of mitochondrial function through a process known as retrograde (RTG) pathway [159, 161]. Here we investigated how cells adapt to carbon source-dependent stress during PDS and stationary (STAT) phases, periods characterized by metabolic reprogramming, including reversal of carbon flow through glycolysis and activation of the glyoxylate cycle [159, 162], as well as during a shift to raffinose as the sole carbon source. To assess this, we introduced a *CIT2*-LacZ reporter into WT and N88S seipin-expressing cells and measured β-galactosidase activity. In WT cells, *CIT2*-LacZ expression significantly increased upon transition from PDS to STAT phase, coinciding with glucose exhaustion. In contrast, the β-gal reporter activity in N88S seipin-expressing cells was reduced by ~30% at both PDS and STAT phases, indicating impaired metabolic adaptation already under basal conditions (**Figure 25 A**). This defect became even more pronounced when cells were shifted to SC-raffinose medium to strongly induce glyoxylate cycle activity.

Whereas WT cells exhibited robust reporter activation, N88S cells showed a ~40-45% reduction (**Figure 25 B**). These findings demonstrate that N88S mutant cells exhibit a marked defect to properly induce the glyoxylate cycle and adapt to energy demands during diauxic shift and when shifted to non-fermentable carbon sources. In agreement with this idea, N88S-seipin expressing cells showed impaired growth on acetate medium as sole carbon source (**Figure 26**).

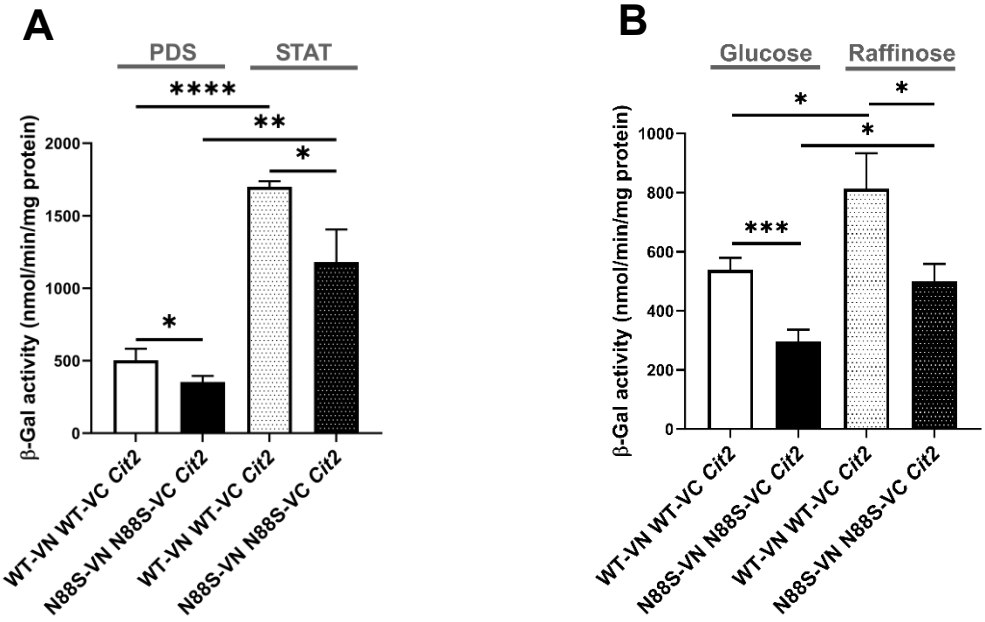

***Figure 25. CIT2* expression is reduced in N88S mutant cells under both basal and non-fermentable growth conditions.** Cells of the indicated genotypes carrying *CIT2*-LacZ were grown in SC-glucose medium and harvested at the post-diauxic shift (PDS) or stationary (STAT) phases **(A)**, or shifted from SC-glucose to SC-raffinose medium and incubated for 6 hours **(B)**. Protein extracts were prepared, and specific β-galactosidase (β-Gal) activity was quantified using o-nitrophenyl-β-D-galactopyranoside (ONPG) as a substrate, with o-nitrophenol release reflecting enzyme activity. Data represent mean ± SD from at least three independent experiments per strain. * $p \leq 0.05$; ** $p \leq 0.01$; *** $p \leq 0.001$; **** $p \leq 0.0001$ (unpaired *t*-test with Welch´s correction).

We next investigated whether acetate utilization in these cells depends on the Krebs cycle, since both TCA and glyoxylate cycles are essential metabolic pathways for growth on acetate as the sole carbon source [163]. Moreover, proteomic and KEGG analyses further revealed reduced levels of proteins from the TCA cycle (Cit1, Mdh2), the glyoxylate cycle (Icl1, Mls1, Cit3), and related processes (Mdh1, Idp2) [10] (**Figure 15**). To test this directly, we compared the growth of WT and N88S mutant strains on glucose or acetate medium, in the presence or absence of sodium arsenite (NaAs, 250 μM). Sodium arsenite inhibits the TCA cycle by targeting the α-ketoglutarate dehydrogenase complex [164]. In the presence of arsenite, both WT and N88S cells displayed similar growth regardless of the carbon source (**Figure 26**). Overall, these results demonstrate that acetate utilization in N88S mutant cells is not limited by the TCA cycle but rather by

defective induction of the glyoxylate cycle, confirming its essential role in metabolic reprogramming and adaptation to non-fermentable carbon sources.

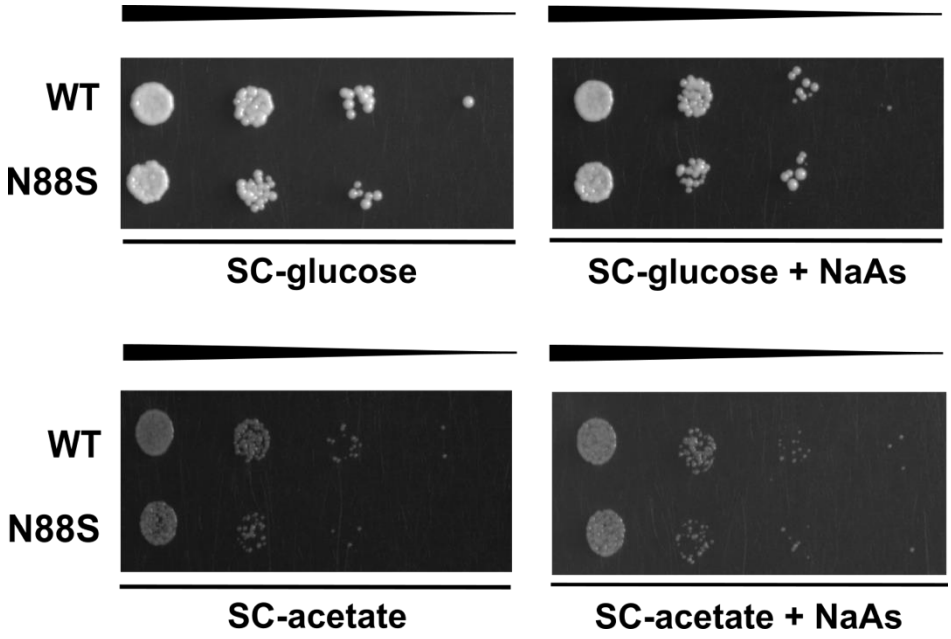

Figure 26. **N88S seipin mutant cells display growth comparable to WT in the presence of sodium arsenite (NaAs) independently of the carbon source.** Cells with the indicated genotypes were grown in SC-glucose medium to the EXP phase and diluted to OD_{600} = 0.1. Tenfold dilution series were spotted onto SC-glucose or SC-acetate plates supplemented (or not) with sodium arsenite (NaAS, 250 μM). Plates were incubated at 26 °C for 2-5 days.

3.5. *MPC1* overexpression exacerbates ER stress but does not contribute to ROS generation upon N88S seipin mutation

Our results indicate that N88S mutant cells exhibit disrupted metabolic coupling between peroxisomal β-oxidation and mitochondrial anaplerosis, likely due to impaired activation of the glyoxylate cycle. From our previous proteomics analysis [10], we also observed reduced protein levels of key metabolite transport/transfer proteins, including the mitochondrial inner membrane carnitine transporter Crc1, which mediates carnitine-dependent transfer of acetyl-CoA from peroxisomes to mitochondria during fatty acid β-oxidation, the mitochondrial succinate-fumarate transporter Sfc1 and the carnitine acetyltransferase *CAT2* (**Figure 15**). Together, these findings suggest that N88S seipin-expressing cells have reduced flux and utilization of peroxisome-derived acetyl-CoA in the glyoxylate cycle, along with defective transport into mitochondria. Consequently, acetyl-CoA or acetyl-carnitine may accumulate in the cytosol while becoming limiting in the mitochondria, thereby restricting TCA cycle activity and energy production, ultimately leading to metabolic stress. To test whether this represents a metabolic bottleneck in acetyl-CoA supply, we overexpressed the mitochondrial pyruvate carrier (*MPC1*), a

nuclear-encoded transporter that facilitates pyruvate uptake into mitochondria, thereby enhancing acetyl-CoA generation via the pyruvate dehydrogenase complex and boosting TCA cycle activity [165]. We first monitored ER stress activation using the UPRE-LacZ reporter. As shown in **Figure 27 A**, *MPC1* overexpression triggered a strong UPR, with a ~13-fold and ~18-fold increase in β-galactosidase reporter activity in WT and N88S mutant cells, respectively. This indicates that while *MPC1* increases mitochondrial acetyl-CoA availability, it also triggers ER stress. Several mechanisms could explain how *MPC1* overexpression induces the UPR. First, excessive mitochondrial import of pyruvate may drive hyperactivation of the TCA cycle, leading to an imbalance in mitochondrial ATP and NADH production [166]. Such shifts in mitochondrial redox state can disrupt ER homeostasis through the ER-mitochondria membrane contact sites**,** where calcium and lipid exchange are tightly regulated. Second, increased mitochondrial metabolism may elevate the demand for protein import, folding, and turnover in the organelle, indirectly contributing to ER stress [166]. Third, metabolic rewiring through *MPC1* may alter lipid synthesis, since acetyl-CoA availability directly feeds into phospholipid and sterol biosynthetic pathways. In fact, perturbation in inositol metabolism and phospholipid homeostasis were previously established as ER stressors in N88S seipin-expressing cells [10]. Next, we assessed ROS generation using the DHE probe (**Figure 27 B**). The results revealed that ROS levels remained unaltered in both WT and N88S cells upon *MPC1* overexpression. This suggests that enhanced incorporation of pyruvate and conversion to acetyl-CoA do not contribute to oxidative stress in the yeast model of N88S seipinopathy.

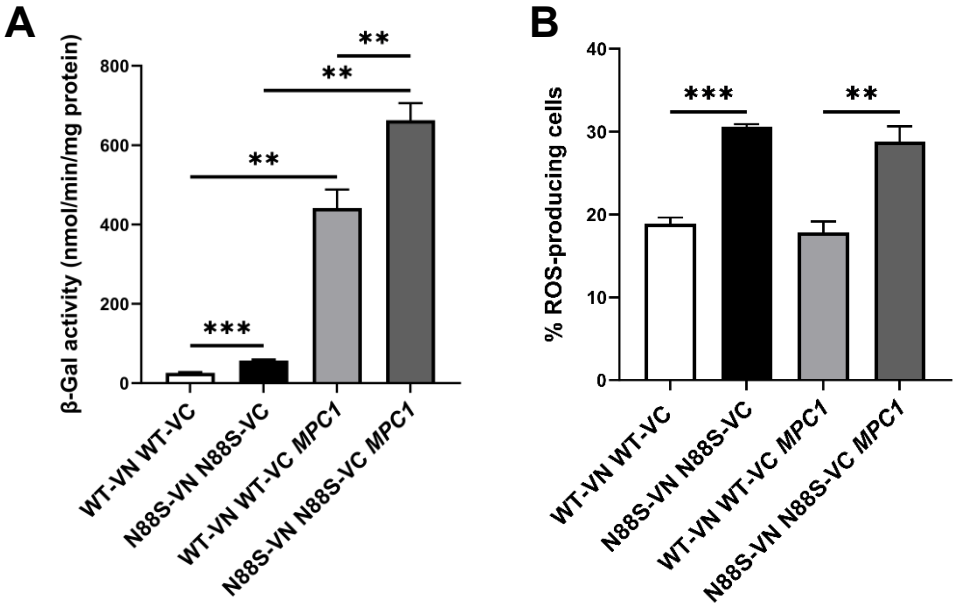

***Figure 27. MPC1* overexpression did not alter the levels of ROS production in WT and N88S seipin mutant cells. (A)** Cells with the specified genotypes carrying pRS315-UPRE-LacZ or pRS315-UPRE-LacZ-

ADH1pr-*MPC1*- ADH1t were grown in SC-glucose and allowed to reach the post-diauxic shift (PDS) phase. Protein extracts were prepared, and specific β-galactosidase (β-Gal) activity was measured using o-nitrophenyl-β-D-galactopyranoside (ONPG) as a substrate, with the amount of o-nitrophenol released indicating enzyme activity. At least 3 independent experiments for each strain were performed. **(B)** Cells with the indicated genotypes were grown in SC-glucose medium to stationary phase, and ROS levels were assessed in cells labeled with dihydroethidium (DHE) via flow cytometry using the FL3 channel. Cells were centrifuged and washed twice with PBS buffer. At least 3 independent experiments were conducted. ** $p \leq 0.01$; *** $p \leq 0.001$ (unpaired *t*-test with Welch´s correction).

3.6. Cytosolic misrouting of acetyl-CoA potentiates ER stress and contributes to oxidative damage in N88S mutant cells

In *S. cerevisiae*, acetyl-CoA is synthesized in four subcellular compartments: the cytosol, mitochondria, peroxisomes, and nucleus. Among these, peroxisomes constitute a particularly rich source of acetyl-CoA owing to their exclusive role in fatty acid β-oxidation [167, 168]. Peroxisomal acetyl-CoA can either be metabolized within the glyoxylate cycle or transferred to mitochondria through the carnitine shuttle system. Because the peroxisomal membrane is impermeable to acetyl-CoA, this transfer requires conversion of acetyl-CoA to acetyl-carnitine by carnitine acetyltransferase 2 Cat2, whose protein levels are decreased in N88S mutant cells (**Figure 15**). Once exported, acetyl-carnitine is reconverted to acetyl-CoA inside mitochondria, where it supports TCA cycle activity [169]. Based on our earlier observation that N88S mutant cells exhibit impaired utilization of peroxisome-derived acetyl-CoA, we hypothesized that dysfunction of the carnitine shuttle system may contribute to acetyl-CoA mislocalization and subsequent metabolic stress. To address this, we engineered two genetically modified backgrounds: one overexpressing the endogenous *CAT2* gene (hereafter $CAT2_{mit}$) to enhance mitochondrial and peroxisomal carnitine acetyltransferase activity, and a second strain expressing a modified *CAT2* variant (hereafter $CAT2_{cyt}$) engineered for exclusive cytosolic localization by removal of its native mitochondrial and peroxisomal targeting sequences [146]. This design allowed us to directly test whether manipulation of acetyl-CoA subcellular distribution impacts key disease phenotypes, including the ER stress response. Quantitative analysis of the UPRE-LacZ reporter activity (**Figure 28**) revealed significant activation of the UPR in WT and N88S mutant cells expressing both *CAT2* variants. In the $CAT2_{mit}$ background, the UPR reporter activity increased ~20-fold in WT and ~12-fold in N88S cells relative to their counterparts. Remarkably, the $CAT2_{cyt}$ variant induced even stronger responses, with ~22-fold and ~17-fold activation in WT and N88S seipin-expressing cells, respectively (**Figure 28**). These findings demonstrate that perturbations in acetyl-CoA compartmentalization, and particularly its cytosolic misrouting, is a more potent contributor to the activation of the ER stress response. This

is consistent with a model in which excess cytosolic acetyl-CoA significantly perturbs ER homeostasis, likely through altered lipid metabolism or changes in redox balance.

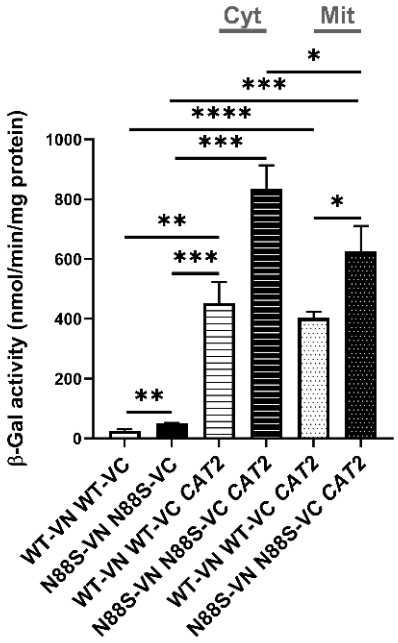

Figure 28. **Changes in acetyl-CoA subcellular distribution triggers the UPR in WT and N88S seipin mutant cells.** Cells with the specified genotypes expressing pRS315-UPRE-LacZ, pRS315-UPRE-LacZ-ADH1pr-*CAT2*$_{cyt}$-ADH1t or pRS315-UPRE-LacZ-ADH1pr-*CAT2*$_{mit}$-ADH1t were grown in SC-glucose and allowed to reach the post-diauxic shift (PDS) phase. Protein extracts were prepared, and specific β-galactosidase (β-Gal) activity was measured using o-nitrophenyl-β-D-galactopyranoside (ONPG) as a substrate, with the amount of o-nitrophenol released indicating enzyme activity. At least 3 independent experiments for each strain were performed. * $p \leq 0.05$; ** $p \leq 0.01$; *** $p \leq 0.001$; **** $p \leq 0.0001$ (unpaired *t*-test with Welch´s correction).

In parallel, we assessed ROS levels in these strains. The results showed that the expression of both *CAT2* variants increased the generation of ROS in WT and N88S seipin-expressing cells. Notably, in the N88S background, the expression of *CAT2*$_{cyt}$ increased ROS levels (~90 %) to a greater extent than those observed in N88S *CAT2*$_{mit}$ -expressing cells (~33%) (**Figure 29**).

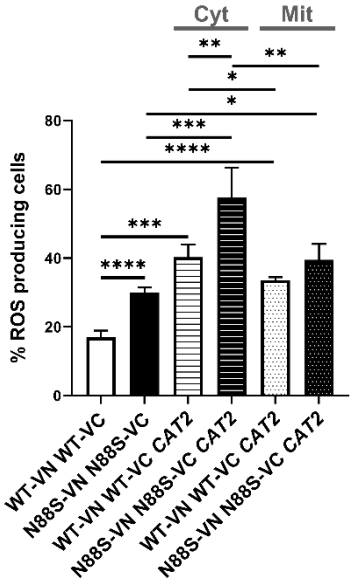

***Figure 29*. N88S cytosolic *CAT2* cells induced more ROS production.** Cells with the specified genotypes expressing pRS315-UPRE-LacZ, pRS315-UPRE-LacZ-ADH1pr-*CAT2*$_{cyt}$-ADH1t or pRS315-UPRE-LacZ-ADH1pr-*CAT2*$_{mit}$-ADH1t were grown in SC-glucose medium to stationary (STAT) phase, and ROS levels were assessed in cells labeled with dihydroethidium (DHE) via flow cytometry using the FL3 channel. Cells were centrifuged, washed twice with water, At least 3 independent experiments were performed for each strain. * $p \leq 0.05$; ** $p \leq 0.01$; *** $p \leq 0.001$; **** $p \leq 0.0001$ (unpaired *t*-test with Welch´s correction).

These results indicate that cytosolic accumulation of acetyl-CoA is not only a trigger for ER stress, but also a key driver of oxidative stress and damage, further supporting our initial hypothesis of impaired acetyl-CoA compartmentalization in disease-related metabolic dysfunctions. Notably, we observed a growth defect in N88S mutant cells overexpressing the cytosolic *CAT2* variant (*CAT2*$_{cyt}$) once they reached stationary phase, but not for cells expressing the peroxisomal/mitochondrial variant (*CAT2*$_{mit}$) (**Figure 30**)

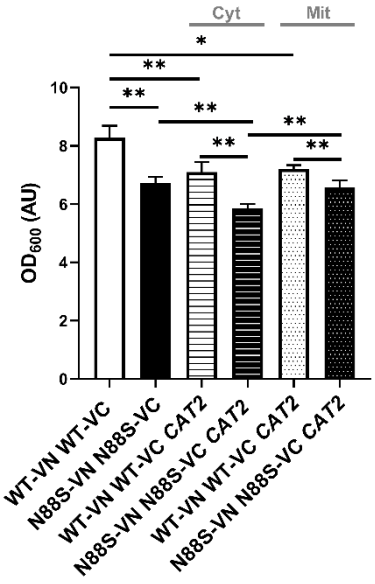

***Figure 30*. Mutant N88S cells expressing the cytosolic *CAT2* showed growth defects at STAT phase.** Overnight precultures of SC-glucose grown cells with the specified genotypes expressing pRS315-UPRE-

LacZ, pRS315-UPRE-LacZ-ADH1pr-*CAT2*$_{cyt}$-ADH1t or pRS315-UPRE-LacZ-ADH1pr-*CAT2*$_{mit}$-ADH1t were diluted to OD_{600}=0.15 in fresh medium. The growth was determined accordingly after a 48-hour incubation period. Data were obtained from at least 3 independent experiments for each strain. * $p \leq 0.05$; ** $p \leq 0.01$ (unpaired *t*-test with Welch´s correction).

As *S. cerevisiae* is auxotrophic for carnitine [131, 170], acetyl-carnitine shuttle activity is intrinsically limited under standard growth conditions. To determine whether exogenous carnitine supplementation could alleviate the stress phenotypes associated with cytosolic mislocalization of acetyl-CoA, *CAT2*$_{cyt}$-overexpressing cells were cultured in media supplemented with L-carnitine. Supplementation failed to reduce ROS accumulation, with levels remaining at ~20–25% in WT and ~40% in N88S seipin-expressing cells upon overexpression of *CAT2*$_{cyt}$ (**Figure 31**). These findings indicate that although carnitine supplementation modulates acetyl-CoA trafficking in yeast, it does not mitigate the cytotoxic consequences of its cytosolic accumulation. Rather, persistent ROS generation in N88S mutant cells arises from aberrant subcellular distribution and compartmentalization defects, likely reflecting impaired flux through the glyoxylate cycle (**Figure 31**).

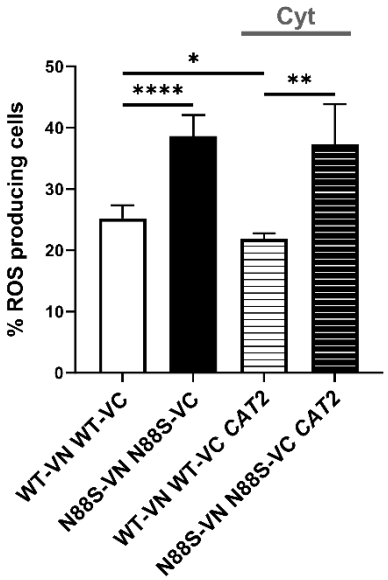

Figure 31. **Carnitine supplementation had no effect in ROS production in N88S seipin expressing cells.** Cells with the indicated genotypes expressing pRS315-UPRE-LacZ or pRS315-UPRE-LacZ-ADH1pr-*CAT2*$_{cyt}$-ADH1t were grown in SC-glucose medium supplemented with L-carnitine (100 mg/L) until stationary (STAT) phase, and ROS levels were assessed in cells labeled with dihydroethidium (DHE) via flow cytometry using the FL3 channel. Cells were centrifuged, washed twice with water, and diluted to OD600=0.5, at least 3 independent experiments for each strain. * $p \leq 0.05$; ** $p \leq 0.01$; **** $p \leq 0.0001$ (unpaired *t*-test with Welch´s correction).

3.7. Cytosolic acetyl-CoA fuels lipid biosynthesis and promotes oxidative stress in N88S seipin expressing cells

To investigate the downstream metabolic fate of mislocalized cytosolic acetyl-CoA, we next examined its potential diversion into lipid biosynthesis pathways. Because acetyl-CoA is the primary substrate for FA synthesis, we employed the well-characterized fatty acid synthase (FAS) inhibitor cerulenin, a covalent and irreversible inhibitor of the β-ketoacyl-ACP synthase domain, which effectively blocks the elongation of acyl chains and suppresses *de novo* lipogenesis [171, 172]. Treatment of WT and N88S *CAT2*$_{cyt}$-expressing strains with cerulenin (1 µg/mL) reduced ROS levels after 1 hour (**Figure 32 A**). Importantly, this was associated with decreased lipid peroxidation (**Figure 32 B**).

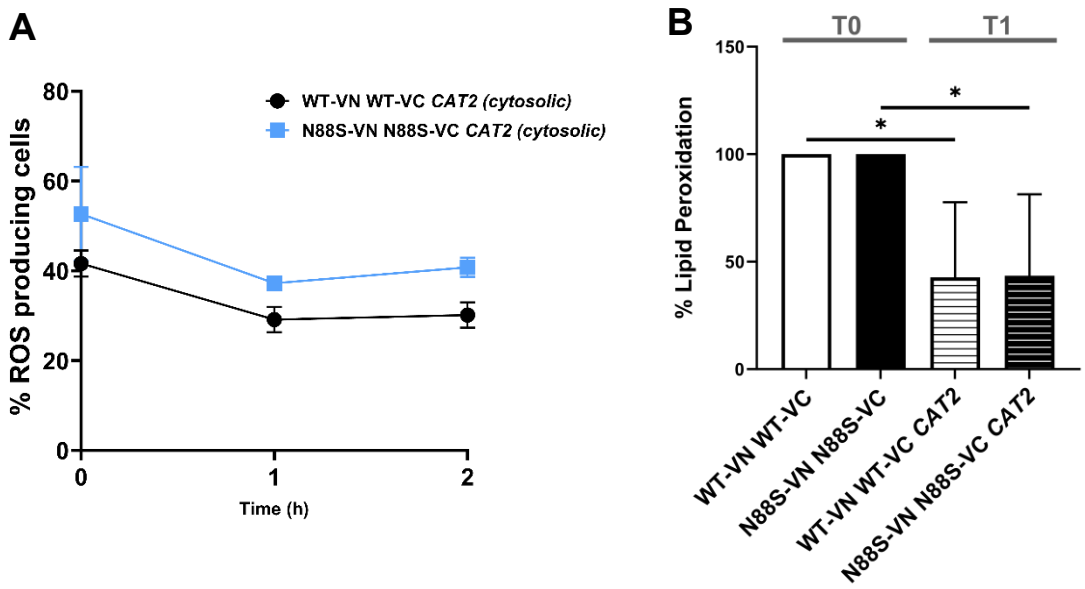

Figure 32. **Cerulenin attenuates oxidative stress in WT and N88S seipin mutant cells expressing cytosolic *CAT2*.** WT and N88S seipin mutant cells were grown in SC-glucose medium to stationary phase and incubated with 1 µg/mL cerulenin for 2 h (A) or 1 h (B) after which ROS levels were quantified using the DHE probe (A) and lipid peroxidation was assessed as the percentage of colony-forming units relative to time 0 (B). Data represents the mean ± SEM from at least three independent experiments. * $p \leq 0.05$ (one-way ANOVA).

These results provide strong evidence that excess cytosolic acetyl-CoA is actively funneled into FA biosynthesis and that this metabolic flux contributes to oxidative stress through enhanced lipid peroxidation. Finally, since acetyl-CoA can serve as a substrate for epigenetic regulation via histone acetylation [173, 174], we assessed global histone H3 acetylation by Western blot. No significant differences were observed between WT and N88S seipin-expressing cells upon overexpression of cytosolic *CAT2* (data not shown), indicating that histone acetylation does not act as a major sink for excess cytosolic acetyl-CoA under these conditions. Consistent with this, acetyl-coenzyme A

synthetase (Acs) activity, which supplies acetyl-CoA for histone acetylation, was increased in N88S mutant cells overexpressing cytosolic *CAT2* relative to its N88S mutant counterpart, suggesting that acetyl-CoA availability for histone acetylation is not limiting (**Figure 33**). On the other hand, excessive activation of the acetyl-coenzyme A synthetase at PDS phase likely feeds further the cytosolic acetyl-CoA pool and may contribute to its deleterious effects in N88S seipin-expressing cells.

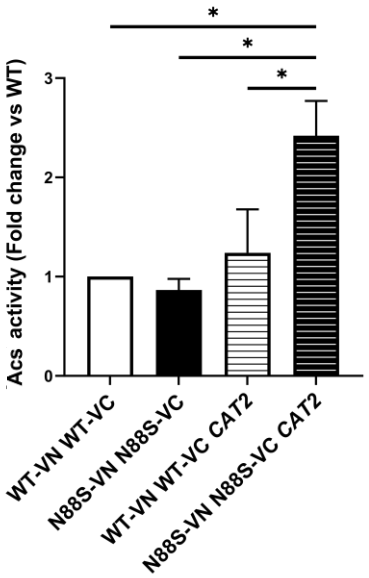

Figure 33. **The activity of acetyl-coenzyme A synthetase (Acs) was increased in N88S mutant cells overexpressing cytosolic *CAT2*.** Acs enzymatic activity was measured in cells grown in SC-glucose medium to PDS phase. Results are mean±SD of at least three independent experiments. * $p \leq 0.05$ (unpaired *t*-test with Welch´s correction).

Altogether, our results indicate that metabolic dysfunction exhibited by N88S mutant cells are not due to a global deficit in acetyl-CoA synthesis, but rather to its impaired compartmentalization and misrouting. Specifically, peroxisome-derived acetyl-CoA fails to reach mitochondria efficiently and instead accumulates in the cytosol, where it is redirected into lipid biosynthesis, fueling ROS production and ER stress. Therefore, we posit that cytosolic acetyl-CoA-driven lipogenesis is a key contributor to cellular dysfunction in N88S mutant cells.

4. Conclusion

Our study demonstrates that the N88S seipin mutation disrupts the interplay between lipid and protein metabolism, linking altered phospholipid homeostasis, miscompartmentalized acetyl-CoA, and oxidative stress to the cellular pathophysiology of seipinopathy. Using our yeast model of N88S seipinopathy, we previously showed that inositol and neutral lipid metabolism, as well as cellular iron homeostasis, are significantly impaired [10]. Central to this phenotype is the accumulation of phosphatidic acid (PA), reflecting a reduction in phospholipid biosynthetic flux and impaired inositol metabolism. This metabolic imbalance interferes with the activity of the Opi1p transcriptional repressor, resulting in derepression of *INO1* and elevated Ino1 levels [10]. Notably, PA accumulation and altered inositol metabolism contribute to ER stress independently of seipin misfolding, highlighting that lipid dysregulation alone can act as a driver of ER dysfunction [10]. In addition to perturbations in phospholipid and inositol metabolism, this study identified a previously unrecognized metabolic feedback loop that amplifies oxidative stress through mislocalized cytosolic acetyl-CoA. In N88S mutant cells, acetyl-CoA is inefficiently imported into mitochondria via the carnitine-dependent shuttle and is poorly channeled into the glyoxylate and TCA cycles. Instead, it is redirected into *de novo* FA synthesis, and these FAs are subsequently processed in peroxisomes via β-oxidation, regenerating cytosolic acetyl-CoA and establishing a futile cycle. This cycle exacerbates lipid peroxidation and ROS production. In fact, short-term inhibition of FA synthase partially mitigates oxidative stress, confirming that redirected lipogenesis directly contributes to cellular damage. This mechanistic framework explains the elevated ROS levels observed in N88S cells and links cytosolic acetyl-CoA miscompartmentalization to excessive FA turnover and peroxisome proliferation. The N88S mutation therefore produces a dual pathogenic signature. As a proteinopathy, it is characterized by misfolded seipin accumulation in the ER, which overwhelms the ER-associated degradation (ERAD) and the unfolded protein response (UPR) [9, 10]. As a lipidopathy, it arises from both disruptions in inositol and phospholipid homeostasis, which are key drivers of the ER stress response [10], and from impaired acetyl-CoA flux that fuels futile cycles of FA synthesis and oxidation, thereby amplifying oxidative stress and cellular damage. Together, these intertwined defects establish a self-reinforcing network in which ER stress, lipid peroxidation, and ROS generation likely potentiate one another, providing a mechanistic link between metabolic dysfunction and lipid storage phenotypes in N88S seipinopathy that is a common feature shared with other neurodegenerative disorders.

These findings also redefine a framework for potential therapeutic strategies. Interventions should aim not only to mitigate ROS or inhibit lipogenesis but also to restore proper metabolic compartmentalization and interrupt the self-amplifying lipid futile cycle. Enhancing mitochondrial import and utilization of acetyl-CoA via the Cat2-assisted carnitine shuttle can relieve cytosolic acetyl-CoA accumulation and reduce substrate flow into de novo FA synthesis. Redirecting cytosolic acetyl-CoA into sterol or phospholipid biosynthesis can buffer its accumulation while restoring membrane lipid homeostasis. Stimulating phospholipid synthesis, which is impaired in N88S cells [10], may serve a dual purpose as it may sequester excess acetyl-CoA and stabilize ER architecture, potentially alleviating ER stress associated with seipin misfolding. Additionally, modulating lipogenic transcriptional programs through AMPK activation or SREBP suppression in mammalian cells may further recalibrate lipid synthesis to match the cellular energy and redox demands.

Importantly, peroxisome proliferation in N88S mutant cells appears to be a compensatory adaptation rather than a simple consequence of lipotoxicity. Peroxisomal proliferation increases the capacity to promote the β-oxidation of FA derived from mislocalized acetyl-CoA, partially alleviating lipid accumulation. Peroxisomes also contribute to redox homeostasis through regulation of glutathione metabolism, which can compensate, at least partially, for diminished catalase activity and elevated ROS levels [9]. Therapeutic approaches that fine-tune peroxisomal function while redirecting acetyl-CoA flux could therefore synergistically reduce oxidative damage and restore metabolic balance. Taken together, a multifaceted strategy that promotes mitochondrial utilization of acetyl-CoA, enhances phospholipid synthesis, fine-tunes lipogenic transcription, and optimizes peroxisomal function provides a rational framework to disrupt the futile cycle at multiple nodes. Such an approach not only mitigates lipotoxicity and oxidative stress but also restores lipid metabolism, preserves membrane integrity, and supports adaptive cellular mechanisms critical for the survival of N88S seipin-expressing cells under physiological and environmental stress.

In summary, our findings provide an integrated mechanistic model for N88S seipinopathy, demonstrating how subtle disruptions in phospholipid metabolism, acetyl-CoA miscompartmentalization, and oxidative stress converge to perturb both protein and lipid homeostasis. This work underscores the central role of seipin in coordinating lipid balance, redox homeostasis, and ER function, and highlights the importance of targeting metabolic compartmentalization and peroxisomal adaptation as potential therapeutic

avenues to tackle the cellular dysfunctions in N88S seipin-associated motor neuron diseases.

References

1. Schwarz, D.S. and M.D. Blower, *The endoplasmic reticulum: structure, function and response to cellular signaling.* Cellular and Molecular Life Sciences, 2016. **73**(1): p. 79-94.
2. Prinz, W.A., A. Toulmay, and T. Balla, *The functional universe of membrane contact sites.* Nat Rev Mol Cell Biol, 2020. **21**(1): p. 7-24.
3. Olzmann, J.A. and P. Carvalho, *Dynamics and functions of lipid droplets.* Nature Reviews Molecular Cell Biology, 2019. **20**(3): p. 137-155.
4. Costa, V. and V. Teixeira, *Oxidative stress in N88S seipinopathy: novel insights into the mechanisms of neurodegeneration and therapeutic avenues.* Neural Regen Res, 2023. **18**(8): p. 1719-1720.
5. Walther, T.C., J. Chung, and R.V. Farese, Jr., *Lipid Droplet Biogenesis.* Annu Rev Cell Dev Biol, 2017. **33**: p. 491-510.
6. Salo, V.T., *Seipin—still a mysterious protein?* Frontiers in Cell and Developmental Biology, 2023. **Volume 11 - 2023**.
7. Arlt, H., et al., *Seipin forms a flexible cage at lipid droplet formation sites.* Nature Structural & Molecular Biology, 2022. **29**(3): p. 194-202.
8. Binns, D., et al., *Seipin Is a Discrete Homooligomer.* Biochemistry, 2010. **49**(50): p. 10747-10755.
9. Nogueira, V., et al., *Causative links between ER stress and oxidative damage in a yeast model of human N88S seipinopathy.* Free Radical Biology and Medicine, 2022. **192**: p. 165-181.
10. Ribeiro, M.O., et al., *N88S seipin-related seipinopathy is a lipidopathy associated with loss of iron homeostasis.* Cell Communication and Signaling, 2025. **23**(1): p. 10.
11. Fan, H.-d., et al., *Seipin mutation at glycosylation sites activates autophagy in transfected cells via abnormal large lipid droplets generation.* Acta Pharmacologica Sinica, 2015. **36**(4): p. 497-506.
12. Wright, Z.J., N.E. Tharp, and B. Bartel, *ER nests are specialized ER subdomains in Arabidopsis where peroxisomes and lipid droplets form.* Developmental Cell, 2025. **60**(15): p. 2061-2080.e4.
13. Hammoudeh, N., et al., *Mammalian lipid droplets: structural, pathological, immunological and anti-toxicological roles.* Progress in Lipid Research, 2023. **91**: p. 101233.
14. Zhang, C., et al., *Bacterial lipid droplets bind to DNA via an intermediary protein that enhances survival under stress.* Nature Communications, 2017. **8**(1): p. 15979.
15. Lundquist, P.K., K.K. Shivaiah, and R. Espinoza-Corral, *Lipid droplets throughout the evolutionary tree.* Prog Lipid Res, 2020. **78**: p. 101029.
16. Kong, J., et al., *Spatiotemporal contact between peroxisomes and lipid droplets regulates fasting-induced lipolysis via PEX5.* Nat Commun, 2020. **11**(1): p. 578.
17. Kamerkar, S., et al., *Metabolic and immune-sensitive contacts between lipid droplets and endoplasmic reticulum reconstituted in vitro.* Proc Natl Acad Sci U S A, 2022. **119**(24): p. e2200513119.
18. Zadoorian, A., X. Du, and H. Yang, *Lipid droplet biogenesis and functions in health and disease.* Nat Rev Endocrinol, 2023. **19**(8): p. 443-459.
19. Dalhaimer, P., *Lipid Droplets in Disease.* Cells, 2019. **8**(9).
20. Kumari, R.M., et al., *Concept of lipid droplet biogenesis.* European Journal of Cell Biology, 2023. **102**(4): p. 151362.
21. Yen, C.L., et al., *Thematic review series: glycerolipids. DGAT enzymes and triacylglycerol biosynthesis.* J Lipid Res, 2008. **49**(11): p. 2283-301.

22. Yang, H., et al., *Sterol esterification in yeast: a two-gene process.* Science, 1996. **272**(5266): p. 1353-6.
23. Dahlqvist, A., et al., *Phospholipid:diacylglycerol acyltransferase: an enzyme that catalyzes the acyl-CoA-independent formation of triacylglycerol in yeast and plants.* Proc Natl Acad Sci U S A, 2000. **97**(12): p. 6487-92.
24. Sandager, L., et al., *Storage lipid synthesis is non-essential in yeast.* J Biol Chem, 2002. **277**(8): p. 6478-82.
25. Ben M'barek, K., et al., *ER Membrane Phospholipids and Surface Tension Control Cellular Lipid Droplet Formation.* Dev Cell, 2017. **41**(6): p. 591-604.e7.
26. Wang, G., et al., *Fat storage-inducing transmembrane proteins: beyond mediating lipid droplet formation.* Cellular & Molecular Biology Letters, 2022. **27**(1): p. 98.
27. Choudhary, V., et al., *A conserved family of proteins facilitates nascent lipid droplet budding from the ER.* J Cell Biol, 2015. **211**(2): p. 261-71.
28. Fei , W., et al., *Fld1p, a functional homologue of human seipin, regulates the size of lipid droplets in yeast.* Journal of Cell Biology, 2008. **180**(3): p. 473-482.
29. Choudhary, V., et al., *Seipin and Nem1 establish discrete ER subdomains to initiate yeast lipid droplet biogenesis.* J Cell Biol, 2020. **219**(7).
30. Wang, S., et al., *Seipin and the membrane-shaping protein Pex30 cooperate in organelle budding from the endoplasmic reticulum.* Nature Communications, 2018. **9**(1): p. 2939.
31. Joshi, A.S., et al., *Lipid droplet and peroxisome biogenesis occur at the same ER subdomains.* Nature Communications, 2018. **9**(1): p. 2940.
32. Henne, W.M., M.L. Reese, and J.M. Goodman, *The assembly of lipid droplets and their roles in challenged cells.* Embo j, 2018. **37**(12).
33. Arribat, Y., et al., *Spastin mutations impair coordination between lipid droplet dispersion and reticulum.* PLOS Genetics, 2020. **16**(4): p. e1008665.
34. Wan, N., et al., *Spartin-mediated lipid transfer facilitates lipid droplet turnover.* Proceedings of the National Academy of Sciences, 2024. **121**(3): p. e2314093121.
35. Thiam, A.R., R.V. Farese, Jr., and T.C. Walther, *The biophysics and cell biology of lipid droplets.* Nat Rev Mol Cell Biol, 2013. **14**(12): p. 775-86.
36. Xu, N., et al., *The FATP1-DGAT2 complex facilitates lipid droplet expansion at the ER-lipid droplet interface.* J Cell Biol, 2012. **198**(5): p. 895-911.
37. Thiam, A.R., et al., *COPI buds 60-nm lipid droplets from reconstituted water-phospholipid-triacylglyceride interfaces, suggesting a tension clamp function.* Proc Natl Acad Sci U S A, 2013. **110**(33): p. 13244-9.
38. Xu, D., et al., *Rab18 promotes lipid droplet (LD) growth by tethering the ER to LDs through SNARE and NRZ interactions.* J Cell Biol, 2018. **217**(3): p. 975-995.
39. Wilfling, F., et al., *Triacylglycerol synthesis enzymes mediate lipid droplet growth by relocalizing from the ER to lipid droplets.* Dev Cell, 2013. **24**(4): p. 384-99.
40. Pol, A., S.P. Gross, and R.G. Parton, *Review: biogenesis of the multifunctional lipid droplet: lipids, proteins, and sites.* J Cell Biol, 2014. **204**(5): p. 635-46.
41. Walther, T.C. and R.V. Farese, Jr., *The life of lipid droplets.* Biochim Biophys Acta, 2009. **1791**(6): p. 459-66.
42. Kilwein, M.D. and M.A. Welte, *Lipid droplet motility and organelle contacts.* Contact (Thousand Oaks), 2019. **2**.
43. Gong, J., et al., *Fsp27 promotes lipid droplet growth by lipid exchange and transfer at lipid droplet contact sites.* Journal of Cell Biology, 2011. **195**(6): p. 953-963.
44. Grahn, T.H., et al., *FSP27 and PLIN1 interaction promotes the formation of large lipid droplets in human adipocytes.* Biochem Biophys Res Commun, 2013. **432**(2): p. 296-301.

45. Reddy, B.J., et al., *Load-induced enhancement of Dynein force production by LIS1-NudE in vivo and in vitro.* Nat Commun, 2016. **7**: p. 12259.
46. Guimaraes, S.C., et al., *Peroxisomes, lipid droplets, and endoplasmic reticulum "hitchhike" on motile early endosomes.* J Cell Biol, 2015. **211**(5): p. 945-54.
47. Zhang, Z., et al., *Roles of lipid droplets and related proteins in metabolic diseases.* Lipids Health Dis, 2024. **23**(1): p. 218.
48. Xu, W., et al., *Differential Roles of Cell Death-inducing DNA Fragmentation Factor-α-like Effector (CIDE) Proteins in Promoting Lipid Droplet Fusion and Growth in Subpopulations of Hepatocytes.* J Biol Chem, 2016. **291**(9): p. 4282-93.
49. Nguyen, T.B., et al., *DGAT1-Dependent Lipid Droplet Biogenesis Protects Mitochondrial Function during Starvation-Induced Autophagy.* Dev Cell, 2017. **42**(1): p. 9-21.e5.
50. Greenberg, A.S., et al., *The role of lipid droplets in metabolic disease in rodents and humans.* J Clin Invest, 2011. **121**(6): p. 2102-10.
51. Olzmann, J.A. and P. Carvalho, *Dynamics and functions of lipid droplets.* Nat Rev Mol Cell Biol, 2019. **20**(3): p. 137-155.
52. Miner, G.E., et al., *PLIN5 interacts with FATP4 at membrane contact sites to promote lipid droplet-to-mitochondria fatty acid transport.* Dev Cell, 2023. **58**(14): p. 1250-1265.e6.
53. Wang, H., et al., *Perilipin 5, a lipid droplet-associated protein, provides physical and metabolic linkage to mitochondria.* J Lipid Res, 2011. **52**(12): p. 2159-2168.
54. Hu, L., et al., *Mfn2/Hsc70 Complex Mediates the Formation of Mitochondria-Lipid Droplets Membrane Contact and Regulates Myocardial Lipid Metabolism.* Adv Sci (Weinh), 2024. **11**(14): p. e2307749.
55. Fan, H. and Y. Tan, *Lipid Droplet-Mitochondria Contacts in Health and Disease.* Int J Mol Sci, 2024. **25**(13).
56. Jarc, E. and T. Petan, *Lipid Droplets and the Management of Cellular Stress.* Yale J Biol Med, 2019. **92**(3): p. 435-452.
57. Kaushik, S. and A.M. Cuervo, *Degradation of lipid droplet-associated proteins by chaperone-mediated autophagy facilitates lipolysis.* Nat Cell Biol, 2015. **17**(6): p. 759-70.
58. Sztalryd, C. and D.L. Brasaemle, *The perilipin family of lipid droplet proteins: Gatekeepers of intracellular lipolysis.* Biochim Biophys Acta Mol Cell Biol Lipids, 2017. **1862**(10 Pt B): p. 1221-1232.
59. Schulze, R.J., et al., *Hepatic Lipophagy: New Insights into Autophagic Catabolism of Lipid Droplets in the Liver.* Hepatol Commun, 2017. **1**(5): p. 359-369.
60. Ohsaki, Y., et al., *PML isoform II plays a critical role in nuclear lipid droplet formation.* Journal of Cell Biology, 2016. **212**(1): p. 29-38.
61. Grabner, G.F., et al., *Lipolysis: cellular mechanisms for lipid mobilization from fat stores.* Nat Metab, 2021. **3**(11): p. 1445-1465.
62. Zechner, R., F. Madeo, and D. Kratky, *Cytosolic lipolysis and lipophagy: two sides of the same coin.* Nature Reviews Molecular Cell Biology, 2017. **18**(11): p. 671-684.
63. Vaquero, M.E., et al., *Properties, structure, and applications of microbial sterol esterases.* Applied Microbiology and Biotechnology, 2016. **100**(5): p. 2047-2061.
64. Watkins, P.A., *Very-long-chain acyl-CoA synthetases.* J Biol Chem, 2008. **283**(4): p. 1773-7.
65. Henry, S.A., S.D. Kohlwein, and G.M. Carman, *Metabolism and regulation of glycerolipids in the yeast Saccharomyces cerevisiae.* Genetics, 2012. **190**(2): p. 317-49.
66. Klug, Y.A., et al., *Mechanism of lipid droplet formation by the yeast Sei1/Ldb16 Seipin complex.* Nat Commun, 2021. **12**(1): p. 5892.

67. Guillén-Navarro, E., et al., *A new seipin-associated neurodegenerative syndrome.* J Med Genet, 2013. **50**(6): p. 401-9.
68. Ito, D. and N. Suzuki, *Molecular pathogenesis of seipin/BSCL2-related motor neuron diseases.* Ann Neurol, 2007. **61**(3): p. 237-50.
69. Wang, H., et al., *Seipin is required for converting nascent to mature lipid droplets.* Elife, 2016. **5**.
70. Fei, W., X. Du, and H. Yang, *Seipin, adipogenesis and lipid droplets.* Trends Endocrinol Metab, 2011. **22**(6): p. 204-10.
71. Cui, W., et al., *Seipin deficiency-induced lipid dysregulation leads to hypomyelination-associated cognitive deficits via compromising oligodendrocyte precursor cell differentiation.* Cell Death Dis, 2024. **15**(5): p. 350.
72. Craveiro Sarmento, A.S., et al., *Exploring Seipin: From Biochemistry to Bioinformatics Predictions.* Int J Cell Biol, 2018. **2018**: p. 5207608.
73. Sui, X., et al., *Cryo–electron microscopy structure of the lipid droplet–formation protein seipin.* Journal of Cell Biology, 2018. **217**(12): p. 4080-4091.
74. Grippa, A., et al., *The seipin complex Fld1/Ldb16 stabilizes ER-lipid droplet contact sites.* J Cell Biol, 2015. **211**(4): p. 829-44.
75. Choudhary, V. and R. Schneiter, *A Unique Junctional Interface at Contact Sites Between the Endoplasmic Reticulum and Lipid Droplets.* Frontiers in Cell and Developmental Biology, 2021. **Volume 9 - 2021**.
76. Fei, W., et al., *A role for phosphatidic acid in the formation of "supersized" lipid droplets.* PLoS Genet, 2011. **7**(7): p. e1002201.
77. Combot, Y., et al., *Seipin localizes at endoplasmic-reticulum-mitochondria contact sites to control mitochondrial calcium import and metabolism in adipocytes.* Cell Rep, 2022. **38**(2): p. 110213.
78. Craveiro Sarmento, A.S., et al., *The worldwide mutational landscape of Berardinelli-Seip congenital lipodystrophy.* Mutat Res Rev Mutat Res, 2019. **781**: p. 30-52.
79. Guo, J., et al., *Motor neuron degeneration in a mouse model of seipinopathy.* Cell Death Dis, 2013. **4**(3): p. e535.
80. Yagi, T., et al., *N88S seipin mutant transgenic mice develop features of seipinopathy/BSCL2-related motor neuron disease via endoplasmic reticulum stress.* Hum Mol Genet, 2011. **20**(19): p. 3831-40.
81. Yuan, W., M. Veenhuis, and I.J. van der Klei, *The birth of yeast peroxisomes.* Biochim Biophys Acta, 2016. **1863**(5): p. 902-10.
82. Wróblewska, J.P. and I.J. van der Klei, *Peroxisome Maintenance Depends on De Novo Peroxisome Formation in Yeast Mutants Defective in Peroxisome Fission and Inheritance.* Int J Mol Sci, 2019. **20**(16).
83. Islinger, M., et al., *The peroxisome: an update on mysteries 2.0.* Histochem Cell Biol, 2018. **150**(5): p. 443-471.
84. Pascual-Ahuir, A., S. Manzanares-Estreder, and M. Proft, *Pro- and Antioxidant Functions of the Peroxisome-Mitochondria Connection and Its Impact on Aging and Disease.* Oxid Med Cell Longev, 2017. **2017**: p. 9860841.
85. Dixit, E., et al., *Peroxisomes are signaling platforms for antiviral innate immunity.* Cell, 2010. **141**(4): p. 668-81.
86. Jansen, R.L.M., et al., *Comparative Genomics of Peroxisome Biogenesis Proteins: Making Sense of the PEX Proteins.* Front Cell Dev Biol, 2021. **9**: p. 654163.
87. Mullen, R.T., C.R. Flynn, and R.N. Trelease, *How are peroxisomes formed? The role of the endoplasmic reticulum and peroxins.* Trends Plant Sci, 2001. **6**(6): p. 256-61.
88. Smith, J.J. and J.D. Aitchison, *Peroxisomes take shape.* Nat Rev Mol Cell Biol, 2013. **14**(12): p. 803-17.

89. Jansen, R.L.M. and I.J. van der Klei, *The peroxisome biogenesis factors Pex3 and Pex19: multitasking proteins with disputed functions.* FEBS Lett, 2019. **593**(5): p. 457-474.
90. Agrawal, G. and S. Subramani, *Emerging role of the endoplasmic reticulum in peroxisome biogenesis.* Front Physiol, 2013. **4**: p. 286.
91. Aranovich, A., et al., *PEX16 contributes to peroxisome maintenance by constantly trafficking PEX3 via the ER.* J Cell Sci, 2014. **127**(Pt 17): p. 3675-86.
92. Montilla-Martinez, M., et al., *Distinct Pores for Peroxisomal Import of PTS1 and PTS2 Proteins.* Cell Rep, 2015. **13**(10): p. 2126-34.
93. Ma, C., et al., *Redox-regulated cargo binding and release by the peroxisomal targeting signal receptor, Pex5.* J Biol Chem, 2013. **288**(38): p. 27220-27231.
94. Purdue, P.E., X. Yang, and P.B. Lazarow, *Pex18p and Pex21p, a novel pair of related peroxins essential for peroxisomal targeting by the PTS2 pathway.* J Cell Biol, 1998. **143**(7): p. 1859-69.
95. Di Cara, F., R.A. Rachubinski, and A.J. Simmonds, *Distinct Roles for Peroxisomal Targeting Signal Receptors Pex5 and Pex7 in Drosophila.* Genetics, 2019. **211**(1): p. 141-149.
96. Hagstrom, D., et al., *The unique degradation pathway of the PTS2 receptor, Pex7, is dependent on the PTS receptor/coreceptor, Pex5 and Pex20.* Mol Biol Cell, 2014. **25**(17): p. 2634-43.
97. Skowyra, M.L., P. Feng, and T.A. Rapoport, *Towards solving the mystery of peroxisomal matrix protein import.* Trends Cell Biol, 2024. **34**(5): p. 388-405.
98. Braverman, N., et al., *An isoform of pex5p, the human PTS1 receptor, is required for the import of PTS2 proteins into peroxisomes.* Hum Mol Genet, 1998. **7**(8): p. 1195-205.
99. Matsumura, T., H. Otera, and Y. Fujiki, *Disruption of the interaction of the longer isoform of Pex5p, Pex5pL, with Pex7p abolishes peroxisome targeting signal type 2 protein import in mammals. Study with a novel Pex5-impaired Chinese hamster ovary cell mutant.* J Biol Chem, 2000. **275**(28): p. 21715-21.
100. Hasan, S., H.W. Platta, and R. Erdmann, *Import of proteins into the peroxisomal matrix.* Frontiers in Physiology, 2013. **Volume 4 - 2013**.
101. Kondrashov, F.A., et al., *Evolution of glyoxylate cycle enzymes in Metazoa: evidence of multiple horizontal transfer events and pseudogene formation.* Biol Direct, 2006. **1**: p. 31.
102. Palmieri, L., et al., *The mitochondrial dicarboxylate carrier is essential for the growth of Saccharomyces cerevisiae on ethanol or acetate as the sole carbon source.* Mol Microbiol, 1999. **31**(2): p. 569-77.
103. Kunze, M., et al., *A central role for the peroxisomal membrane in glyoxylate cycle function.* Biochim Biophys Acta, 2006. **1763**(12): p. 1441-52.
104. Hanson, R.W. and L. Reshef, *REGULATION OF PHOSPHOENOLPYRUVATE CARBOXYKINASE (GTP) GENE EXPRESSION.* Annual Review of Biochemistry, 1997. **66**(Volume 66, 1997): p. 581-611.
105. Nakatsukasa, K., et al., *The Ubiquitin Ligase SCF(Ucc1) Acts as a Metabolic Switch for the Glyoxylate Cycle.* Mol Cell, 2015. **59**(1): p. 22-34.
106. Rosenkrantz, M., et al., *Mitochondrial and nonmitochondrial citrate synthases in Saccharomyces cerevisiae are encoded by distinct homologous genes.* Mol Cell Biol, 1986. **6**(12): p. 4509-15.
107. Graybill, E.R., et al., *Functional comparison of citrate synthase isoforms from S. cerevisiae.* Arch Biochem Biophys, 2007. **465**(1): p. 26-37.
108. Padalko, V., F. Posnik, and M. Adamczyk, *Mitochondrial Aconitase and Its Contribution to the Pathogenesis of Neurodegenerative Diseases.* International Journal of Molecular Sciences, 2024. **25**(18): p. 9950.
109. Chaves, R.S., et al., *Isocitrate lyase localisation in Saccharomyces cerevisiae cells.* Gene, 1997. **198**(1-2): p. 165-9.

110. Gabay-Maskit, S., et al., *A piggybacking mechanism enables peroxisomal localization of the glyoxylate cycle enzyme Mdh2 in yeast.* J Cell Sci, 2020. **133**(24).
111. Duntze, W., et al., *Studies on the regulation and localization of the glyoxylate cycle enzymes in Saccharomyces cerevisiae.* Eur J Biochem, 1969. **10**(1): p. 83-9.
112. Beeckmans, S., *Glyoxylate Cycle*, in *eLS*.
113. Simpson-Lavy, K. and M. Kupiec, *Glucose Inhibits Yeast AMPK (Snf1) by Three Independent Mechanisms.* Biology (Basel), 2023. **12**(7).
114. Turcotte, B., et al., *Transcriptional regulation of nonfermentable carbon utilization in budding yeast.* FEMS Yeast Res, 2010. **10**(1): p. 2-13.
115. Schöler, A. and H.J. Schüller, *A carbon source-responsive promoter element necessary for activation of the isocitrate lyase gene ICL1 is common to genes of the gluconeogenic pathway in the yeast Saccharomyces cerevisiae.* Mol Cell Biol, 1994. **14**(6): p. 3613-22.
116. Roth, S., J. Kumme, and H.J. Schüller, *Transcriptional activators Cat8 and Sip4 discriminate between sequence variants of the carbon source-responsive promoter element in the yeast Saccharomyces cerevisiae.* Curr Genet, 2004. **45**(3): p. 121-8.
117. Bui, T.H.D. and K. Labedzka-Dmoch, *RetroGREAT signaling: The lessons we learn from yeast.* IUBMB Life, 2024. **76**(1): p. 26-37.
118. Laera, L., et al., *The transcription factors ADR1 or CAT8 are required for RTG pathway activation and evasion from yeast acetic acid-induced programmed cell death in raffinose.* Microb Cell, 2016. **3**(12): p. 621-631.
119. Du, Z., et al., *Cat8 Response to Nutritional Changes and Interaction With Ehrlich Pathway Related Factors.* Frontiers in Microbiology, 2022. **Volume 13 - 2022**.
120. Raja, V., et al., *Cardiolipin-deficient cells depend on anaplerotic pathways to ameliorate defective TCA cycle function.* Biochim Biophys Acta Mol Cell Biol Lipids, 2019. **1864**(5): p. 654-661.
121. Guaragnella, N., et al., *Analysis of Mitochondrial Retrograde Signaling in Yeast Model Systems.* Methods Mol Biol, 2021. **2276**: p. 87-102.
122. Cai, L. and B.P. Tu, *Acetyl-CoA drives the transcriptional growth program in yeast.* Cell Cycle, 2011. **10**(18): p. 3045-6.
123. Bradshaw, P.C., *Acetyl-CoA Metabolism and Histone Acetylation in the Regulation of Aging and Lifespan.* Antioxidants (Basel), 2021. **10**(4).
124. Shi, L. and B.P. Tu, *Acetyl-CoA and the regulation of metabolism: mechanisms and consequences.* Curr Opin Cell Biol, 2015. **33**: p. 125-31.
125. Bricker, D.K., et al., *A Mitochondrial Pyruvate Carrier Required for Pyruvate Uptake in Yeast, Drosophila, and Humans.* Science, 2012. **337**(6090): p. 96-100.
126. van den Berg, M.A., et al., *The two acetyl-coenzyme A synthetases of Saccharomyces cerevisiae differ with respect to kinetic properties and transcriptional regulation.* J Biol Chem, 1996. **271**(46): p. 28953-9.
127. van Roermund, C.W.T., et al., *Peroxisomal Fatty Acid Uptake Mechanism in Saccharomyces cerevisiae*.* Journal of Biological Chemistry, 2012. **287**(24): p. 20144-20153.
128. Yocum, H.C., S. Bassett, and N.A. Da Silva, *Enhanced production of acetyl-CoA-based products via peroxisomal surface display in Saccharomyces cerevisiae.* Proceedings of the National Academy of Sciences, 2022. **119**(48): p. e2214941119.
129. van Rossum, H.M., et al., *Requirements for Carnitine Shuttle-Mediated Translocation of Mitochondrial Acetyl Moieties to the Yeast Cytosol.* mBio, 2016. **7**(3).

130. Strijbis, K. and B. Distel, *Intracellular Acetyl Unit Transport in Fungal Carbon Metabolism.* Eukaryotic Cell, 2010. **9**(12): p. 1809-1815.
131. van Roermund, C.W., et al., *Molecular characterization of carnitine-dependent transport of acetyl-CoA from peroxisomes to mitochondria in Saccharomyces cerevisiae and identification of a plasma membrane carnitine transporter, Agp2p.* Embo j, 1999. **18**(21): p. 5843-52.
132. Chen, Y., et al., *Ach1 is involved in shuttling mitochondrial acetyl units for cytosolic C2 provision in Saccharomyces cerevisiae lacking pyruvate decarboxylase.* FEMS Yeast Res, 2015. **15**(3).
133. Bonifacino, J.S. and B.S. Glick, *The mechanisms of vesicle budding and fusion.* Cell, 2004. **116**(2): p. 153-66.
134. Rinaldi, T., et al., *Mitochondrial diseases and the role of the yeast models.* FEMS Yeast Res, 2010. **10**(8): p. 1006-22.
135. Brodsky, J.L. and W.R. Skach, *Protein folding and quality control in the endoplasmic reticulum: Recent lessons from yeast and mammalian cell systems.* Curr Opin Cell Biol, 2011. **23**(4): p. 464-75.
136. Goeckeler, J.L. and J.L. Brodsky, *Molecular chaperones and substrate ubiquitination control the efficiency of endoplasmic reticulum-associated degradation.* Diabetes Obes Metab, 2010. **12 Suppl 2**(Suppl 2): p. 32-8.
137. Goffeau, A., et al., *Life with 6000 genes.* Science, 1996. **274**(5287): p. 546, 563-7.
138. Nielsen, J., *Yeast Systems Biology: Model Organism and Cell Factory.* Biotechnol J, 2019. **14**(9): p. e1800421.
139. Fraczek, M.G., S. Naseeb, and D. Delneri, *History of genome editing in yeast.* Yeast, 2018. **35**(5): p. 361-368.
140. Sharma, N., et al., *alpha-Synuclein budding yeast model: toxicity enhanced by impaired proteasome and oxidative stress.* J Mol Neurosci, 2006. **28**(2): p. 161-78.
141. Mohammadi, S., et al., *Scope and limitations of yeast as a model organism for studying human tissue-specific pathways.* BMC Syst Biol, 2015. **9**: p. 96.
142. Janke, C., et al., *A versatile toolbox for PCR-based tagging of yeast genes: new fluorescent proteins, more markers and promoter substitution cassettes.* Yeast, 2004. **21**(11): p. 947-62.
143. Longtine, M.S., et al., *Additional modules for versatile and economical PCR-based gene deletion and modification in Saccharomyces cerevisiae.* Yeast, 1998. **14**(10): p. 953-61.
144. Yofe, I. and M. Schuldiner, *Primers-4-Yeast: a comprehensive web tool for planning primers for Saccharomyces cerevisiae.* Yeast, 2014. **31**(2): p. 77-80.
145. Li, D., et al., *Excess diacylglycerol at the endoplasmic reticulum disrupts endomembrane homeostasis and autophagy.* BMC Biol, 2020. **18**(1): p. 107.
146. Cordente, A.G., et al., *Modulating aroma compounds during wine fermentation by manipulating carnitine acetyltransferases in Saccharomyces cerevisiae.* FEMS Microbiol Lett, 2007. **267**(2): p. 159-66.
147. Kakimoto, Y., et al., *Visualizing multiple inter-organelle contact sites using the organelle-targeted split-GFP system.* Scientific Reports, 2018. **8**(1): p. 6175.
148. Gietz, R.D. and R.H. Schiestl, *Large-scale high-efficiency yeast transformation using the LiAc/SS carrier DNA/PEG method.* Nat Protoc, 2007. **2**(1): p. 38-41.
149. Laadan, B., et al., *Identification of an NADH-dependent 5-hydroxymethylfurfural-reducing alcohol dehydrogenase in Saccharomyces cerevisiae.* Yeast, 2008. **25**(3): p. 191-8.
150. Teixeira, V., et al., *Target of Rapamycin Complex 1 (TORC1), Protein Kinase A (PKA) and Cytosolic pH Regulate a Transcriptional Circuit for Lipid Droplet Formation.* Int J Mol Sci, 2021. **22**(16).

151. Turkolmez, S., et al., *Peroxisomal NAD(H) Homeostasis in the Yeast Debaryomyces hansenii Depends on Two Redox Shuttles and the NAD+ Carrier, Pmp47.* Biomolecules, 2023. **13**(9): p. 1294.
152. Samokhvalov, V., V. Ignatov, and M. Kondrashova, *Inhibition of Krebs cycle and activation of glyoxylate cycle in the course of chronological aging of Saccharomyces cerevisiae. Compensatory role of succinate oxidation.* Biochimie, 2004. **86**(1): p. 39-46.
153. Ding, J., et al., *Overexpression of acetyl-CoA synthetase in Saccharomyces cerevisiae increases acetic acid tolerance.* FEMS Microbiol Lett, 2015. **362**(3): p. 1-7.
154. Steels, E.L., R.P. Learmonth, and K. Watson, *Stress tolerance and membrane lipid unsaturation in Saccharomyces cerevisiae grown aerobically or anaerobically.* Microbiology (Reading), 1994. **140 (Pt 3)**: p. 569-76.
155. Ott, J., et al., *Comparison of human PEX knockout cell lines suggests a dual role of PEX1 in peroxisome biogenesis.* Biol Chem, 2023. **404**(2-3): p. 209-219.
156. Ferreira, M.J., et al., *Glutathione and peroxisome redox homeostasis.* Redox Biol, 2023. **67**: p. 102917.
157. Lefevre, S.D., et al., *The significance of peroxisome function in chronological aging of Saccharomyces cerevisiae.* Aging Cell, 2013. **12**(5): p. 784-93.
158. Vegusdal, A., et al., *Beta-oxidation, esterification, and secretion of radiolabeled fatty acids in cultivated Atlantic salmon skeletal muscle cells.* Lipids, 2004. **39**(7): p. 649-58.
159. Liu, Z. and R.A. Butow, *A transcriptional switch in the expression of yeast tricarboxylic acid cycle genes in response to a reduction or loss of respiratory function.* Mol Cell Biol, 1999. **19**(10): p. 6720-8.
160. Zampar, G.G., et al., *Temporal system-level organization of the switch from glycolytic to gluconeogenic operation in yeast.* Mol Syst Biol, 2013. **9**: p. 651.
161. Rothermel, B.A., et al., *Transactivation by Rtg1p, a basic helix-loop-helix protein that functions in communication between mitochondria and the nucleus in yeast.* J Biol Chem, 1995. **270**(49): p. 29476-82.
162. Galdieri, L., et al., *Transcriptional regulation in yeast during diauxic shift and stationary phase.* Omics, 2010. **14**(6): p. 629-38.
163. Lee, Y.J., et al., *TCA cycle-independent acetate metabolism via the glyoxylate cycle in Saccharomyces cerevisiae.* Yeast, 2011. **28**(2): p. 153-166.
164. Samokhvalov, V.A., et al., *[Arsenite-induced lipid peroxidation in Saccharomyces cerevisiae].* Mikrobiologiia, 2003. **72**(3): p. 308-11.
165. Bricker, D.K., et al., *A mitochondrial pyruvate carrier required for pyruvate uptake in yeast, Drosophila, and humans.* Science, 2012. **337**(6090): p. 96-100.
166. Gebert, M., et al., *The Unfolded Protein Response: A Double-Edged Sword for Brain Health.* Antioxidants, 2023. **12**(8): p. 1648.
167. Wang, Z., et al., *Key enzymes involved in the utilization of fatty acids by Saccharomyces cerevisiae: a review.* Front Microbiol, 2023. **14**: p. 1294182.
168. Krivoruchko, A., et al., *Microbial acetyl-CoA metabolism and metabolic engineering.* Metab Eng, 2015. **28**: p. 28-42.
169. van Roermund, C.W.T., et al., *Molecular characterization of carnitine‐dependent transport of acetyl‐CoA from peroxisomes to mitochondria in Saccharomyces cerevisiae and identification of a plasma membrane carnitine transporter, Agp2p.* The EMBO Journal, 1999. **18**(21): p. 5843-5852.
170. Lv, X., et al., *Dual regulation of cytoplasmic and mitochondrial acetyl-CoA utilization for improved isoprene production in Saccharomyces cerevisiae.* Nature Communications, 2016. **7**(1): p. 12851.

171. Knoll, L.J., D.R. Johnson, and J.I. Gordon, *Biochemical studies of three Saccharomyces cerevisiae acyl-CoA synthetases, Faa1p, Faa2p, and Faa3p.* Journal of Biological Chemistry, 1994. **269**(23): p. 16348-16356.
172. Johnson, D.R., et al., *Genetic analysis of the role of Saccharomyces cerevisiae acyl-CoA synthetase genes in regulating protein N-myristoylation.* J Biol Chem, 1994. **269**(27): p. 18037-46.
173. An, Y.J., et al., *Lactate as a major epigenetic carbon source for histone acetylation via nuclear LDH metabolism.* Experimental & Molecular Medicine, 2023. **55**(10): p. 2238-2247.
174. Jo, C., et al., *Histone acylation marks respond to metabolic perturbations and enable cellular adaptation.* Experimental & Molecular Medicine, 2020. **52**(12): p. 2005-2019.